Proteomic And Transcriptomic Analyses Reveal Novel Aspects Of Post-Transcriptional Regulation In *Saccharomyces cerevisiae*

Gregory A. Cary

A dissertation
submitted in partial fulfillment of the
requirements for the degree

Doctor of Philosophy

University of Washington
2013

Reading Committee:
Aimée Dudley, Chair
David Goodlett
David Morris

Program Authorized to Offer Degree:
Molecular and Cellular Biology

University of Washington

Abstract

Proteomic And Transcriptomic Analyses Reveal Novel Aspects Of Post-Transcriptional Regulation In *Saccharomyces cerevisiae*

Gregory A. Cary

Chair of the Supervisory Committee:
Aimée Dudely, Ph.D.
Genome Sciences

Although gene expression begins with transcription, there are a variety of mechanisms that cells use to control and tune expression post-transcriptionally. Many post-transcriptional regulatory functions including translational regulation, transcript surveillance, intracellular RNA localization, and RNA decay occur in organelles known as RNA granules. RNA granules, such as processing (P)-bodies, are cytoplasmic accumulations of translationally repressed mRNA and associated proteins that are ubiquitous among eukaryotes. Much of what is known about RNA granule biology has been observed through genetic and cytological experimentation and very few biochemical enrichments of these structures have been reported. In this work I present an affinity enrichment strategy for Dhh1, a conserved core component of P-bodies, from the budding yeast *Saccharomyces cerevisiae.* We identify proteins co-enriching with Dhh1 using tandem mass spectrometry and show that many known RNA granule proteins are enriched by this approach. We go on to compare the association of

proteins with the complex across two environmental conditions to examine the effect of stress induction on RNA granule assemblies. We find that metabolic enzymes and molecular chaperones are typically more abundant in the stress-induced P-body complex and demonstrate that one chaperone, YDJ1, is involved in the stress-induced aggregation of several P-body proteins into cytoplasmic foci. We also identify RNA co-enriching with Dhh1 and detect several classes of catalytic RNA as well as a strong enrichment for the mRNA encoding the P-body protein PAT1. Finally, I present and discuss the characterization of a yeast strain that exhibits sensitivity to the drug puromycin. The puromycin-sensitive strain incorporates the drug into nascent proteins *in vivo* and I discuss how this is a unique and useful approach for the detection of protein biosynthesis. The techniques developed and employed in this dissertation provide novel perspectives on post-transcriptional regulatory processes and enable further investigations into how these regulatory programs are executed within the cell.

Table of Contents

List of Figures

List of Tables

Acknowledgements

I would like to express my deepest appreciation to my advisor, Dr. Aimée Dudley, for allowing me to perform this research with her and for her continued support. Aimée accepted me into the lab without the benefit of a rotation, during which she may have learned how woefully little I knew about both yeast and biochemistry. Throughout my dissertation research she has always been available to offer advice and guidance, but has also allowed me the independence and space to struggle and make mistakes, which is a necessity for growth. I am grateful for her patience, support, and guidance throughout this project.

I would also like to extend my gratitude to my supervisory committee, including Dr. David Morris (GSR) and Dr. David Goodlett who both read and provided critical feedback on this dissertation as well as throughout my research. Thanks also to Dr. John Aitchison, Dr. Joseph Nadeau, and Dr. Karol Bomsztyk for their support and guidance along the way. Many thanks also to the directors and administrators of the MCB program for their guidance and steady encouragement.

This work would not have been possible without the support of members of the Dudley lab who provided continuous scientific, moral, and gastronomical assistance. Chief among them is Dr. Dani Vinh who worked with me, and at times critically challenged me, to achieve the highest quality results and was a true catalyst for success in these efforts.

Finally, I am immeasurably grateful to the support of my friends and family. From the time I arrived in Seattle, I have been surrounded by friends who have been immensely supportive of my efforts and understanding of my general absence due to my scholarly pursuits. The love and support of my family including my sister, Leslie, brother-in-law, Don, and their children Natalie, Owen and Liam has been a source of great strength for me over these years. The opportunity watch these kids grow, to build Legos™ and play with Polly Pockets™ together, and to read stories with them – to be an uncle – has provided exceptional respite from the trials of graduate school. To my wife, Sara, I cannot thank you enough for your encouragement throughout this process. You have been a source of constant inspiration and comfort throughout the many ups and downs of graduate school and I am eternally grateful to you for your love and steadfast support. I'm not sure how I could have managed without you.

Chapter 1: Background & Introduction

Defining the regulatory mechanisms involved in gene expression is a fundamental objective of modern biology. Recently, the ability to measure total RNA abundance coupled with techniques developed to interrogate vast networks of protein-DNA interactions have led to a detailed understanding of transcriptional control. However, transcriptional regulation is only the first of many steps needed to express functional proteins at the correct levels. Transcript maturation, localization, and decay all play critical parts in determining the time, place, and amount of protein produced. Recent work in a variety of organisms has underscored the importance of post-transcriptional regulation in an array of biological processes, including response to nutrient deprivation in yeast[1,2], metabolic diseases in mammals[3], developmental processes in worms[4], and the control of one of the most frequently altered genes in cancer (p53)[5]. Post-transcriptional regulatory processes are central to the appropriate and optimal expression of gene products. While steady state transcript levels are commonly reported measurements of gene expression, they are not always well correlated with protein expression levels[6,7]. Therefore, a more complete understanding of gene expression necessitates more detailed knowledge of how transcripts are regulated post-transcriptionally.

Protein-RNA interactions are a key component of many of many post-transcriptional regulatory processes. The collection of proteins associated with a particular mRNA at a given time is known as the messenger ribonucleoprotein (mRNP)

complex and includes proteins that associate with transcripts generally (e.g. the mRNA cap binding protein, eIF4E[8]) as well as sequence-specific RNA binding proteins (e.g. the Puf family proteins[9]). These proteins work in concert to shepherd a transcript through its life cycle, dictating where and when it will be translated and at which point it will be degraded[10]. Therefore, elucidating the combinatorial array of protein-mRNA interactions is central to gaining insight into post-transcriptional regulation.

Cytoplasmic RNA Granules

Association between mRNPs and cytoplasmic RNA granules represents one mechanism through which cells can regulate the post-transcriptional fate of mRNA. RNA granules are aggregates of translationally silenced mRNA and accompanying proteins that appear as cytoplasmic foci[11,12]. These structures have been associated with many post-transcriptional regulatory processes including mRNA localization[13], aberrant mRNA surveillance[14], and mRNA decay[15,16]. Transcripts associated with RNA granules can be maintained in the translationally silent state indefinitely, primed to return to translation when and where it is beneficial to the cell, or can be targeted for degradation. In this way accumulation of mRNP within RNA granules is a way for cells to rationalize transcript content and modify gene expression programs post-transcriptionally.

While RNA granules are found throughout eukaryotic lineages, germ-line cells and neurons are examples of two cell types that contain specialized RNA granules that are employed for specific functions unique to these cells. Germ cells contain mRNP

aggregates known as germ cell granules (GCG), comprised of maternal mRNA required for germ cell specification during early embryogenesis. Once an embryo reaches an appropriate developmental stage, the translational repression is released and incorporated mRNAs are expressed[11,12]. Neurons contain mRNP aggregates, neuronal granules (NG), which are transported from the soma to distal sites of translation where exogenous stimuli can lead to swift adaptations in localized protein synthesis via de-repression of these transcripts. This mechanism is important for various aspects of neuronal physiology including guidance of growing neuronal processes as well fine-tuning cellular aspects of learning and memory at synapses[13].

RNA granules such as processing (P)-bodies (PB) and stress granules (SG) are common among all eukaryotes examined and therefore represent a more general class. SG and PB are both dynamic aggregates of non-translating mRNAs that are rapidly induced by stress to form cytoplasmic foci[11,17]. They are distinguished primarily based on their protein components, with SGs containing components of the translation initiation machinery and PBs containing RNA decay factors[11,18,19,20]. However, there are a number of proteins that PB and SG share in common, and it has been reported that these granules can interact and exchange components *in vivo*[21]. In the following sections I will review what is currently known about PB and SG complexes, with special focus on granule composition and dynamics.

PBs are the most thoroughly characterized RNA granule in yeast, beginning in 2003 with the discovery of cytoplasmic foci containing decapping factors and the 5'-3' exonuclease[20]. PB have been shown to be dynamic, stress-induced aggregates of

translationally silenced mRNA along with various RNA degradation factors[19] [Table 1.1]. In yeast, mRNA decay is initiated by deadenylation of the transcript by the Ccr4p/Pop2p/Not1-5p complex[22]. The subsequent decapping step is inhibited by the poly(A) binding protein (Pab1p) and decapping only begins when the poly(A) tail is shorter than 12 nucleotides, the minimum length for Pab1p binding[23]. Removal of the 5' cap is achieved by the decapping complex including the catalytic Dcp2p and associated decapping enhancers such as Dcp1p, Edc3p, Dhh1p, and Pat1p/Lsm1-7p[16]. Finally transcripts are terminally degraded primarily by the cytoplasmic 5'-3' exonuclease Kem1p[24]. All of these proteins have been shown to co-localize to PB foci *in vivo*. PBs have also been found to contain proteins associated with transcript-specific RNA decay processes, such as nonsense mediated decay (NMD) in yeast[14] and the RNA-induced silencing complex (RISC)[25] in metazoans.

Certain translation initiation factors localize to PB including Pab1p, the cap-binding protein (eIF4E), and a scaffold protein (eIF4G) that mediates the interaction of the cap with Pab1p. These components accumulate within PB especially during stress conditions[26]. This co-localization may reflect associations between PB and SG aggregates *in vivo* as SG typically consist of these, and other, translation initiation factors along with various ribosomal subunits[27].

PBs also contain various proteins involved in retrotransposition. PB proteins have been shown to be involved in the assembly of Ty retrotransposon virus-like particles[28,29,30], promotion of transposition[31], and may be involved in the post-transcriptional shift from a translation substrate to genomic RNA for the Ty3 transcript[32].

Table 1.1 RNA granule proteins in *S. cerevisiae*

	Protein / Complex	Function
P-body Core	Ccr4 / Pop2 / Not1-5	Cytoplasmic de-adenylase complex
	Dcp2 / Dcp1	Decapping enzyme complex
	Kem1 (Xrn1)	5'-3' Exonuclease
	Edc3	Decapping activator
	Dhh1	DExD/H-box helicase; decapping activator & translational repressor
	Pat1	Decapping activator & translational repressor
	Lsm1-7	Heteroheptameric Sm-like complex involved in decapping
	Scd6	Repressor of translation initiation
Stress Granule	Pab1	Poly(A) binding protein
	Cdc33	mRNA cap binding protein (eIF4E)
	TIF4631 / TIF4632	Translation initiation factor eIF4G
	Rpg1 / Prt1 / Nip1	Translation initiation factor eIF3 (subunits a, b & c)
	Pbp1	Component of glucose deprivation induced stress granules
	Pbp4	Pbp1 binding protein
	Pub1	Poly(A)+ RNA binding protein
	Lsm12	Protein of unknown function, may have a role in RNA processing
P-body Associated	Nam7 / Upf3 / Ebs1	Nonsense mediated decay
	YGR109W-A	Retrotransposon TYA Gag
	Dcs1 / Dcs2	Cap scavenger
	Pby1	Putative tubulin tyrosine ligase
	Smy2	COPII vesicle formation

In what are likely similar interactions between PB and transposons, PB are also associated with a number of viruses[33,34] and are altered during viral infection[35,36]. Because retrotransposons and retroviruses are entities that rely heavily on post-transcriptional regulatory processes for their life cycles, their interaction with and regulation by PB emphasize the central role of these granules in cellular post-transcriptional regulatory processes.

RNA Granules Are Stress Induced and Highly Dynamic

An important characteristic of PB to emerge from their investigation in yeast is that PBs typically exist in balance with translation. Generally, perturbations that prevent translation – such as drugs, mutations or stress – lead to an increase in the size and number of PB foci[17]. The inverse is also true; for example cycloheximide treatment, which prevents ribosomal translocation and traps RNAs with translating ribosomes, leads to a decrease in the size and number of PB foci[17]. Furthermore, as cells are released from stress, PB are reduced in a manner dependent on functional translation initiation[26]. Some PB components can mediate both translational silencing and PB induction. Over-expression of the decapping enhancers Dhh1p and Pat1p represses translation and stimulates PB formation, whereas deletion of either of these factors has the inverse effect[23]. The identification of this relationship has led to the development of a model in which mRNA association with PB and other RNA granules is involved with the regulation of translational activity particularly in response to environmental perturbations.

PB are induced to aggregate rapidly by a variety of cellular stresses including glucose depletion from the media, osmotic stress, UV irradiation[37], acidic stress[38], DNA damage[39], and entry into stationary phase[17]. These foci can disaggregate just as rapidly once the stress is relieved[40]. PB are also regulated by cell cycle processes and are involved in yeast mating[41] and recent work from our own lab has demonstrated that PBs are unidirectionally transferred from the mother cell to the daughter during the cell cycle [Garmendia Torres and Dudley, personal communication].

The accumulation of PB proteins into cytoplasmic foci does not appear to be a random aggregation process but rather a direct result of various cell signaling cascades. For example, while salt stress induces PB aggregation in yeast, deletion of the gene encoding the Hog1 MAP kinase, the effector kinase of the osmotic shock signal transduction pathway, prevents the accumulation of PB foci even in the presence of high salt[17]. PB protein accumulation can also be induced by the cAMP-dependant protein kinase (PKA)[42]. The catalytic subunits of PKA localize to PB under some, but not all stress conditions[43]. Finally, the kinases Pkh1/2 and Pkc1, which are involved in regulating cellular growth in response to nutrient availability, have been shown to stimulate PB accumulation and affect mRNA decay under specific stress conditions[44]. Taken together, these results show that while PBs aggregate following a variety of stresses, PB accumulation is a controlled physiological response to specific environmental states. Because these environmental conditions also typically alter other aspects of gene expression, such as transcription, it is reasonable to speculate that PBs may also play a role in that gene expression response.

PBs are very dynamic entities. Fluorescence recovery after photobleaching (FRAP) experiments have been used to interrogate the real-time dynamics of specific PB components. One set of FRAP experiments demonstrated that in a human cell line Dcp1 fluorescence returns to steady-state levels within one minute of photobleaching, indicating a high rate of protein exchange between PB and the cytoplasm. In contrast, the fluorescence of another PB component, Dcp2 does not recover from FRAP, indicating that Dcp2 is stably associated with PB[45]. In addition PBs interact with the cytoskeleton leading to dynamic intracellular localization. Microtubule disruption by treatment with benomyl or temperature sensitive mutations leads to the accumulation of PB components[46]. In mammalian cells, the microtubule motor proteins kinesin and dynein are involved in PB and SG dynamics[47]. Myosins also associate with PB[48] and are necessary for PB formation[49]. These experiments highlight the dynamic nature of PBs *in vivo*, both at the level of protein components shuttling in and out of PB as well as PB transport within the cell.

Functional Implications of RNA Granule Aggregation

The molecular interactions underlying induced PB assembly have been identified in yeast. For example, RNA is critical for assembly and when they are treated with ribonuclease, PB foci are greatly reduced[17]. Furthermore, the PB components Edc3p and Lsm4p contain self-aggregation domains that are critical for the assembly of PB foci[50]. Destruction of the interaction domains in these two proteins completely inhibits the formation of microscopically detectable PB without significantly affecting either mRNA decay or translational silencing. Intriguingly, metazoan cells also display

functional mRNA decay, NMD, and RNA-mediated gene silencing in the absence of visible PB[51].

Despite thorough characterization, the functional relevance of the induced aggregation of mRNP into PB remains an unresolved question. While the protein components of PB primarily consist of cellular RNA decay machinery, there is no direct evidence demonstrating enzymatic activity of these proteins within PB[16] or of changes in mRNA decay when PB foci are depleted[50,51]. In addition, the constituent mRNAs are not necessarily destined for degradation as transcripts can be released back to translation following sequestration in PB[40,52]. There are indications that sequestration of mRNAs into RNA granule compartments may be a requirement for cell viability and long term survival[53,42]. Finally, it has not been demonstrated whether the PB complex exists ubiquitously, even when not induced to aggregate by stress, but at levels below the microscopic detection limit. Therefore, the nature of sub-microscopic PB must be examined in relation to the induced complexes in order to discern the functional implications of aggregation.

The fundamental question of how granules are selective for specific mRNPs remains unclear. For example, mammalian cells under stress sequester transcripts such as GAPDH, β-actin, c-MYC, Igf-II, and H19 into SG[54], while the stress-induced transcripts for Hsp90[54] and Hsp70[55] are excluded from SG and are directed toward translating polyribosomes. How these various transcripts are differentiated in the cytoplasm remains a crucial question. One likely explanation could be that this specificity is mediated by the interaction of *trans*-acting factors with *cis*-elements

within mRNA. For example, the RISC is a component of both metazoan SG and PB and the interaction of specific non-coding RNAs with their cognate mRNA targets is one mechanism by which individual transcripts could be targeted to accumulate into RNA granules[51]. Another example is *trans*-acting AU-rich element (ARE) binding proteins that interact with AREs within the 3' UTR of specific transcripts and are also located in mammalian SG and PB[18,56]. In yeast, the Rbp1p protein associates with the 3' end of the mitochondrial porin transcript, localizes to PB and modulates transcript stability[57]. Finally, the yeast Puf3p, which specifically binds to nuclear transcripts of mitochondrial function[9], is known to co-localize with PB proteins and this interaction is associated with regulation of the target transcripts[58]. Trans-acting RNA binding proteins likely mediate mRNP association with RNA granules, however it remains to be determined how these interactions are coordinated.

While protein-RNA interactions are at least partially responsible for the partitioning of transcripts to RNA granules, there are various classes of RNA granules within a single cell at any given time. Both PB and SG are composed of proteins that are unique to each granule, although there are several proteins that can exist in either. The core PB component Dhh1p has been shown to co-localize with both Edc3p, a core PB protein, and Pab1p, a canonical SG protein, following stress induction[59]. PB and SG can also physically interact within the cell and constituent mRNAs can transition between the granules[60,21]. Determining how mRNP complexes are partitioned between different RNA granules is an important step in understanding how the cell determines which transcripts are to be degraded, which are to be translated and which are to be stored for later translation.

Technologies for Global Analysis of Post-transcriptional Regulation

The study of post-transcriptional regulatory processes has only recently begun to leverage the power of global methods analogous to those that have been applied so effectively in the study of transcription, such as ChIP-Seq and RNA expression analysis. Recently high-throughput technologies such as polysome profiling[61], ribosome affinity purification[62], and ribosome footprinting[63] have enabled unprecedented insights into translational activity including processes such as ribosome initiation, elongation rates and pausing sites[64]. These approaches all rely on ribosome association with a transcript as a readout for translational activity. While ribosome association is clearly a very useful proxy, it does not always correlate well with the active translation of substrate mRNA. For example, transcripts may contain structural elements that allow ribosome binding but prevent active translation of the full transcript such as upstream open reading frames or iron response element hairpins in the 5' UTR. Furthermore, SGs have been shown to contain both non-translating mRNA and ribosomal subunits. The ability to globally measure the protein products of translation would be a powerful complementary approach to these ribosome-based assays and would provide an additional perspective onto translational activity.

While a variety of techniques exist to assay translational activity, there are currently no approaches to globally access non-translating pools of mRNA within the cell. Given their central role in post-transcriptional regulation, as well as the balance that exists between translational activity and RNA granule accumulation, RNA granules are good candidates for compartments in which one might gain access to non-

translating mRNA. While it is possible to visualize RNA granules, these investigations give little insight into their functional relevance in post-transcriptional gene regulation.

A few biochemical enrichments of RNA granules have been reported. In 2004 Kanai *et al.* identified a number of proteins involved in neuronal RNA transport in biochemical association with a kinesin motor protein[65]. In another study, proteins co-immunoprecipitating with Dcp1 were identified by mass spectrometry. These included many known components of RNA granules, such as Edc3, p54/rck, and Hedls, but did not capture several other core components, most notably Dcp2[56]. The high stringency TAP system has also been used to identify proteins co-precipitating with Dhh1[66] and Pat1[67]. Recently work by Mitchell *et al.* identified transcripts associated with TAP-tagged P-body proteins including Dhh1, Pat1, Lsm1, and Sbp1[68]. However, none of these approaches demonstrated the specific enrichment of RNA granule proteins along with specific RNAs. Two papers by Kato *et al.* come the closest to this goal when they demonstrated the enrichment of RNA granule proteins through selective precipitation with biotinylated isoxazole (b-isox) compound[69,70]. The authors show that the presence of domains of low-complexity within RNA granule proteins is both necessary and sufficient to stimulate precipitation of these proteins when cell lysates are treated with the drug. The authors also characterize the RNA that co-precipitates using this approach and identify features common to RNA granule substrates, for example long 3' UTR with binding sites for known RNA granule proteins. While RNA granule proteins and associated RNAs are enriched by precipitation with b-isox, this approach is not a direct probe for RNA granule proteins per se as it depends on the presence of low-

complexity regions within RNA granule proteins for enrichment. Therefore it has the potential to capture other proteins with similar structural or sequence elements that are not strictly components of cellular RNA granules.

One of the most crucial and unaddressed questions surrounding the study of mRNP aggregates is that there has been no comprehensive analysis of constituent RNAs. Enumerating the protein and mRNA components of PB in yeast, and elucidating whether and how their composition changes in response to different stimuli are critical tasks for understanding the functional implications of RNA granule induction. Furthermore, the signals responsible for the induction of specific mRNP aggregates and how they are partitioned into PB, SG, or other RNA granules within the cell are currently unclear. Finally, the flux of mRNPs through PB, SG and polysomes remains to be conclusively demonstrated and likely will not be until both the components and underlying regulatory mechanisms have been identified.

The yeast *Saccharomyces cerevisiae* has been an extremely potent model organism for studying eukaryotic cell biology. *S cerevisiae* has a relatively small genome and is fairly simple to manipulate genetically using the tools accessible by homologous recombination. It is also easy to generate the large amount of starting material required for biochemical analysis by growth in large batch culture. Because RNA granule structures are largely conserved across eukaryotic lineages, it is logical to pursue enrichment of RNA granules from yeast as a means to understand their composition and dynamics.

In this thesis I will present the work I have accomplished to address these questions and challenges. First, I will describe our approach to enriching RNA granules from yeast cells as well as the analysis of co-enriching proteins and RNA using systems-level technologies and analyses. Using this approach we identify previously unrecognized aspects of RNA granule biology in yeast. I will then describe work done to enable the development of protein-centric translational assays in yeast using the small molecule puromycin as a probe for translational activity. Finally I will discuss the implications of this work in the broader context of gaining a better understanding of post-transcriptional regulatory processes, not only in yeast but also across eukaryotes and why these questions might be especially critical for elucidating neurodegenerative pathologies.

References

[1] McCarthy, J. E. Posttranscriptional control of gene expression in yeast. *Microbiology and molecular biology reviews : MMBR* **62**, 1492-1553 (1998).

[2] Hinnebusch, A. G. Translational regulation of GCN4 and the general amino acid control of yeast. *Annual review of microbiology* **59**, 407-450, doi:10.1146/annurev.micro.59.031805.133833 (2005).

[3] Kim, W. & Kyung Lee, E. Post-transcriptional regulation in metabolic diseases. *RNA biology* **9**, 772-780, doi:10.4161/rna.20091 (2012).

[4] Nousch, M. & Eckmann, C. R. Translational control in the Caenorhabditis elegans germ line. *Advances in experimental medicine and biology* **757**, 205-247, doi:10.1007/978-1-4614-4015-4_8 (2013).

[5] Freeman, J. A. & Espinosa, J. M. The impact of post-transcriptional regulation in the p53 network. *Briefings in functional genomics* **12**, 46-57, doi:10.1093/bfgp/els058 (2013).

[6] Gunawardana, Y. & Niranjan, M. Bridging the gap between transcriptome and proteome measurements identifies post-translationally regulated genes. *Bioinformatics*, doi:10.1093/bioinformatics/btt537 (2013).

[7] Lee, M. V. *et al.* A dynamic model of proteome changes reveals new roles for transcript alteration in yeast. *Mol Syst Biol* **7**, 514, doi:10.1038/msb.2011.48 (2011).

[8] Tharun, S. & Parker, R. Targeting an mRNA for decapping: displacement of translation factors and association of the Lsm1p-7p complex on deadenylated yeast mRNAs. *Molecular cell* **8**, 1075-1083 (2001).

[9] Gerber, A., Herschlag, D. & Brown, P. O. Extensive association of functionally and cytotopically related mRNAs with Puf family RNA-binding proteins in yeast. *Plos Biol* **2**, E79, doi:10.1371/journal.pbio.0020079 (2004).

[10] Hieronymus, H. & Silver, P. A. A systems view of mRNP biology. *Genes & development* **18**, 2845-2860, doi:10.1101/gad.1256904 (2004).

[11] Anderson, P. & Kedersha, N. RNA granules. *The Journal of Cell Biology* **172**, 803-808, doi:10.1083/jcb.200512082 (2006).

[12] Anderson, P. & Kedersha, N. RNA granules: post-transcriptional and epigenetic modulators of gene expression. *Nat Rev Mol Cell Biol* **10**, 430-436, doi:10.1038/nrm2694 (2009).

[13] Rodriguez, A. J., Czaplinski, K., Condeelis, J. S. & Singer, R. H. Mechanisms and cellular roles of local protein synthesis in mammalian cells. *Current Opinion in Cell Biology* **20**, 144-149, doi:10.1016/j.ceb.2008.02.004 (2008).

[14] Sheth, U. & Parker, R. Targeting of aberrant mRNAs to cytoplasmic processing bodies. *Cell* **125**, 1095-1109, doi:10.1016/j.cell.2006.04.037 (2006).

[15] Chen, C. Y. & Shyu, A. B. Deadenylation and P-bodies. *Advances in experimental medicine and biology* **768**, 183-195, doi:10.1007/978-1-4614-5107-5_11 (2013).

[16] Franks, T. M. & Lykke-Andersen, J. The control of mRNA decapping and P-body formation. *Molecular cell* **32**, 605-615, doi:10.1016/j.molcel.2008.11.001 (2008).

[17] Teixeira, D., Sheth, U., Valencia-Sanchez, M. A., Brengues, M. & Parker, R. Processing bodies require RNA for assembly and contain nontranslating mRNAs. *RNA* **11**, 371-382, doi:10.1261/rna.7258505 (2005).

[18] Anderson, P. & Kedersha, N. Stress granules: the Tao of RNA triage. *Trends Biochem Sci* **33**, 141-150, doi:10.1016/j.tibs.2007.12.003 (2008).

[19] Parker, R. & Sheth, U. P bodies and the control of mRNA translation and degradation. *Molecular cell* **25**, 635-646, doi:10.1016/j.molcel.2007.02.011 (2007).

[20] Sheth, U. & Parker, R. Decapping and decay of messenger RNA occur in cytoplasmic processing bodies. *Science (New York, N.Y.)* **300**, 805-808, doi:10.1126/science.1082320 (2003).

[21] Stoecklin, G. & Kedersha, N. Relationship of GW/P-bodies with stress granules. *Advances in experimental medicine and biology* **768**, 197-211, doi:10.1007/978-1-4614-5107-5_12 (2013).

[22] Parker, R. & Song, H. The enzymes and control of eukaryotic mRNA turnover. *Nat Struct Mol Biol* **11**, 121-127, doi:10.1038/nsmb724 (2004).

[23] Coller, J. & Parker, R. Eukaryotic mRNA decapping. *Annu. Rev. Biochem.* **73**, 861-890, doi:10.1146/annurev.biochem.73.011303.074032 (2004).

[24] Meyer, S., Temme, C. & Wahle, E. Messenger RNA turnover in eukaryotes: pathways and enzymes. *Critical Reviews in Biochemistry and Molecular Biology* **39**, 197-216, doi:10.1080/10409230490513991 (2004).

[25] Chan, S. P. & Slack, F. J. microRNA-mediated silencing inside P-bodies. *RNA biology* **3**, 97-100 (2006).

[26] Brengues, M. & Parker, R. Accumulation of polyadenylated mRNA, Pab1p, eIF4E, and eIF4G with P-bodies in Saccharomyces cerevisiae. *Molecular biology of the cell* **18**, 2592-2602, doi:10.1091/mbc.E06-12-1149 (2007).

[27] Grousl, T. *et al.* Robust heat shock induces eIF2alpha-phosphorylation-independent assembly of stress granules containing eIF3 and 40S ribosomal subunits in budding yeast, Saccharomyces cerevisiae. *J Cell Sci* **122**, 2078-2088, doi:10.1242/jcs.045104 (2009).

[28] Beliakova-Bethell, N. *et al.* Virus-like particles of the Ty3 retrotransposon assemble in association with P-body components. *RNA* **12**, 94-101, doi:10.1261/rna.2264806 (2006).

[29] Checkley, M. A., Nagashima, K., Lockett, S. J., Nyswaner, K. M. & Garfinkel, D. J. P-body components are required for Ty1 retrotransposition during assembly of retrotransposition-competent virus-like particles. *Molecular and cellular biology* **30**, 382-398, doi:10.1128/mcb.00251-09 (2010).

[30] Larsen, L. S. *et al.* Ty3 nucleocapsid controls localization of particle assembly. *Journal of virology* **82**, 2501-2514, doi:10.1128/jvi.01814-07 (2008).

[31] Dutko, J. A., Kenny, A. E., Gamache, E. R. & Curcio, M. J. 5' to 3' mRNA decay factors colocalize with Ty1 gag and human APOBEC3G and promote Ty1 retrotransposition. *Journal of virology* **84**, 5052-5066, doi:10.1128/jvi.02477-09 (2010).

[32] Sandmeyer, S. B. & Clemens, K. A. Function of a retrotransposon nucleocapsid protein. *RNA biology* **7**, 642-654 (2010).

[33] Gimenez-Barcons, M. *et al.* The cellular decapping activators LSm1, Pat1, and Dhh1 control the ratio of subgenomic to genomic Flock House virus RNAs. *Journal of virology* **87**, 6192-6200, doi:10.1128/jvi.03327-12 (2013).

[34] Beckham, C. J. *et al.* Interactions between brome mosaic virus RNAs and cytoplasmic processing bodies. *Journal of virology* **81**, 9759-9768, doi:10.1128/jvi.00844-07 (2007).

[35] Lloyd, R. E. Regulation of stress granules and P-bodies during RNA virus infection. *Wiley interdisciplinary reviews. RNA* **4**, 317-331, doi:10.1002/wrna.1162 (2013).

[36] Reineke, L. C. & Lloyd, R. E. Diversion of stress granules and P-bodies during viral infection. *Virology* **436**, 255-267, doi:10.1016/j.virol.2012.11.017 (2013).

[37] Gaillard, H. & Aguilera, A. A novel class of mRNA-containing cytoplasmic granules are produced in response to UV-irradiation. *Molecular biology of the cell* **19**, 4980-4992, doi:10.1091/mbc.E08-02-0193 (2008).

[38] Iwaki, A. & Izawa, S. Acidic stress induces the formation of P-bodies, but not stress granules, with mild attenuation of bulk translation in Saccharomyces cerevisiae. *The Biochemical journal* **446**, 225-233, doi:10.1042/bj20120583 (2012).

[39] Tkach, J. M. *et al.* Dissecting DNA damage response pathways by analysing protein localization and abundance changes during DNA replication stress. *Nature cell biology* **14**, 966-976, doi:10.1038/ncb2549 (2012).

[40] Brengues, M., Teixeira, D. & Parker, R. Movement of eukaryotic mRNAs between polysomes and cytoplasmic processing bodies. *Science (New York, N.Y.)* **310**, 486-489, doi:10.1126/science.1115791 (2005).

[41] Ka, M., Park, Y. U. & Kim, J. The DEAD-box RNA helicase, Dhh1, functions in mating by regulating Ste12 translation in Saccharomyces cerevisiae. *Biochemical and biophysical research communications* **367**, 680-686, doi:10.1016/j.bbrc.2007.12.169 (2008).

[42] Ramachandran, V., Shah, K. H. & Herman, P. K. The cAMP-dependent protein kinase signaling pathway is a key regulator of P body foci formation. *Molecular cell* **43**, 973-981, doi:10.1016/j.molcel.2011.06.032 (2011).

[43] Tudisca, V. *et al.* Differential localization to cytoplasm, nucleus or P-bodies of yeast PKA subunits under different growth conditions. *European journal of cell biology* **89**, 339-348, doi:10.1016/j.ejcb.2009.08.005 (2010).

[44] Luo, G., Costanzo, M., Boone, C. & Dickson, R. C. Nutrients and the Pkh1/2 and Pkc1 protein kinases control mRNA decay and P-body assembly in yeast. *The Journal of biological chemistry* **286**, 8759-8770, doi:10.1074/jbc.M110.196030 (2011).

[45] Aizer, A. *et al.* The dynamics of mammalian P body transport, assembly, and disassembly in vivo. *Molecular biology of the cell* **19**, 4154-4166, doi:10.1091/mbc.E08-05-0513 (2008).

[46] Sweet, T. J., Boyer, B., Hu, W., Baker, K. E. & Coller, J. Microtubule disruption stimulates P-body formation. *RNA* **13**, 493-502, doi:10.1261/rna.355807 (2007).

[47] Loschi, M., Leishman, C. C., Berardone, N. & Boccaccio, G. L. Dynein and kinesin regulate stress-granule and P-body dynamics. *J Cell Sci* **122**, 3973-3982, doi:10.1242/jcs.051383 (2009).

[48] Chang, W. *et al.* Myo2p, a class V myosin in budding yeast, associates with a large ribonucleic acid-protein complex that contains mRNAs and subunits of the RNA-processing body. *RNA* **14**, 491-502, doi:10.1261/rna.665008 (2008).

[49] Lindsay, A. J. & McCaffrey, M. W. Myosin Va is required for P body but not stress granule formation. *The Journal of biological chemistry* **286**, 11519-11528, doi:10.1074/jbc.M110.182808 (2011).

[50] Decker, C. J., Teixeira, D. & Parker, R. Edc3p and a glutamine/asparagine-rich domain of Lsm4p function in processing body assembly in Saccharomyces cerevisiae. *The Journal of Cell Biology* **179**, 437-449, doi:10.1083/jcb.200704147 (2007).

[51] Eulalio, A., Behm-Ansmant, I., Schweizer, D. & Izaurralde, E. P-body formation is a consequence, not the cause, of RNA-mediated gene silencing. *Molecular and cellular biology* **27**, 3970-3981, doi:10.1128/mcb.00128-07 (2007).

[52] Bhattacharyya, S. N., Habermacher, R., Martine, U., Closs, E. I. & Filipowicz, W. Relief of microRNA-mediated translational repression in human cells subjected to stress. *Cell* **125**, 1111-1124, doi:10.1016/j.cell.2006.04.031 (2006).

[53] Lavut, A. & Raveh, D. Sequestration of highly expressed mRNAs in cytoplasmic granules, P-bodies, and stress granules enhances cell viability. *PLoS Genet* **8**, e1002527, doi:10.1371/journal.pgen.1002527 (2012).

[54] Stöhr, N. *et al.* ZBP1 regulates mRNA stability during cellular stress. *The Journal of Cell Biology* **175**, 527-534, doi:10.1083/jcb.200608071 (2006).

[55] Kedersha, N. & Anderson, P. Stress granules: sites of mRNA triage that regulate mRNA stability and translatability. *Biochem Soc Trans* **30**, 963-969, doi:10.1042/ (2002).

[56] Fenger-Gron, M., Fillman, C., Norrild, B. & Lykke-Andersen, J. Multiple processing body factors and the ARE binding protein TTP activate mRNA decapping. *Molecular cell* **20**, 905-915, doi:10.1016/j.molcel.2005.10.031 (2005).

[57] Jang, L., Buu, L. & Lee, F. J. Determinants of Rbp1p localization in specific cytoplasmic mRNA-processing foci, P-bodies. *The Journal of biological chemistry* **281**, 29379-29390, doi:10.1074/jbc.M601573200 (2006).

[58] Lee, S. *et al.* Learning a prior on regulatory potential from eQTL data. *PLoS Genet* **5**, e1000358, doi:10.1371/journal.pgen.1000358 (2009).

[59] Swisher, K. D. & Parker, R. Localization to, and effects of Pbp1, Pbp4, Lsm12, Dhh1, and Pab1 on stress granules in Saccharomyces cerevisiae. *PloS one* **5**, e10006, doi:10.1371/journal.pone.0010006 (2010).

[60] Balagopal, V. & Parker, R. Polysomes, P bodies and stress granules: states and fates of eukaryotic mRNAs. *Current Opinion in Cell Biology*, doi:10.1016/j.ceb.2009.03.005 (2009).

[61] Pospisek, M. & Valasek, L. Polysome profile analysis--yeast. *Methods in enzymology* **530**, 173-181, doi:10.1016/b978-0-12-420037-1.00009-9 (2013).

[62] Halbeisen, R. E., Scherrer, T. & Gerber, A. Affinity purification of ribosomes to access the translatome. *Methods (San Diego, Calif.)*, 1-5, doi:10.1016/j.ymeth.2009.04.003 (2009).

[63] Ingolia, N. T., Ghaemmaghami, S., Newman, J. R. & Weissman, J. S. Genome-wide analysis in vivo of translation with nucleotide resolution using ribosome profiling. *Science (New York, N.Y.)* **324**, 218-223, doi:10.1126/science.1168978 (2009).

[64] Ingolia, N. T., Lareau, L. F. & Weissman, J. S. Ribosome profiling of mouse embryonic stem cells reveals the complexity and dynamics of mammalian proteomes. *Cell* **147**, 789-802, doi:10.1016/j.cell.2011.10.002 (2011).

[65] Kanai, Y., Dohmae, N. & Hirokawa, N. Kinesin transports RNA: isolation and characterization of an RNA-transporting granule. *Neuron* **43**, 513-525, doi:10.1016/j.neuron.2004.07.022 (2004).

[66] Drummond, S. P. *et al.* Diauxic shift-dependent relocalization of decapping activators Dhh1 and Pat1 to polysomal complexes. *Nucleic acids research* **39**, 7764-7774, doi:10.1093/nar/gkr474 (2011).

[67] Bahassou-Benamri, R. *et al.* Subcellular localization and interaction network of the mRNA decay activator Pat1 upon UV stress. *Yeast (Chichester, England)* **30**, 353-363, doi:10.1002/yea.2968 (2013).

[68] Mitchell, S. F., Jain, S., She, M. & Parker, R. Global analysis of yeast mRNPs. *Nat Struct Mol Biol* **20**, 127-133, doi:10.1038/nsmb.2468 (2013).

[69] Kato, M. *et al.* Cell-free formation of RNA granules: low complexity sequence domains form dynamic fibers within hydrogels. *Cell* **149**, 753-767, doi:10.1016/j.cell.2012.04.017 (2012).

[70] Han, T. W. *et al.* Cell-free formation of RNA granules: bound RNAs identify features and components of cellular assemblies. *Cell* **149**, 768-779, doi:10.1016/j.cell.2012.04.016 (2012).

Chapter 2: Systems level analyses of the yeast P-body complex identify novel functional interactions

Gregory A. Cary[1,2], Dani B. N. Vinh[1], Patrick May[3], Rolf Kuestner[1], Young-Ah Goo[4], David R. Goodlett[4], Aimee M. Dudley[1]

[1]Institute for Systems Biology, Seattle WA

[2]Molecular and Cellular Biology Program, University of Washington, Seattle WA

[3]Luxembourg Centre for Systems Biomedicine

[4]Department of Pharmaceutical Sciences, University of Maryland, Baltimore, Maryland

Abstract

Cytoplasmic RNA granules are dynamic aggregates of non-translating RNA that are conserved across eukaryotic lineages. Given their central role in an array of post-transcriptional regulatory processes, there has been considerable interest in developing a better understanding of how these granules accumulate and which RNAs are targeted to these structures. With a few exceptions, most of what is known regarding RNA granule biology has been observed by genetic or cytological analyses. In this work we develop a method to enrich RNA granule complexes from yeast cells by immunoprecipiatation of the RNA granule protein Dhh1-GFP and demonstrate the specificity and integrity of these complexes by proteomic analyses. Despite their dynamic nature, we enrich the majority of the core processing body (PB) complex and show using quantitative mass spectrometry that these proteins reflect primarily *in vivo* interactions. We also examine the association of identified proteins under two different environmental conditions to examine the effect of stress induction on RNA granule assemblies. We detect an increased association of a number of metabolic enzymes and protein chaperones in the stress induced complex and go on to demonstrate that one of these chaperones, Ydj1p, is crucial for the induction of large cytoplasmic aggregates under stress conditions. Finally, we measure RNA associated with Dhh1-GFP and identify mitochondrially encoded catalytic RNAs as a class that is robustly enriched. In addition, we find that the mRNA for the core P-body component Pat1 is strongly and reproducibly enriched across all of our samples and we observe a small phenotypic benefit to the expression of the Pat1 mRNA that is not attributable to the

expression of the Pat1 protein. This work demonstrates the utility of global analysis of RNA granule complexes as we identify new components and reinforce previous functional associations.

Introduction

Post-transcriptional regulation of gene expression is critical to a variety of biological processes of interest[1,2,3,4,5]. Although there are many mechanisms by which expression is regulated post-transcriptionally, the association of transcripts with cytoplasmic RNA granules has emerged as a ubiquitous process central to the control of transcripts within the cell[6,7]. There are a variety of RNA granules, typically distinguished based on their associated proteins. For example, processing bodies (PB) are comprised of RNA decay enzymes and decay co-factors[8,9], whereas stress granules (SG) contain a variety of translation factors and ribosomal subunits[10,11,12]. RNA granules appear to be a location within the cell where non-translating mRNA accumulates[13]. Overexpression of the PB proteins Pat1[14] and Dhh1[15,16] is known to both repress translational activity and induce the accumulation of PB proteins into cytoplasmic foci[17,18]. Thus, a balance exists between translational activity and RNA granule accumulation. As translation is repressed (e.g. in response to stress), RNA granule proteins increasingly accumulate into large cytoplasmic aggregates containing translationally quiescent mRNP. Due to this relationship, there is considerable interest in defining the processes through which RNA granules accumulate and regulate the fates of constituent mRNPs.

Much of what is known about RNA granules is based on genetic and cytological observations of RNA granule proteins. However, several biochemical enrichments of RNA granules have been described, including the enrichment of neuronal RNA transport granules by affinity enrichment of a kinesin motor protein[19], immunoprecipitation of the core PB protein Dcp1[20], and enrichment of RNA granule proteins using the high stringency TAP system[21,22]. Recently work by Mitchell *et al.* identified transcripts associated with TAP-tagged PB proteins including Dhh1, Pat1, Lsm1, and Sbp1[23]. Finally, employing a remarkably different approach, Kato *et al.* precipitated both RNA granule proteins and RNA by treating cell lysates with the small molecule biotinylated isoxazole and characterized the protein requirements for this association[24]. To date there has not been a method described to specifically enrich RNA granule complexes that explores both the protein and RNA constituents.

Here, we describe a method developed to specifically enrich RNA granule proteins from yeast lysate based on their physical association with the known PB component, Dhh1. The identity of the co-precipitating proteins, determined by tandem mass spectrometry, supports the specific enrichment of RNA granules. We use this approach to compare RNA granules isolated from yeast cells in both uninduced and stress induced conditions. By comparing the conditional enrichments of constituent proteins, we identify proteins within the complex that are involved in the aggregation into large cytoplasmic foci and confirm this effect experimentally. We also identify co-enriched RNA transcripts. We reproducibly identify several classes of catalytic RNAs encoded by the mitochondrial genome that had not previously been shown to

physically interact with PB. Finally, we identify a phenotypic benefit of Pat1 RNA that is separable from the Pat1 protein, which suggests a potential functional role for this transcript.

Methods

Yeast strains, PB induction & fast filtering

Yeast strains used in this study [Table 2.1] are isogenic to FY4[25]. Plasmids indicated are from the molecular barcoded yeast ORF (MoBY) plasmid library (ThermoScientific)[26]. All media and manipulation of yeast was performed as described[27]. For immunoprecipitation experiments, strains harboring a Dhh1-GFP fusion protein were used. Overnight cultures were diluted into 200 ml fresh medium and grown to OD 2.0. Additional media was then added to dilute the cultures to OD 0.2 in 2 L YPD. These cultures were grown for approximately 3 doublings to O.D. 1.0, at which point the cells were collected by filtration (Millipore Nitocellulose Membrane Filter Type: 0.65µm DAWP #DAWP09025), re-suspended from the filter into 50 ml conical tubes containing 20 ml of the same growth medium, and pelleted for 3 minutes at 3000 x g. Cell pellets were then frozen in liquid nitrogen (+Glu, YPD samples, PB uninduced), or rinsed in YEP medium lacking glucose, pelleted again and resuspended into 2 L of YEP for induction. Induction was allowed to proceed for 30 minutes, at which point cells were filtered, and cell pellets were frozen as above (-Glu, YEP samples, PB induced). For SILAC cultures, synthetic complete (SC) media lacking lysine and arginine amino acids was used. To this media, we added heavy labeled arginine (^{13}C6-^{15}N4) and lysine (^{13}C6-^{15}N2). The BY4741 strain was grown in SCD (2% glucose) media to a

Table 2.1 *S. cerevisiae* strains used in this study.

Strain	Genotype	Reference
YAD1	MATa *his3Δ1 leu2Δ0 met15Δ0 ura3Δ0*	[25]
YAD49	MATa *his3Δ1 leu2Δ0 met15Δ0 ura3Δ0* DHH1-GFP::HIS3MX6	[28]
YAD50	MATa *his3Δ1 leu2Δ0 met15Δ0 ura3Δ0* EDC3-GFP::HIS3MX6	[28]
YAD52	MATa *his3Δ1 leu2Δ0 met15Δ0 ura3Δ0* LSM1-GFP::HIS3MX6	[28]
YAD53	MATa *his3Δ1 leu2Δ0 met15Δ0 ura3Δ0* PAT1-GFP::HIS3MX6	[28]
GC01	MATa *his3Δ1 leu2Δ0 met15Δ0 ura3Δ0* DHH1-GFP::HIS3MX6 *ydj1Δ::kanMX*	This study
GC02	MATa *his3Δ1 leu2Δ0 met15Δ0 ura3Δ0* DHH1-GFP::HIS3MX6 *hsp104Δ::kanMX*	This study
GC03	MATa *his3Δ1 leu2Δ0 met15Δ0 ura3Δ0* DHH1-GFP::HIS3MX6 *ssa1Δ::kanMX*	This study
GC04	MATa *his3Δ1 leu2Δ0 met15Δ0 ura3Δ0* DHH1-GFP::HIS3MX6 *ssa2Δ::kanMX*	This study
GC05	MATa *his3Δ1 leu2Δ0 met15Δ0 ura3Δ0* DHH1-GFP::HIS3MX6 *hsp82Δ::kanMX*	This study
GC06	MATa *his3Δ1 leu2Δ0 met15Δ0 ura3Δ0* DHH1-GFP::HIS3MX6 *hsc82Δ::kanMX*	This study
GC07	MATa *his3Δ1 leu2Δ0 met15Δ0 ura3Δ0* LSM1-GFP::HIS3MX6 *ydj1Δ::kanMX*	This study
GC08	MATa *his3Δ1 leu2Δ0 met15Δ0 ura3Δ0* EDC3-GFP::HIS3MX6 *ydj1Δ::kanMX*	This study
GC09	MATa *his3Δ1 leu2Δ0 met15Δ0 ura3Δ0* DHH1-GFP::HIS3MX6 *ydj1Δ::kanMX* + MoBY-YDJ1	This study
GC10	MATa *his3Δ1 leu2Δ0 met15Δ0 ura3Δ0* DHH1-GFP::HIS3MX6 *ydj1Δ::kanMX* + MoBY-SIS1	This study
GC11	MATa *his3Δ1 leu2Δ0 met15Δ0 ura3Δ0* DHH1-GFP::HIS3MX6 *ydj1Δ::kanMX* + MoBY-HSP104	This study
GC12	MATa *his3Δ1 leu2Δ0 met15Δ0 ura3Δ0* DHH1-GFP::HIS3MX6 *ydj1Δ::kanMX* + MoBY-SSA1	This study
GC13	MATa *his3Δ1 leu2Δ0 met15Δ0 ura3Δ0* DHH1-GFP::HIS3MX6 *ydj1Δ::kanMX* + MoBY-SSA2	This study
GC14	MATa *his3Δ1 leu2Δ0 met15Δ0 ura3Δ0* DHH1-GFP::HIS3MX6 *ydj1Δ::kanMX* + MoBY-HSP82	This study
GC15	MATa *his3Δ1 leu2Δ0 met15Δ0 ura3Δ0* DHH1-GFP::HIS3MX6 *ydj1Δ::kanMX* + MoBY-HSC82	This study
DV100	MATa *his3Δ1 leu2Δ0 met15Δ0 ura3Δ0 pat1Δ::URA3-GFP*::HIS3MX6	This study
DV110	MATa *his3Δ1 leu2Δ0 met15Δ0 ura3Δ0* PAT1-STOP-GFP::HIS3MX6	This study

density of OD 1. This culture was then diluted 1:500 to OD ~ 0.002 into SCD containing the heavy amino acids. These cultures were allowed to grow for a total of 9 doublings, to OD ~1.2, at which point the cells were filtered, pelleted and frozen as above.

For assessment of PB induction in other strains, cells were grown to mid-log phase (OD ~ 0.7) and pelleted by centrifugation 5 minutes at 3000 x g. Cell pellets were washed in YEP media lacking glucose and resuspended in YEP. Cells were induced in YEP media for 30 minutes. Induced cells were fixed in 3.7% formaldehyde in PBS for 2 minutes at room temperature, followed by a 10-minute incubation in PBS on ice.

Microscopy

The induction of PB proteins was checked prior to lysis by fixing a small aliquot of both the uninduced and the induced 2 L culture and examining aggregation status of Dhh1-GFP by microscopy. In addition, a small amount of the cell pellet from the uninduced condition was fixed and examined for induction to verify that the collection of cells had not induced PB aggregates. Fixed cells were imaged using a DeltaVision deconvolution imaging system (Applied Precision, Issaquah, WA) outfitted with an Olympus IX-71 wide field microscope. Cells were imaged with a PlanApo 60x oil objective (N.A. 1.42) using differential interference contrast (DIC) bright field illumination and a 250W xenon LED transillumination light source. For GFP fluorescence imaging a polychroic beam splitter was used along with excitation 490/20 and emission 528/38 bandpass filters. A set of up to 30, 0.2 micron z-sections were captured for each image, deconvolved, and exported as tiff files. Tiff files were imported into ImageJ to generate image stacks and image levels were adjusted to be identical across all images and z-stack projections were made

Cryolysis and anti-GFP IP

Cell pellets stored at -80º C were released into a pre-cooled Retsch PM-100 planetary ball mill grinding jar. Grinding was performed at 600 rpm in 2-minute cycles with rotation reversal at 1 minute. Jars were re-chilled in liquid nitrogen between grinding cycles. Samples were ground until >90% lysis was achieved, as assessed by microscopic examination, which typically occurred after 5 to 10 cycles of grinding. Cell powder was then collected and returned to -80º C for storage.

Cell powder was resuspended in 1.5 volumes cold buffer consisting of 30 mM K-Hepes (pH 7.4), 150 mM KCl, 2 mM $MgCl_2$, 0.1% Tw20, 0.2% NP-40, 1 mM DTT, 1/100 dilution of protease inhibitor (Sigma) and 1/1000 dilution RNase-In (Ambion / Millipore). The resuspended powder was then briefly pre-cleared by centrifugation 5 minutes at 3000 x g and 4º C. The supernatant from this spin was then added to protein G beads that had previously been cross-linked with Roche anti-GFP. Crosslinking was performed using 20 mM dimethyl pimelimidate. Lysate and antibody-linked beads were incubated for 30 minutes at 4º C with constant rotation. The beads were then collected by magnetic separation and washed twice with IP buffer. The beads were then divided for elution of protein and RNA: 88% of the beads were used to elute protein and 12% were used to elute RNA. For elution of protein, a solution of 0.1% SDS in 30 mM Hepes (pH 7.4) was added to the bead pellet and incubated for 10 minutes at 60º C. The beads were then pelleted again, and the supernant was collected as the IP fraction. For elution of RNA beads were resuspended in 200 µl TES (10 mM Tris (pH 7.5), 1 mM EDTA, 0.5% SDS) and an equal volume of acid phenol was added. Phenol:chloroform extraction was performed and the extracted aqueous phase

was precipitated with cold ethanol. Washed ethanol pellets were resuspended in 30 µl TE and stored at -80º C.

For I-DIRT immunoprecipitations, cell powder from heavy BY and light Dhh1-GFP were resuspended and pre-cleared as described above. Protein concentration of the suspended lysates was quantitated using the BCA protein assay (Pierce) and lysates were mixed in a 1:1 ratio based on protein concentration. The immunoprecipitation was performed as described above, although no RNA was eluted from these preparations.

Proteomics

A small amount of protein eluted from beads was measured by western blot (Clontech monoclonal anti-GFP JL-8, Cat# 632381) to demonstrate immuno-enrichment and silver stain gel (Pierce Silver Stain for Mass Spectrometry, Cat# 24600) to test for IP-specific bands. IP fractions were reduced, alkylated, and trypsinized *in solution* using an established SDS/Urea-based denaturing protocol[29]. Tryptic digestions were acidified and desalted by UltraMicroSpin Vydac C18 silica column (Nest Group, Inc) following manufacture's specifications. Digested and cleaned samples were submitted to the University of Washington School of Pharmacy Mass Spectrometry Facility for tandem mass spectrometry analysis by LTQ-Velos or LTQ-Orbitrap.

Tandem mass spectra were converted to universal mzXML file format and searched against a database consisting of translation of all known yeast open reading frames (SGD), know contaminant proteins, and a decoy library prepared by randomization of the library using a perl script available from the Matrix Science

website (http://www.matrixscience.com/help/decoy_help.html). Searches were performed using X!Tandem[30] with the following parameters: tolerable tryptic termini = 1; identifications based on b- and y-ions; parent mass tolerance = 3.00; fixed modifications include carboxyamidomethylation of cysteine (57.02); variable modifications include oxidation of methionine (15.99). Tandem mass spectra peptide assignments were validated by PeptideProphet[31] and protein assignments validated by Protein Prophet[32], available in the current TPP distribution (http://tools.proteomecenter.org/wiki/index.php?title=Software:TPP). Protein probabilities yielding a 0.05 FPR threshold were applied to the resulting protein lists and lists were filtered to exclude proteins identified in any experiment with fewer than two unique peptides. Only proteins identified in at least two independent IP samples were considered in the final filtered list. Gene ontology (GO) category enrichments for detected proteins were assessed using the YeastMine toolset available from the SGD website (http://yeastmine.yeastgenome.org/yeastmine/). All reported p-values have been corrected for multiple hypothesis testing using Benjamini Hochberg.

For spectral count quantitation experiments, paired –Glu and +Glu samples were analyzed using the same mass spectrometer on the same day and two technical replicate injections were performed of each sample to assess reproducibility of spectral count numbers. Tandem mass spectral counts for each protein were normalized using the APEX program[33,34] (version 1.1.0) available from the JCVI website (http://pfgrc.jcvi.org/index.php/bioinformatics/apex.html). Briefly, estimated observability scores for the yeast proteome were downloaded and input into the program along with the prot.xml files output by the TPP. APEX normalization was then

performed for all proteins lower than the 0.05 FPR threshold. The APEX-normalized value for each protein within a sample was further normalized to the normalized value for Dhh1 in that sample.

The mass spectrometry data from the I-DIRT IP samples were analyzed using a similar approach as described above with the following important differences. Database searches were performed including the following variable modifications: SILAC heavy arginine: $^{13}C6$-$^{15}N4$ (10.01), and SILAC heavy lysine: $^{13}C6$-$^{15}N2$ (8.01). Following assessment of peptide and protein identifications by PeptideProphet and Protein Prophet, quantitative SILAC ratios for proteins were determined using XPRESS software[35]. Precursor ion elution profiles of heavy vs. light peptides were determined with a mass tolerance of 0.05 (>5s) and the area under the curve (AUC) was used to determine a SILAC ratio for each peptide.

Microarray

Acid phenol extracted, ethanol precipitated RNA was prepared from input and bead fractions. 5 µg input RNA and 200 ng IP RNA were fragmented and hybridized to a custom Agilent microarray per manufacturer's directions. The array was subsequently washed and incubated with the S9.6 antibody (ATCC clone hb-8730) and Cy3 labeled anti-mouse antibody as described[36]. Following the final antibody wash, slides were dried by brief low speed (600 rpm) centrifugation and immediately scanned and feature extraction was performed using an Agilent G2565CA Microarray Scanner and control software. The antibody approach produced background signal that was not well estimated by the feature background. To remove this background, signal from array features that do not hybridize to any yeast transcripts was measured and

subtracted. Background subtracted signal was log transformed, pairs of Input and IP arrays were normalized by cyclic loess implemented in the limma Bioconductor package[37], and transcript replicate probes were averaged. Finally, we applied a threshold to remove transcripts that exhibited low abundance and high variability or that were saturated on the total RNA array.

Growth Assays

For liquid growth assays, strains were grown overnight and diluted into fresh YPD the following day. Cells were grown for 2-3 doublings at which point cells were counted and cells were resuspended in either YPD media or YPD media containing 0.18 µg/ml cycloheximide at a cell concentration of 3,333 cells/ml. 150 µl of these cell suspensions, corresponding to 500 cells, was added to each well of a tissue culture treated, flat bottomed, 96-well plate. There were at least five biological replicates performed for each mutant and Pat-STOP strain background. Plates were sealed with sterile, gas-permeable, optical adhesive sealing film for microplates and incubated in a Sunrise 96-well optical plate reader (Tecan Austria GmbH, Austria) controlled by the Tecan Magellan v6.55 software. Cells were grown at 30º C with continuous shaking. Prior to reading, the plate was subjected to 15 seconds of high intensity shaking, and the OD_{600} was read using the Tecan accuracy method. Growth was measured for 4-5 days or until the OD of the wells exhibiting growth had plateaued.

The amount of time in lag phase was estimated for each well by calculating the timepoint at which each well surpassed 25% of the OD in the media-specific blank well. For each strain, the amount of time in lag for YPD was subtracted from the amount of

time in lag for the YPD media containing cycloheximide to generate a relative lag time for each replicate.

Results

Enrichment Strategy

We used an immunoprecipitation (IP) strategy to enrich RNA granule components from yeast cell lysate. The enrichment protocol was designed to minimize the experimental impacts on the dynamic nature RNA granule aggregates. We used GFP as an affinity tag in order to assess the induction state of granules *in vivo* prior to IP[38]. Cells were collected from culture using rapid filtration instead of centrifugation because in early tests we determined that pelleting cells by centrifugation slightly induced aggregation of a PB protein in an otherwise uninduced culture, while filtration minimized this effect [*data not shown*]. Cell pellets were frozen in liquid nitrogen and remained frozen throughout lysis by cryolysing cells in a planetary ball mill[39]. Finally, immunoprecipitations were performed rapidly using high affinity anti-GFP antibodies pre-conjugated to magnetic beads.

Employing this approach, we enriched GFP tagged Dhh1 and Edc3, two core components of PB, from cells that were induced to form PB foci by 30 minutes of glucose starvation [FIG 2.1A]. Western blot confirmed the depletion of GFP from the unbound fractions and enrichment in the IP fractions for both proteins [FIG 2.1B], and silver stains of the IP fractions revealed an intense band of the appropriate size for each bait protein along with many other IP-specific bands not detectable in a negative

control IP from a lysate containing no GFP [FIG 2.1C]. To identify the proteins co-precipitating with each bait protein, the IP fractions were trypsinized and subjected to tandem mass spectrometry. While both proteins co-immunoprecipitated with several known RNA granule proteins, the Dhh1-GFP complex enriched more of the core PB proteins. Several components of the Lsm1-7 heptamer were not identified in the Edc3-GFP complex, and while Dhh1p, Pat1p, and Xrn1p were identified in the Edc3-GFP complex, they were all detected more abundantly in the Dhh1-GFP complex [FIG 2.1D]. For example, using total independent spectra as a proxy for protein abundance within the preparation, eight of the top ten proteins identified by the Dhh1-GFP IP are known RNA granule components whereas the top ten most abundant proteins in the Edc3-GFP IP contain only three known RNA granule proteins. Because the Dhh1-GFP IP enriched more of the core PB components, we restricted our analyses of RNA granule enrichments to the Dhh1-GFP complex.

Proteomic Analysis Of Dhh1-GFP Complex

Five Dhh1-GFP IP samples were analyzed, including two preparations from cells in which PB were not induced (+Glu) and three preparations from cells in which PB were induced to form foci by removal of glucose from the growth media for 30 minutes prior to harvesting (-Glu). Co-precipitating proteins were identified by tandem mass spectrometry followed by database searching and analysis of matched spectra using the Trans-Proteomic Pipeline (TPP). The list of proteins was filtered further to only include proteins identified in any experiment with more than two unique peptides and proteins identified in at least two replicate experimental preparations. This filtering

yielded a list of 332 proteins reproducibly enriched by our Dhh1-GFP IP. To compare the proteins enriched from the uninduced and PB induced conditions, +Glu and -Glu samples were paired and run on the mass spectrometer on the same day with two replicate injections per sample. Tandem mass spectral counts were normalized using the APEX program and we further normalized the APEX score for each protein to the APEX score for Dhh1p in each IP. Normalized spectral counts for each pair of samples was then used to generate a ratio of abundance in the –Glu sample relative to the +Glu sample. Of the 332 proteins in our list, 71 proteins were consistently more abundant in the +Glu condition, 71 proteins were consistently more abundant in the –Glu condition, 101 proteins had contradicting ratios indicating higher abundance in the opposite condition for each replicate, and the remaining 80 proteins were only identified in one of our two replicate spectral counting experiments [FIG 2.2B].

The enriched proteins show statistically significant gene ontology (GO) category enrichment ($p < 1x10^{-8}$) for ribosomal proteins, proteins involved in translation, and RNP granule proteins including components of both cytoplasmic processing bodies and cytoplasmic stress granules [FIG 2.2A]. Many of the core PB components are identified in the Dhh1 complex including the Xrn1p exonuclease, members of the decapping complex including Dcp2p, Dcp1p and Edc3p, as well as the translational repressor and decapping activator Pat1p along with the Lsm1-7p heptamer. Importantly Lsm8p, which forms a nuclear complex with the Lsm2-7 proteins, was not detected in any of our experiments indicating the preferential enrichment of the cytoplasmic Lsm complex. Several core components of PB were not identified in any

of our experiments. Except for Cdc39p, none of the Ccr4/Pop2/Not1-5 deadenylation complex is identified and the core component Scd6p is also absent. In addition to the core components, several PB accessory proteins are identified, including Edc1p, Sbp1p, and proteins involved in nonsense mediated decay Nam7p, Dbp2p, and Ebs1p. There are also a several stress granule components identified including Pab1p, Lsm12p, Pbp1p, Pbp4p and a number of translation factors that are known to co-localize with stress granule foci *in vivo*. The association of ribosomal subunits with the Dhh1-GFP complex is consistent with previous results showing that ribosomal subunits co-purify with Dhh1 by stringent TAP purification[21], Dhh1 co-sediments with polyribosomes on sucrose density gradients[40], PB are observed in close proximity to ribosomes *in vivo*[41], and Dhh1 co-localizes with stress granules, which contain small ribosomal subunits and other translation factors, *in vivo*[42]. The number and abundance of RNA granule proteins identified indicates that IP of Dhh1-GFP enriches RNA granule proteins. Intriguingly, when we compared the normalized spectral counts for the 22 RNA granule proteins identified in both of the spectral count replicates, only 2 proteins, Pbp1p and Lsm5p, were reproducibly more abundant in the –Glu sample, whereas 13 proteins, including many of the core PB proteins, were reproducibly more abundant in the +Glu samples [FIG 2.2B]. This result supports the hypothesis that the core PB proteins form a complex *in vivo* even when they are not detectable as foci microscopically.

In order to assess the specificity of the purification, we performed two SILAC based I-DIRT experiments in which cell lysate from Dhh1-GFP cells induced to form PB

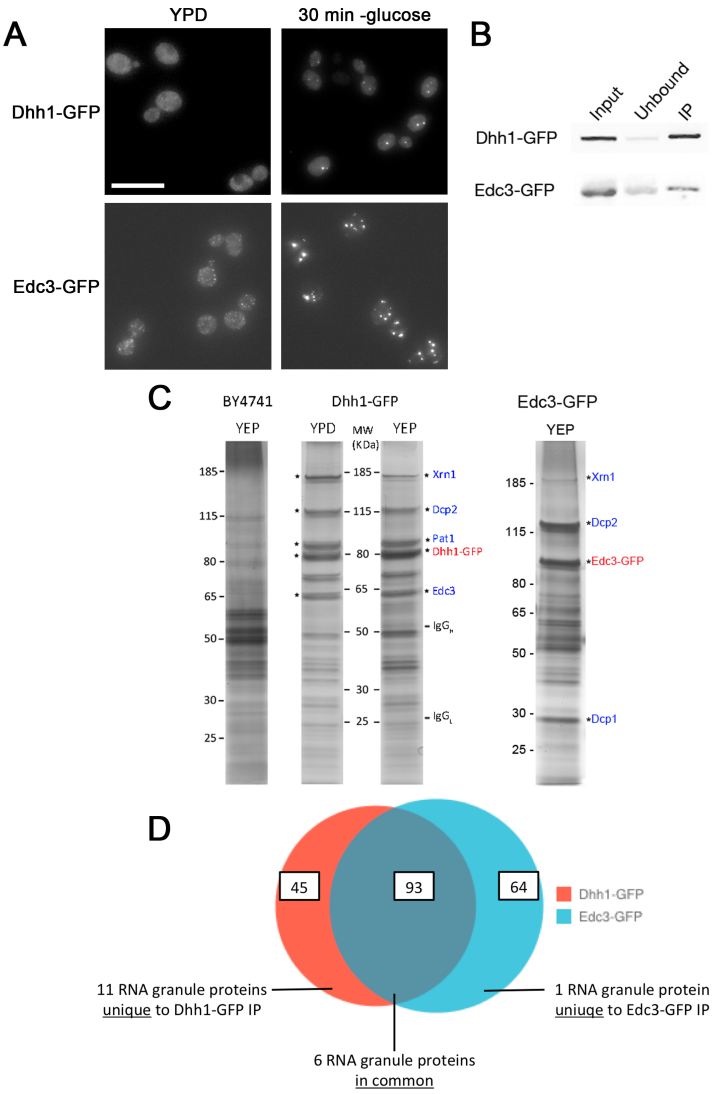

Figure 2.1 Enrichment of yeast P-body proteins.
(A) Induction of yeast P-body protein aggregates by 30 minutes of glucose starvation. Scale bar = 10 μm. (B) Anti-GFP western blot of Dhh1-GFP and Edc3-GFP IP. Equivalent volumes of the input and the undbound fractions are loaded to demonstrate IP depletion of the GFP tagged protein. (C) Silver stain gel of IP fractions from Dhh1-GFP from P-body induced (YEP) and P-body uninduced (YPD) states and Edc3-GFP in the induced state. IP fractions from BY4741 strain are shown as a negative control. Gel lanes are labeled with bait proteins (red) and co-precipitating proteins (blue) identified by tandem mass spectrometry, appropriate molecular weight, and tandem mass spectral count abundance. (E) Overlap of proteins identified by Dhh1-GFP and Edc3-GFP IP. Numbers of total proteins identified in each category (i.e. unique to Dhh1, unique to Edc3, or common to both) are indicated in white boxes. Numbers of RNA granule proteins identified in each IP or in common between the two indicated by the text.

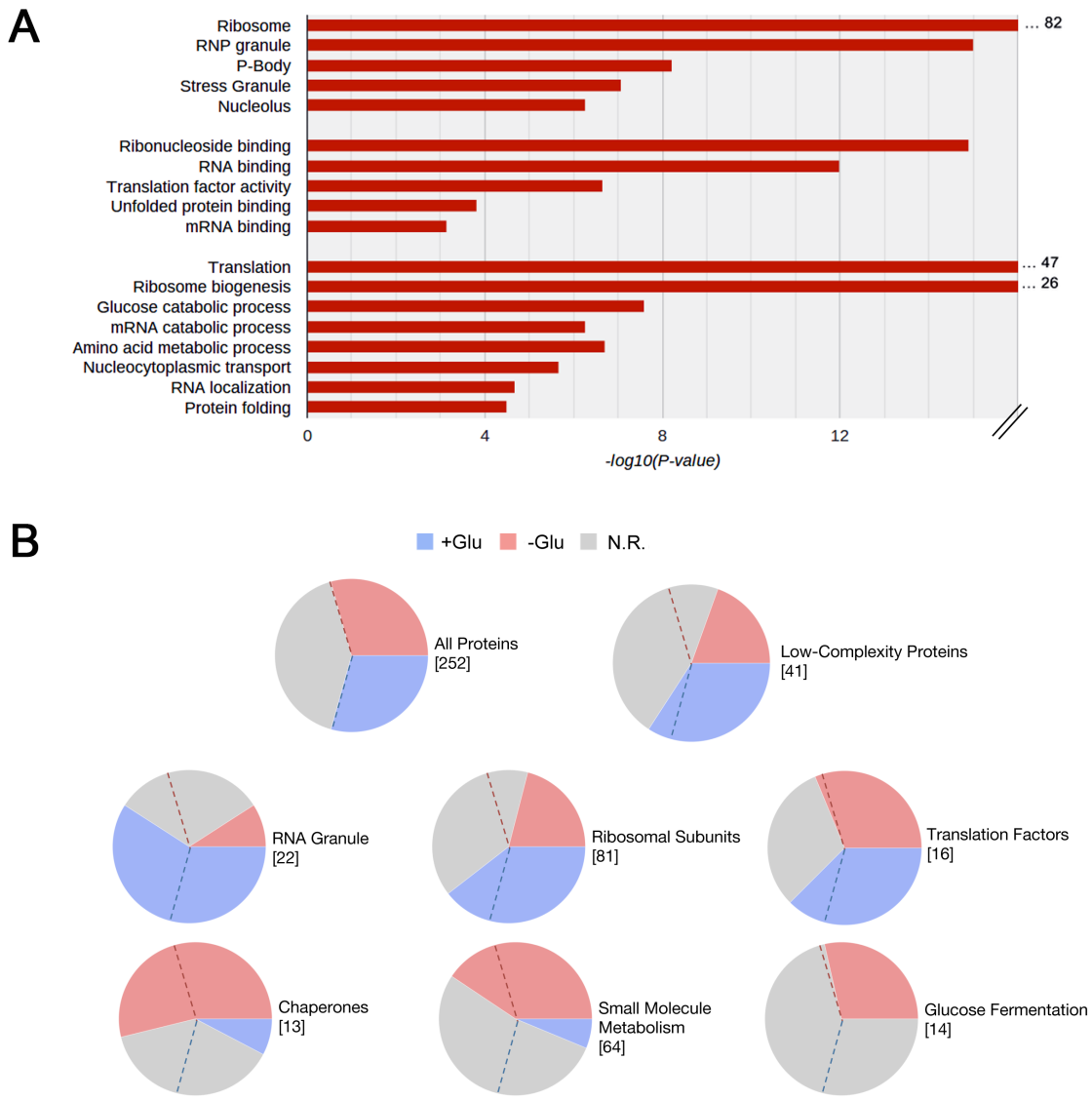

Figure 2.2 Proteomic analysis of Dhh1-GFP IP.

(A) Gene ontology category enrichments from the proteins identified in the Dhh1-GFP IP filtered list. The x-axis is the Benjamini-Hochberg corrected P-value for the enrichment expressed on a -log scale. The axis has been truncated and, where indicated, p-values that are larger than the displayed axis are reported. (B) Conditional enrichment of protein classes showing the proportion of proteins reproducibly more abundant in normal glucose (blue), glucose depletion (red) or no agreement between replicates (grey). In each case, the dotted lines represent the relative proportions in each condition for all proteins. Total number of proteins measured in each category reported in square brackets.

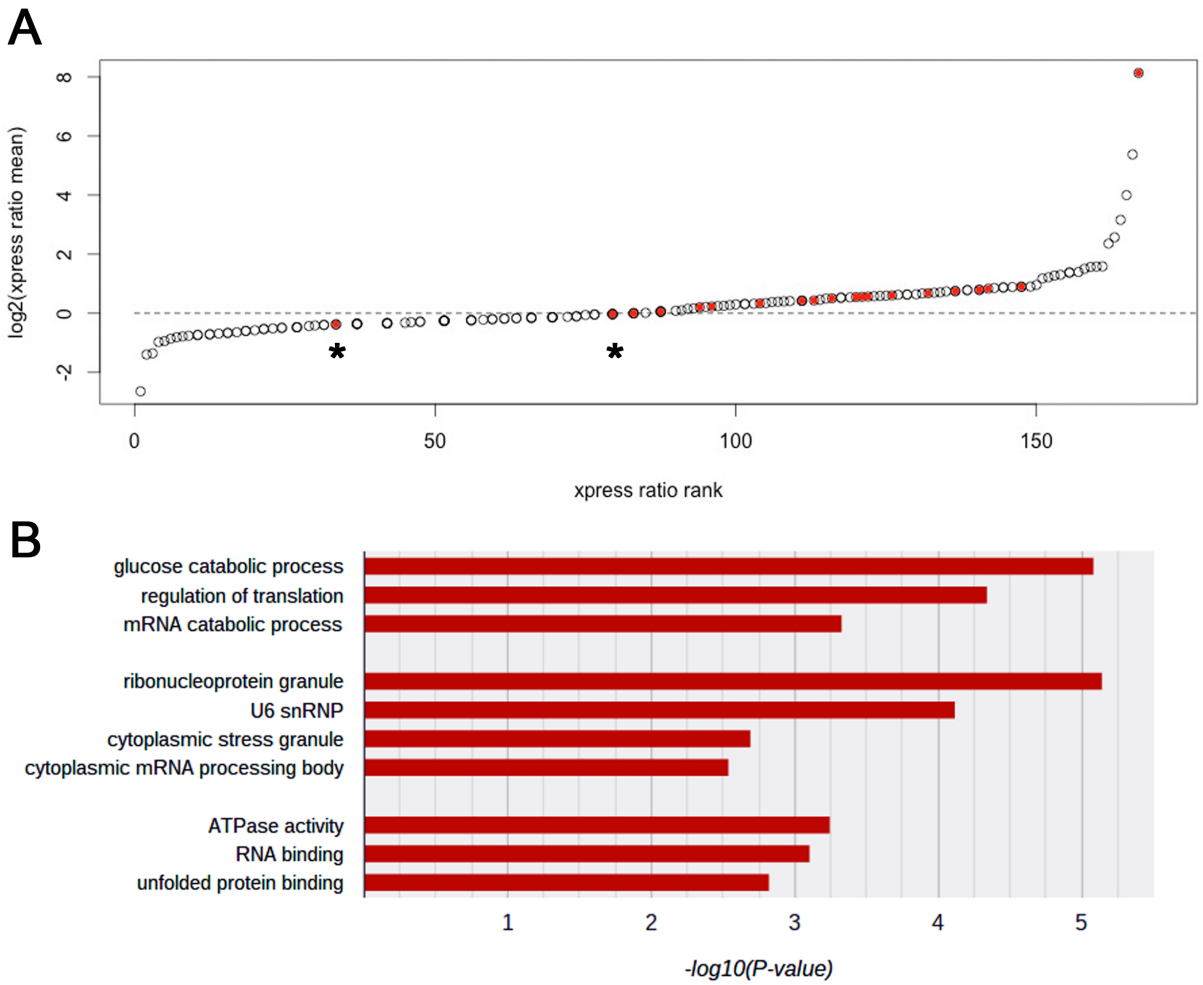

Figure 2.3 I-DIRT results identify Dhh1-GFP IP.

(A) Specificity of RNA granule proteins as demonstrated by I-DIRT data. The log-transformed average ratio of light:heavy for all proteins identified in a sample plotted against the rank of the ratio. Known RNA granule proteins are colored in red. The dotted line corresponds to a 50:50 ratio of light:heavy peptides for given proteins. Two known RNA granule proteins that fall below this threshold - Dcp2p and Dcp1p - are marked with an asterisk. The remaining 11 proteins are all identified with predominantly light peptides. (B) Gene ontology enrichments for the 45 proteins reproducibly identified with predominantly light peptides in both I-DIRT replicate experiments. The x-axis is the Benjamini-Hochberg corrected P-value for the enrichment expressed on a -log scale.every sample tested. Such a result is consistent with a highly dynamic *in vitro* exchange occurring once the two lysates are mixed. This hypothesis is consistent with a result from mammalian cell culture, in which a Dcp1 homolog (Dcp1a) exhibits highly dynamic exchange with PB *in vivo*, recovering from a photobleach to equilibrium levels in under 1 minute[43].

but grown in standard media was mixed 1:1 with lysate from cells not expressing any GFP and grown in isotopically heavy media, and immunoprecipiating proteins were identified by tandem mass spectrometry. Using this approach, proteins that are identified with a predominance of heavy labeled peptides must have interacted with Dhh1-GFP *in vitro*, either as a contaminant or as a dynamical *in vitro* interactor[44]. We found that 11 of the 13 core PB proteins measured in these experiments have a predominantly light I-DIRT ratio, indicating specific *in vivo* interaction, in at least one of our two replicate experiments [FIG 2.3A]. Two core proteins, Dcp1p and Dcp2p, have reproducibly high ratios of heavy labeled peptides. These two proteins are known core components of PB and each protein is identified by tens to hundreds of peptides in

Thus, while we have taken many steps to limit the dynamic exchange between the Dhh1-GFP complex and the lysate, some proteins are still rapidly cycling into the complex *in vitro*. Because of this, we have elected not to use the I-DIRT data as an indication of non-specific interactions, as proteins with predominantly heavy I-DIRT ratios may simply highlight dynamic interactors. Instead, for proteins with light I-DIRT ratios, we interpret the abundance of light peptides as additional evidence that these proteins interact with Dhh1-GFP *in vivo*. There are 45 proteins in our list that have reproducibly light:heavy I-DIRT ratios. The top ontology enrichments for these proteins are for ribonucleoprotein granule components, glucose catabolism, and regulation of translation [FIG 2.3B].

Metabolic Enzymes Enriched With Dhh1-GFP

Metabolic enzymes from a variety of biochemical pathways are reproducibly enriched in the Dhh1-GFP IP. The reproducibly light proteins in the Dhh1-GFP complex measured by the I-DIRT experiment are significantly enriched for proteins involved in the catabolism of glucose (8 proteins, $p = 8.2x10^{-6}$) [FIG 2.3B], indicating that these proteins interact with Dhh1-GFP *in vivo*. 15 proteins identified in the IP overall are components of the glucose fermentation pathway, and none of these proteins are reproducibly more abundant in the uninduced sample while 4 proteins are reproducibly more abundant in the PB induced sample [FIG 2.2B]. In addition, of the 89 proteins annotated as being involved in small molecule metabolic processes, only 4 proteins are reproducibly more abundant in the uninduced condition whereas 26 proteins are reproducibly more abundant in the induced condition [FIG 2.2B]. This indicates that these enzymes are generally more associated with Dhh1 in the condition when PB are induced by glucose depletion. Other groups have reported that many enzymes have specific RNA binding capacity and reproducibly associate with the same transcripts[45]. In addition, Narayanaswamy *et al.*[46] observed that many metabolic enzymes assemble into cytoplasmic foci when cells are limited for various nutrients. They also demonstrated that many enzymes can transition from insoluble to soluble fractions of the cell lysate upon readdition of nutrients. We found a significant overlap between the proteins in the Dhh1-GFP complex and both proteins that were observed to form cytoplasmic foci ($p = 9.5x10^{-16}$) as well as proteins that reversibly transition between insoluble and soluble phases ($p = 4.7x10^{-37}$). These results support a specific interaction between RNA granule complexes and enzymes of metabolism that have the capacity to reversibly assemble into cytoplasmic foci.

Proteins With Low-Complexity Domains Enriched In Dhh1-GFP Complex

Recent reports have identified low-complexity regions within RNA granule proteins and demonstrated the importance of these regions on RNA granule protein aggregation and retention of RNA[24,47]. We tested the proteins in the Dhh1-GFP complex for the presence low-complexity domains. We applied two orthogonal approaches to identify yeast proteins containing low-complexity regions. First, we searched the yeast proteome for low-complexity (LC) sequences using the SEG algorithm. We found 390 proteins that contain an LC region of at least 35 residues. Second, we used the set of putative prion proteins predicted by Alberti *et al*.[48] who used a hidden-markov model approach to predict proteins containing putative prionogenic sequence. The authors identified 178 candidate proteins with potential prion domains and went on to validate many of the top 100 using various criteria commonly ascribed to prion proteins including ability to form foci *in vivo*, ability to form SDS-resistant aggregates, and ability to seed prion aggregation *in vitro*. The proteins within these lists are enriched for GO categories associated with RNP granules, among others. Importantly, these two lists share 72 proteins in common which is significant using a hypergeometric test ($p=1x10^{-44}$) which indicates that both sets of proteins are identifying common features within the proteome, although searching utilizing distinct algorithmic approaches.

Of the 390 yeast proteins that contain LC regions predicted by SEG, we identify 43 that co-precipitate with Dhh1-GFP ($p=8.98x10^{-8}$). Of the 178 proteins predicted to contain putative prion domains, 29 co-precipitate with Dhh1-GFP ($p=6.26x10^{-9}$). In all,

56 of the proteins co-enriching with Dhh1-GFP contain predicted regions of low complexity by at least one of these two measures. 31 proteins in the disordered set are measured at least once in the I-DIRT experiments and 24 of these were measured with predominantly light peptides in at least one experimental replicate, which indicates that most of the predicted LC proteins interact with Dhh1-GFP *in vivo*. There is no strong condition specificity to the interaction of LC proteins as 14 of the 56 LC proteins are reproducibly more abundant in the +Glu samples, whereas 8 proteins are reproducibly more abundant in the -Glu samples [FIG 2.2B]. Of these 56 proteins, 27 are annotated as being components of a RNP complex ($p=4.05x10^{-10}$) and 39 are annotated in nucleic acid metabolic processes ($p=6.25x10^{-8}$). These results demonstrate that proteins containing LC regions are enriched within yeast RNA granules and therefore represent a common feature of RNA granule components across eukaryotes.

Chaperones Enriched With Dhh1-GFP Involved In PB Induction

We identify 18 chaperone proteins in the Dhh1-GFP complex, including 7 members of the Hsp70 family, 2 members of the Hsp40 family, one or both of the practically indistinguishable yeast Hsp90 proteins, and 3 members of the CCT/TRiC chaperonin complex. Seven of these proteins interact *in vivo* based on our I-DIRT results [FIG 2.3B]. Additionally, seven of the identified chaperones are reproducibly more abundant in the PB induced samples while only Cct8p is more abundant in the uninduced condition [FIG 2.2B]. Thus, chaperones are another class of proteins that are broadly more associated with the Dhh1-GFP complex under conditions of stress induction.

The two Hsp40 class chaperones identified - Sis1p and Ydj1p - are both only associated with the Dhh1-GFP complex in the induced condition and are not detected in the complex from the uninduced samples. Given that both of these chaperones are involved in prion protein conformational changes[49] - including the *bona fide* yeast prion proteins Sup35, Ure2, and Rnq1 - we tested whether they are involved in the stress-induced aggregation of RNA granule proteins. While Sis1 is essential, and therefore deletion is lethal, we tested the aggregation of Dhh1-GFP, Lsm1-GFP, and Edc3-GFP in a *ydj1Δ* mutant strain background. The *ydj1Δ* mutant strongly prevented both Dhh1-GFP and Lsm1-GFP from forming foci in both glucose depletion experiments as well as in a saturated culture [FIG 2.4A]. Edc3-GFP aggregation was also inhibited by the *ydj1Δ* mutant, though the effect was not as severe as on Dhh1-GFP and Lsm1-GFP. We also tested *ssa1Δ*, *ssa2Δ*, *hsc82Δ*, *hsp82Δ*, and *hsp104Δ* mutants on the stress induction of Dhh1-GFP foci and found that none of these mutants inhibited Dhh1-GFP accumulation into foci [FIG 2.4B]. Because Ydj1p is an abundant protein chaperone, we tested the expression of these proteins in the *ydj1Δ* background. We found that the *ydj1Δ* mutant reduced the actin-normalized levels of Dhh1-GFP, Lsm1-GFP and Edc3-GFP approximately 4-5 fold relative to levels in wild type strains [FIG 2.4C]. The inhibition of Dhh1-GFP foci formation was complemented by reintroduction of a vector expressing YDJ1, but was not complemented by any of the other chaperones tested [FIG 2.5A]. The addition of a vector expressing SIS1 appeared to partially complement the *ydj1Δ,* so we tested a vector in which SIS1 is placed under the control of a strong, constitutive promoter (TEF plasmid) as opposed to its native promoter (MoBY plasmids). When SIS1 is expressed under the strong promoter, it does appear to

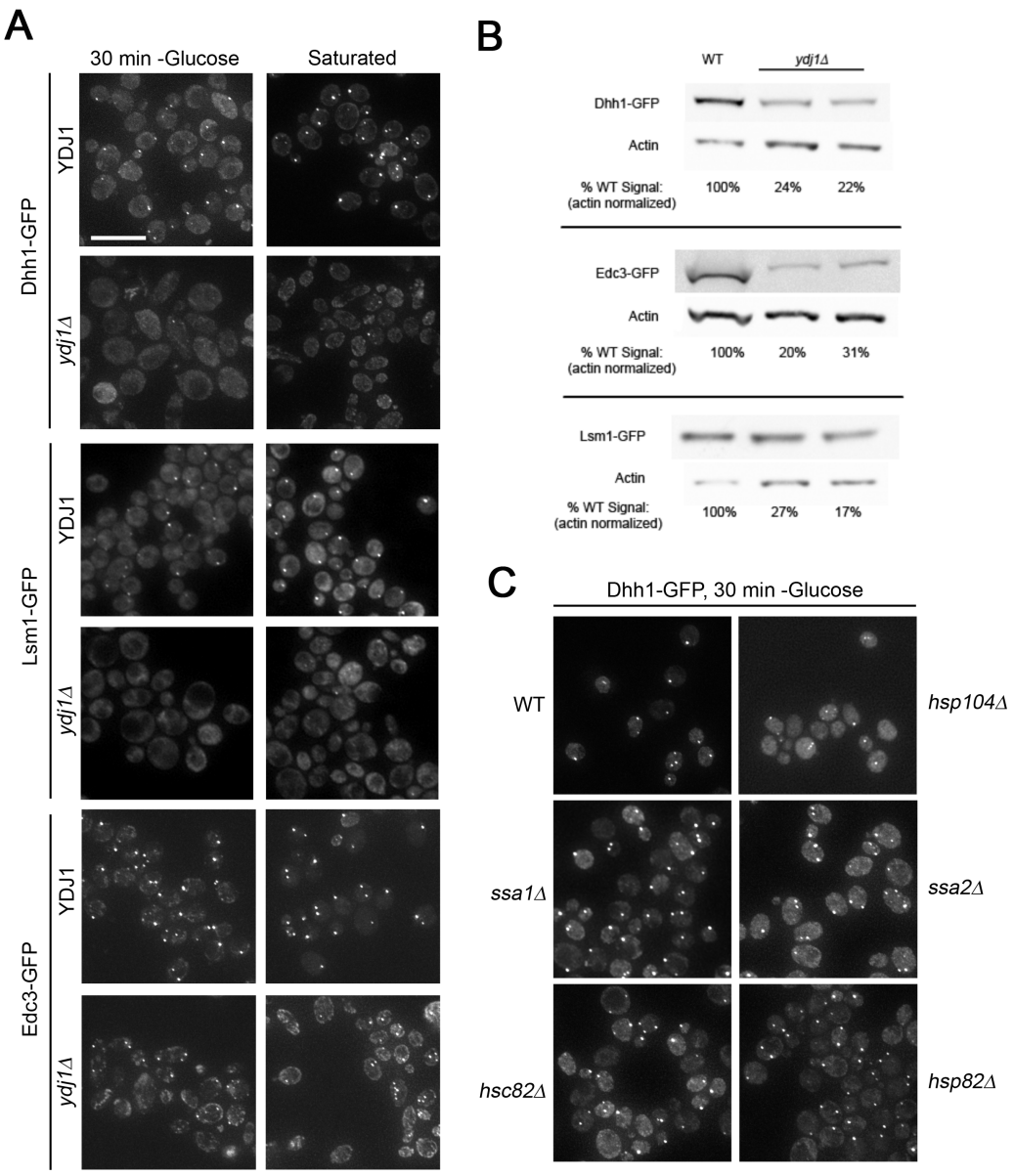

Figure 2.4 Ydj1 is involved in the aggregation of PB proteins.

(A) Microscopic images of Dhh1-GFP, Lsm1-GFP and Edc3-GFP strains in the presence of wild type YDJ1 or mutant (*ydj1Δ*). Example images are shown following 30 minutes of glucose depletion and from a saturated overnight culture for each strain. Scale bar = 10μm. (B) Western blot analysis of Dhh1-GFP, Edc3-GFP and Lsm1-GFP expression in cells wild type for YDJ1 and in two biological replicate *ydj1Δ* mutant strains. Anti-GFP immunoreactivity was normalized to anti-actin loading controls and densitometry was performed to calculate relative expression of WT and mutant strains. (C) Microscopic images of Dhh1-GFP induction in wild type and mutant strains *hsp104Δ*, two Hsp70 mutants (*ssa1Δ* and *ssa2Δ*), and two Hsp90 mutants (*hsc82Δ* and *hsp82Δ*). Cells were induced to form foci by 30 minutes of glucose depletion.

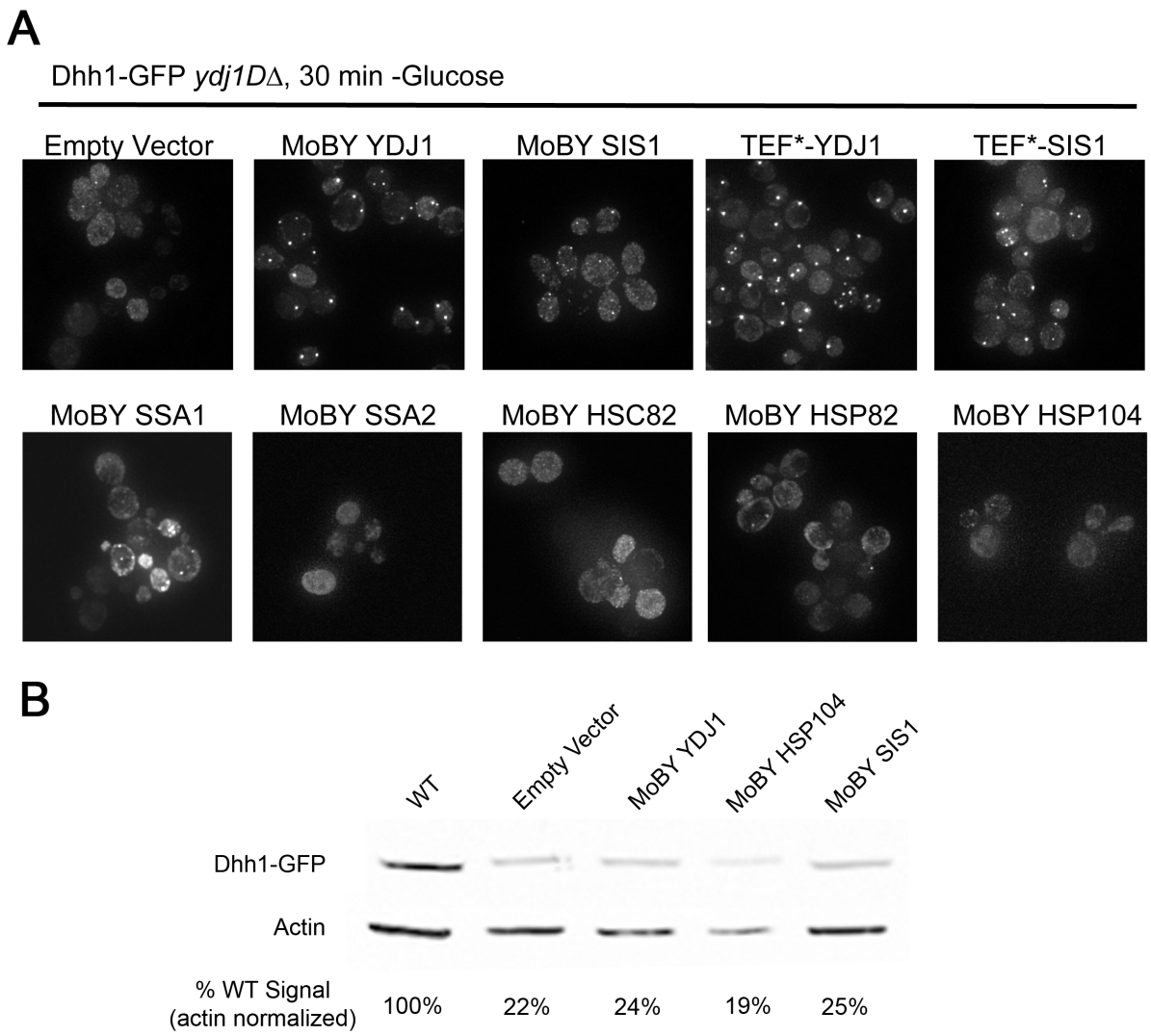

Figure 2.5 Only YDJ1 fully complements the *ydj1Δ* mutant.

(A) Microscopic images of Dhh1-GFP strains mutant for *ydj1Δ* containing the CEN plasmids indicated. MoBY plasmids contain the native promoter and the TEF plasmids are strong, constitutive promoters (*). All strains were induced to form foci by 30 minutes of glucose depletion. (B) Western blot analysis of Dhh1-GFP expression in strains mutant for *ydj1Δ* containing the CEN plasmids indicated. Anti-GFP signal was normalized to anti-actin signal from the same strain.

complement the *ydj1Δ* mutant. Intriguingly, the reduction of protein levels in the *ydj1Δ* background is not complemented by the addition of YDJ1 vector [FIG 2.5B], suggesting that the facilitation of protein aggregation and the effect on protein abundance are distinct functions of Ydj1p. Overexpression of YDJ1 or SIS1 in an otherwise wild type strain had no effect on the aggregation of either Lsm1-GFP or Dhh1-GFP [data not shown]. These results demonstrate that the chaperone YDJ1 is necessary for the accumulation of RNA granule components into cytoplasmic foci, though does not appear to affect all granule components to the same degree. This effect is specifically attributable to YDJ1 as mutations in several other chaperones do not affect foci formation and only YDJ1 can fully complement the mutant.

Analysis of Co-enriched RNA

RNA co-precipitating with Dhh1-GFP was identified using a custom Agilent DNA microarray consisting of 44k probes antisense to the *S. cerevisiae* transcriptome. The probes on the array are designed to hybridize to 10,283 different yeast transcripts including the 6,607 ORF transcripts annotated in the Saccharomyces Genome Database as well as 3,676 non-coding RNAs. There are three distinct probes designed to each transcript distributed across the array. We hybridized RNA eluted from the Dhh1-GFP IP directly to the array and detected RNA::DNA hybridizations using the S9.6 monoclonal antibody and an anti-mouse Cy3-labelled secondary antibody[36]. Total cellular RNA prepared from the lysate used as input to the IP was hybridized to separate arrays on the same slide. Transcripts were considered enriched by the IP if they lay above the 95% confidence interval from a linear regression between the

normalized and thresholded total RNA and IP RNA samples [FIG 2.6A]. Any transcripts that were enriched in more than one biological replicate IP, but not by an IP of GFP alone were considered significantly enriched for these analyses. This analysis resulted in the identification of 70 transcripts as enriched by the Dhh1-GFP IP.

Of the 70 transcripts enriched by our Dhh1-GFP IP, 57 were found enriched at least once in the IP from the uninduced condition and 60 were found enriched at least once in the IP from the induced condition [FIG 2.6B]. 26 of the 70 enriched transcripts (37%) are mRNA that code for verified ORFs, including 4 ORFs encoded within mitochondrial group I introns, and 9 are transcripts for putatitve proteins of unknown function (13%). Of the remaining transcripts, 12 transcripts are dubious ORFs that are unlikely to code for a protein (17%), 13 are stable unannotated transcripts (SUTs) (19%), 3 are cryptic unstable transcripts (CUTs) (4%), 5 correspond to Ty long terminal repeats (LTR) (7%), and 2 are other noncoding transcripts (3%) [FIG 2.6C]. Notably, 25 of the enriched transcripts (36%) are antisense to other transcripts in the genome and 14 enriched transcripts (20%) overlap other annotated transcripts in the sense orientation. Furthermore, 18 of the enriched transcripts (26%) are either paralogous to other genes in the genome (10 transcripts) or are antisense to genes that have paralogs (8 transcripts). Although we enrich 45 transcripts in total with a structural relationship to some other gene in the genome - either antisense, overlapping, or paralogous transcripts - we only find a few examples where both members of the pair are enriched. YHR214W-A and it's antisense transcript SUT1673 are enriched in multiple Dhh1-GFP complexes; YHR214W-A has a paralog YAR068W that is also enriched. Another

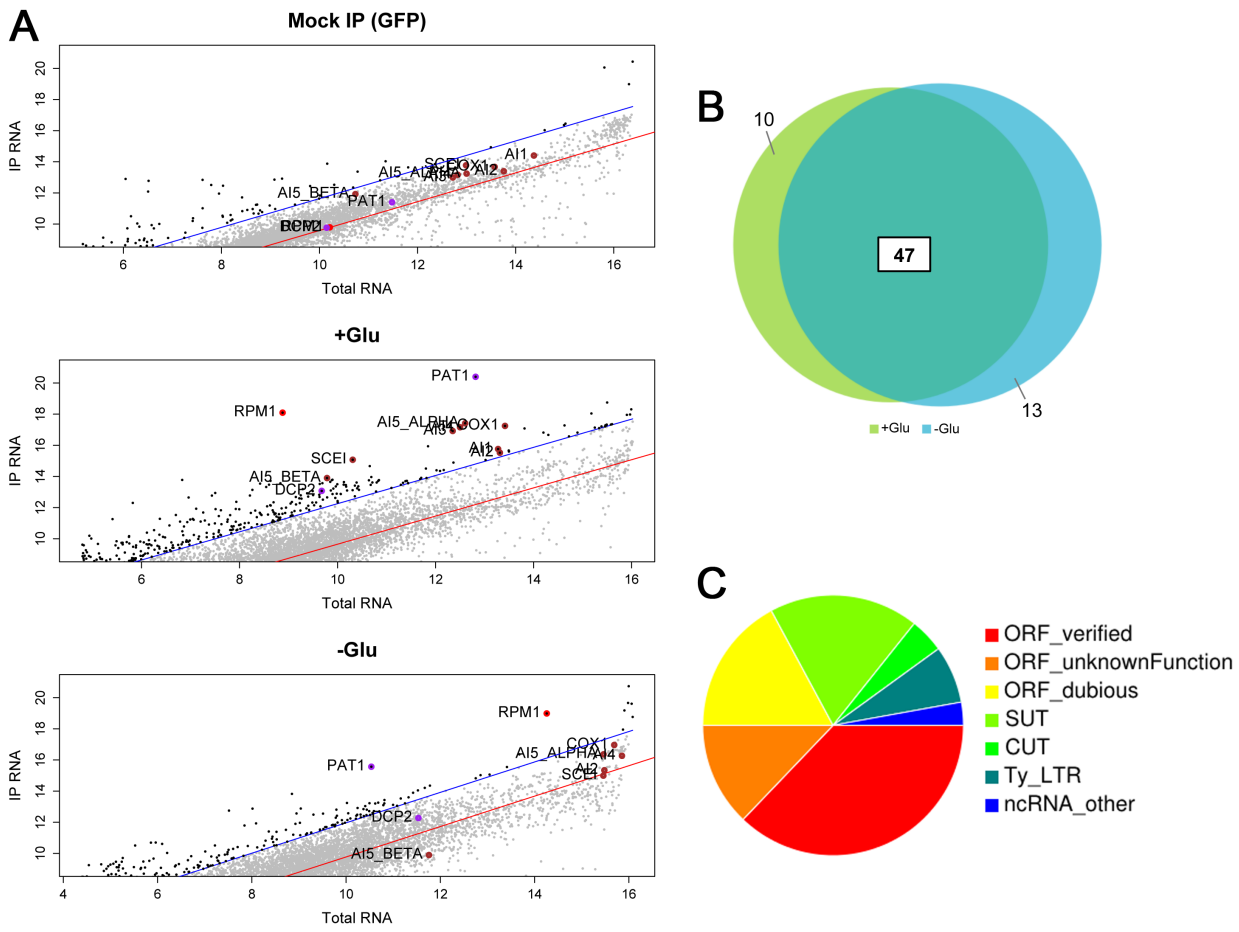

Figure 2.6 Microarray analyses of Dhh1-GFP IP samples.

(A) Representative microarray data from a mock IP (GFP alone) as well as a Dhh1-GFP IP from uninduced (+glucose) and P-body induced (-glucose) conditions. The x-axis in each plot is the log-transformed, normalized array intensity for input (Total) RNA and the y-axis is the log-transformed, normalized array intensity for IP RNA. For each plot, the red line is a linear regression of the signal from total and the signal from IP and the blue lines correspond to the 95% confidence interval. Transcripts above the upper 95% confidence interval are considered enriched (and shaded black) while transcripts that do not reach this threshold are not enriched. Specific transcripts that are enriched and discussed in the text are highlighted and labeld (red= RPM1; brown= mitochondrial group I introns; purple= PAT1 and DCP2). (B) Overlap of transcripts enriched in each condition. The number of each transcripts unique to each category are indicated by the numbers outside of the circles while the number in common is presented in the white box. (C) The proportion of the 70 transcripts representing each identified RNA class.

example of co-enrichment is NTS1-2 and SUT2110 which are both transcribed from the rDNA locus. SUT2110 is antisense to both NTS1-2 and ETS2-2 and overlaps the boundary between the two transcripts. Another example are the pair SUT881 and SUT1704 which are paralogs of each other and both are enriched across multiple preparations. Finally, there are three transcripts enriched which are encoded within subtelomeric Y-elements which are repetitive across the genome - YBL113C, YHR219W and YHR218W-A.

There are only a few gene ontology categories enriched within the identified transcripts - including intron homing ($p=3.92x10^{-6}$), and hydrogen ion transmembrane transport activity ($p=4.92x10^{-3}$) - and the enriched ontologies all correspond to the same subset of transcripts emanating from the mitochondrially encoded Cox1 locus and the introns encoded there. When we considered transcripts that are preferentially enriched by the IP in a condition specific way, we found 13 transcripts associated with Dhh1-GFP only in the induced condition and 10 transcripts associated with Dhh1-GFP only in the uninduced condition [FIG 2.6B]. While there is no apparent similarity among the 13 transcripts enriched from the induced condition, 4 of the 10 transcripts specific to the uninduced condition correspond to Ty LTR transcripts and one other noncoding transcript, SUT1773, which is antisense to a Ty3 LTR. This suggests that the Ty LTR transcripts may be conditionally associated with Dhh1-GFP. It is important to note that these transcripts correspond to Ty LTRs that do not flank functional retroelements, but are LTRs that are abandoned single LTRs within the genome. Finally, we tested for a correlation between the enriched transcripts and the presence of their cognate proteins

within the mass spectrometry data. Of the 332 proteins we enrich by proteomic analysis, we only enrich 1-5 cognate mRNA. This result indicates that we are not broadly enriching both transcripts as well as their cognate protein.

Mitochondrially Encoded Transcripts Enriched

One of the strongest and most reproducibly enriched transcripts is RPM1, the mitochondrially encoded RNA component of mitochondrial RNase P. RPM1 is enriched in 4 out of 7 Dhh1-GFP IP tested but not enriched by IP of GFP alone. Importantly, in the four samples where we detect and enrichment of RPM1, we also detect enrichment of Rpm2p by proteomic analysis of the same IP. Rpm2p is the protein component of the mitochondrial RNase P and has previously been observed to interact with PB[50], though this is the first description of the association of the RPM1 RNA with PB. Several other mitochondrially encoded transcripts are enriched in the Dhh1-GFP complex including Cox1 and several of the self-splicing group I introns encoded within the COX1 locus. The enrichment appears to be greater for the group I introns of Cox1 (AI3, AI4 and AI5-alpha) and less for the group II introns (AI1 and AI2). We designed qPCR assays to test the enrichment of the group I versus group II introns and confirmed that the group I introns are more abundant in the IP RNA than are the group II introns [FIG 2.7]. In addition SCEI is a group I intron encoded within the mitochondrial 21S rRNA locus that is also enriched in the Dhh1-GFP IP. In contrast the group II introns encoded within the Cytochrome B locus are not enriched. We also identify Mss116p in our proteomics results. Mss116p is a DEAD-box helicase that has been demonstrated to assist in the *in vivo* splicing of mitochondrial group I and group II introns. These results

demonstrate that two different classes of mitochondrial RNA processing catalytic RNAs are associated with Dhh1-GFP.

PAT1 mRNA Enriched in Dhh1-GFP Complex

The most reproducibly enriched transcript we identify is the mRNA encoding the PB component Pat1p which is identified in every Dhh1-GFP complex tested but not enriched in the GFP alone negative control. The level of enrichment is also remarkably strong with Pat1 mRNA approximately 25-fold more abundant in the Dhh1-GFP IP RNA than in the total RNA. The enrichment of Pat1 RNA, and the relative level of enrichment, was confirmed by qPCR [FIG 2.7]. In addition, we confirmed by qPCR that the Pat1 RNA enriched in the IP is polyadenylated, which suggests that the Pat1 detected is not simply a decay intermediate. Pat1 is not the only transcript coding for a PB component that is enriched as we also enrich the Dcp2 mRNA. However, in contrast to Pat1, Dcp2 is only identified in the two IPs from the uninduced condition and the level of enrichment is not as strong with an average of 8-fold enrichment over the signal in total RNA. This could indicate conditional regulation of mRNA for PB protein transcripts or possibly translational regulation for assembly of the complex. Alternatively, the mRNA encoding Pat1 may serve an additional function within RNA granules that is distinct from its role coding for the Pat1 protein.

To test the hypothesis that the Pat1 mRNA has a function in PB that is distinct from coding for the Pat1 protein, we generated strains in which two stop codons were engineered early in the coding region of the Pat1 transcript. We show that these strains do not express any detectable Pat1p by western blotting a Pat1-STOP-GFP strain.

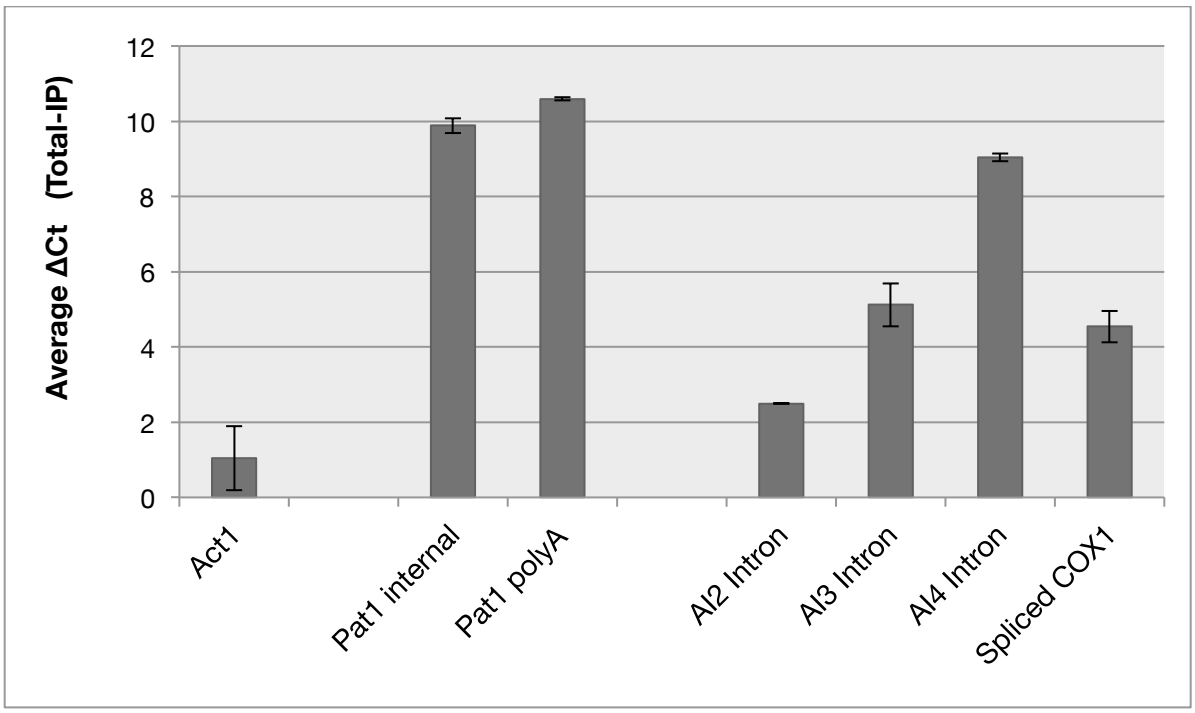

Figure 2.7 Quantitative RT-PCR validation of transcript enrichment.

Data is shown as average change in Ct (ΔCt) between the Total RNA and IP RNA. Data for ACT1 is shown as a negative control for enrichment. PAT1_internal is a primer set internal to the Pat1 transcript and Pat1_polyA is a primer set anchored at the polyA tail of Pat1. AI2, AI3 and AI4 are PCR reactions designed three exemplary introns encoded within the Cox1 locus and the Spliced Cox1 is an intron-spanning PCR reaction that is specific to the spliced Cox1 mRNA.

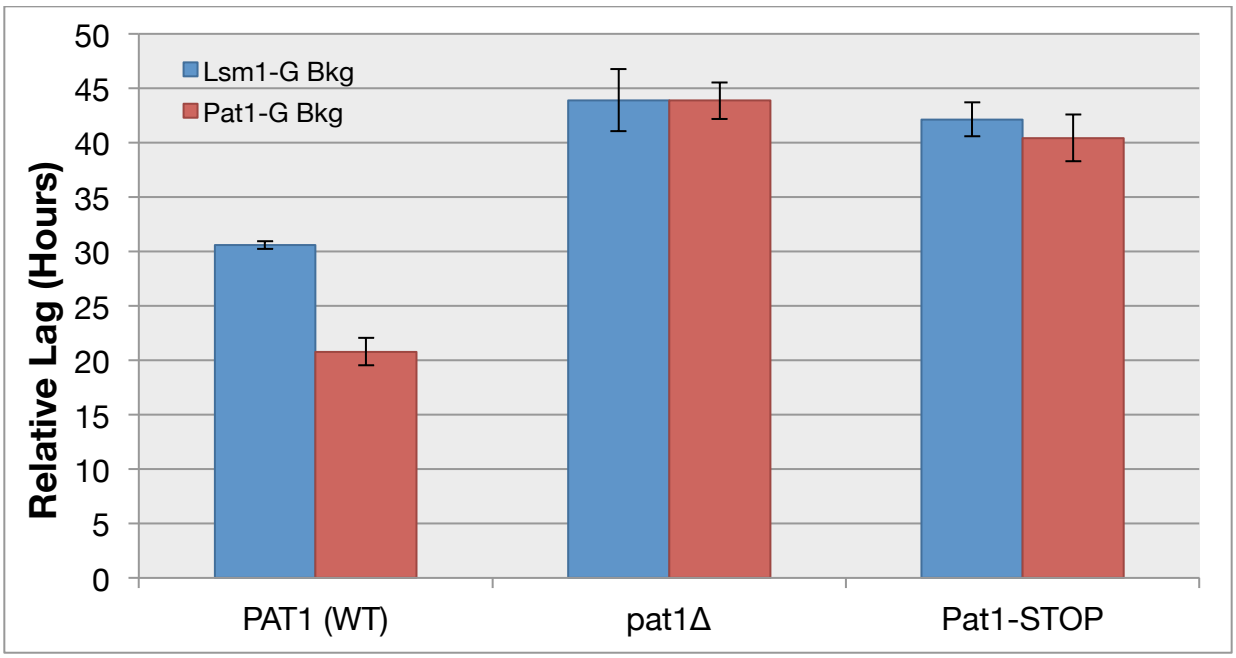

Figure 2.8 Estimated lag phase for Pat1 strains in cycloheximide and YPD media
Average relative lag phase calculated as lag time in cycloheximide media minus lag time in YPD media for each strain, averaged across genetic backgrounds. Two backgrounds are shown Lsm1-GFP (blue) and Pat1-GFP (red) across three different Pat1 genotypes - Pat1 wild type, *pat1Δ*, and Pat1-STOP. Error bars are +/- standard deviation.

Because we have engineered a destabilizing premature termination codon into the Pat1 RNA, we tested for the relative expression of Pat1-STOP and wild type Pat1 RNA by qPCR and found that the Pat1-STOP strains only express 12% of wild type levels of Pat1 [data not shown]. We then grew these strains on conditions for which the *pat1Δ* has reported sensitivity. For most phenotypes tested, there is no difference between the growth of *pat1Δ* strains and the Pat1-STOP strains. However, we did detect a phenotypic benefit to the Pat1-STOP strains compared to *pat1Δ* when grown on media containing cycloheximide [FIG 2.8]. The Pat1-STOP strains have a slightly shorter lag phase on cycloheximide media than do the *pat1Δ* strains in both genetic backgrounds tested (Pat1-STOP-GFP and Pat1-STOP in an Lsm1-GFP background). These differences, while reproducible, do not reach statistical significance for the Lsm1-GFP background, but are significantly different based on the nonparametric Mann Whitney U Test ($p=0.0102$). It is possible the phenotype is small due to the significantly lower amount of RNA expressed in these strains and that if the expression were artificially increased, one might see a larger phenotypic benefit to the presence of the noncoding Pat1 transcripts. We cannot completely rule out the possibility that the Pat1-STOP strains are producing small amounts of Pat1 protein that are undetectable by western blot, but these results suggest there is a phenotypic benefit to the Pat1 RNA that is not due to the expression of protein.

Discussion

In this work we have demonstrated for the first time a specific enrichment of yeast PB complexes by developing and implementing an immunoprecipitation of the

core PB protein Dhh1-GFP. While we reproducibly identify the majority of the core proteins, a specific set of proteins largely absent from our results are the members of the Ccr4/Pop2/Not1-5 cytoplasmic deadenylation complex. One possible explanation for the absence of these proteins is that RNA deadenylation is required for RNA association with PB and is likely one of the earliest steps in the targeting of transcripts to the PB compartment[51]. It is also plausible that the interaction between the Dhh1p subcomplex and the deadenylase subcomplex is simply not high affinity enough to persist in our IP. With this exception in mind, we still identify a majority of the PB core as well as many RNA granule associated proteins.

An important result from these experiments is that the core PB proteins are more abundantly associated with Dhh1-GFP in the condition in which PB are uninduced. This is counterintuitive as naively one might expect that the induction of large PB aggregates would result in the enrichment of many more PB proteins. There are several possible interpretations that could explain these observations. We cannot rule out potential technical limitations, such as the possibility that these differences are due to limited or altered accessibility of PB associated Dhh1-GFP in the stress induced condition. However, a biological interpretation of these results is that these differences reflect RNP re-arrangements in the stress condition. For example, it has been observed that under conditions of stress induction some cellular Dhh1p associates with PB proteins and some Dhh1p associates with stress granule proteins[42]. Supporting this interpretation is our observation that the stress granule associated proteins Pbp1, Cdc33 and Cdc48 are reproducibly more abundant within the Dhh1-GFP complex in

the stress induced condition. Whether biological or technical in origin, the undisputable fact that emerges is that the PB core proteins measured in our IP are together when they are not induced to form cytologically detectable foci.

The enrichment of proteins containing low-complexity regions is yet another example of the similarity between yeast RNA granules and RNA granules found in higher eukaryotes. Previous results identified the importance of proteins containing LC sequences in the induction of PB foci. For example, double deletion of Edc3 and the Q/N rich region of Lsm4 was shown to prohibit the formation of PB *in vivo*[52] and, more generally, the role of Q/N rich domains within proteins in establishing the localization of PB has been demonstrated[53]. The abundance of proteins containing LC domains is further evidence that these features comprise an organizational principle for RNA granule complexes that could allow for rapid state changes in response to environmental perturbations. Similarly, the conditional enrichment of metabolic enzymes within these RNA granule complexes could reflect a common response to environmental stress in which energetically expensive processes are sequestered along with RNA granule associated aggregates. As the reversibility of these metabolic enzyme aggregates have been demonstrated[46], one interpretation could be that they act as storage depots for proteins during stress. This model is highly similar to the model in which PB are involved in the long-term storage of particular transcripts during stressful conditions and the results presented here suggest that these processes may be physically associated within the cell.

The involvement of Ydj1p in the aggregation of PB proteins is an important result. While Ydj1p is known to be involved in stress responses and protein folding[54,55], this is the first demonstration of its necessity for the formation of RNA granule aggregates. Other chaperone proteins have been shown to affect PB aggregation, including the Cct3p chaperonin[56] as well as observations that Hsp90 inhibitors prevent PB and stress granule aggregation in mammalian cell culture[57]. A potentially interesting aspect of Ydj1p association with RNA granule aggregation is the fact that Ydj1 is involved in the conformational changes of prion proteins[49]. Ydj1p is primarily involved in the disaggregation of yeast prions whereas Sis1p tends to stimulate more aggregation of prions. Given the abundance of low complexity and putative prionogenic sequences within RNA granule associated proteins, it is plausible that Ydj1p interacts with these proteins and stimulates their aggregation in an analogous way to its interaction known prions, even though the effect on aggregation is opposite. These interactions will need to be explored in more physical detail to identify the exact mechanisms through which Ydj1p promotes the aggregation of PB proteins *in vivo*.

Because the Dhh1-GFP IP reproducibly and specifically enriches PB and RNA granule proteins, we can confidently explore the reproducibly enriched RNAs as transcripts that associate with the Dhh1-GFP complex. We cannot conclude with certainty that these transcripts represent translationally repressed PB associated transcripts, because we cannot rule out the possibility that the enriched transcripts co-enrich with the ribosomal subunits. However, given that 50% of the transcripts detected in the IP are non-protein coding transcripts, it is highly unlikely that we are

specifically enriching translating mRNAs by association with ribosomal subunits. The prevalence of noncoding transcripts enriched with the Dhh1-GFP complex is an interesting result, although it is difficult to explain. There does not appear to be co-enrichment of structurally associated transcripts - i.e. sense-antisense pairs are not co-enriched - as would be expected for RNA interference mechanisms[58]. However, the enrichment of LTR sequences, Y' elements and RNA antisense to other transcripts is similar to the general classes of RNA associated with ectopically expressed dicer in *S. cerevisiae*[59]. The observation that 25% of the enriched transcripts are members of known paralog groups could be an indication that these transcripts are the result of a transcriptional paralog interference[60]. Finally, as Dhh1 is an RNA helicase it is formally possible that the transcripts enriched by association with Dhh1 do so through some unidentified common structural elements.

These results are the first report of an association between Rpm1 RNA and Dhh1, although the Rpm2p component of mitochondrial RNase P has previously been shown to interact both physically and genetically with a number of PB proteins[50]. These results suggest the possibility that either Rpm1r, transcribed in the mitochondrion, is exported and interacts with Dhh1 RNA granules in the cytoplasm, or that Dhh1 RNA granules are localized within the mitochondrion. A recent report demonstrated that human RNase P localizes to RNA granules within the mitochondrion, and this localization was shown to be important for the processing of RNase P substrates[61]. However a separate study of a large yeast mitochondrial RNA processing complex containing RNase P did not detect any of the abundant RNA processing proteins we

identified in our Dhh1-GFP IP except for Rpm2p[62]. The yeast RPM1 transcript is itself processed and only a portion of the primary transcript is involved in RNase P activity[63] and Rpm2p has been shown to be involved in the maturation of Rpm1r *in vivo*[62,64]. It is possible that association with yeast PB facilitates or otherwise regulates the Rpm2p-mediated maturation of the Rpm1r primary transcript or the assembly of Rpm1r and Rpm2p into the RNase P complex.

The presence of other mitochondrial transcripts within the Dhh1-GFP IP is further indication that Dhh1 RNA granules are associated with mitochondrial RNA processing. The specific enrichment of the both the COX1 mRNA as well as self-splicing introns contained within the COX1 locus along with the Mss116p helicase that is required for efficient *in vivo* splicing suggests a role in mitochondrial splicing activity as opposed to RNA decay, a function typically attributed to the Suv3p helicase[65,66]. The PB genes DHH1 and LSM6 have previously been implicated in the splicing of mitochondrial introns as respiratory deficient mutants in these genes are rescued by removal of the group II introns from the mitochondrial genome[67]. Dhh1-GFP appears to enrich predominantly mitochondrial group I introns, including both AI3 and AI4 from the COX1 gene and SCEI from the 21s rRNA locus, and group II introns are not enriched to the same degree. This could be reflect structural differences between the two classes - group II introns form lariats when spliced whereas group I introns are spliced linearly[68] - and suggests that Dhh1 could be involved in the folding of these introns, which is critical for the splicing activity *in vivo*[69]. Finally, the self-splicing group I and II introns also have the ability to act as mobile elements within the mitochondrial genome.

Because Ty retrotransposons, mobile elements of the nuclear genome, are known to localize to PB for assembly of the virus-like particles that are necessary for the transposition activity[70], it is possible that the association between mitochondrial introns and PB is relevant to the mobility of these elements *in vivo*.

Finally we conclude that the Pat1 mRNA is closely associated with the Dhh1-GFP complex. While the Pat1 mRNA is not the only transcript for a PB protein that is enriched, the level and reproducibility of enrichment is unmatched by any other enriched RNA. Given these results, we explored the possibility that the Pat1 mRNA could possess a functional role within the cell in addition to, and distinguishable from coding for the Pat1 protein. We identified a small, but significant phenotypic benefit to the expression of Pat1 RNA in the form of a reproducible reduction in the length of lag phase for cells grown in cycloheximide media. While we cannot rule out the possibility that some undetectably small amount of Pat1 protein produced in these strains is the cause of this phenotypic benefit, the benefit observed in the Pat1-STOP strains suggests a functional role for the Pat1 mRNA distinct from coding for the Pat1 protein. These results, in combination with the robust co-enrichment of Pat1 mRNA with Dhh1-GFP, suggests a model in which the Pat1 transcript is bifunctional as both coding for the Pat1 protein and as a functional noncoding RNA. This model, while not common, is also not unprecedented; for example the steroid receptor RNA activator (SRA) has numerous functions as a noncoding RNA and is also recognized to encode a protein (SRAP) with its own and overlapping functions[71,72]. These relationships should be explored in more detail to establish which explanation best fits these results.

Finally, this experimental approach can be used for further explorations into yeast RNA granule composition. For example, testing whether one can detect stress-specific compositional changes in the protein and RNA components of these granules when different cell stresses are applied. Alternatively, utilizing combinations of other PB bait proteins could assist in the identification of specific sets of proteins or RNA that are associated with these granules. Ultimately, the uninduced state may be a more interesting condition in which to probe the functions of these complexes as stress induction appears to increase the numbers and abundance of non-RNA granule proteins including protein chaperones and metabolic enzymes. The uninduced conditions by contrast present an opportunity for probing the normal (i.e. non-stress responsive) functions of these complexes in the post-transcriptional regulation of RNA.

References

[1] McCarthy, J. E. Posttranscriptional control of gene expression in yeast. *Microbiology and molecular biology reviews : MMBR* **62**, 1492-1553 (1998).

[2] Kim, W. & Kyung Lee, E. Post-transcriptional regulation in metabolic diseases. *RNA biology* **9**, 772-780, doi:10.4161/rna.20091 (2012).

[3] Anderson, P. Post-transcriptional regulons coordinate the initiation and resolution of inflammation. *Nature reviews. Immunology* **10**, 24-35, doi:10.1038/nri2685 (2010).

[4] Freeman, J. A. & Espinosa, J. M. The impact of post-transcriptional regulation in the p53 network. *Briefings in functional genomics* **12**, 46-57, doi:10.1093/bfgp/els058 (2013).

[5] Nousch, M. & Eckmann, C. R. Translational control in the Caenorhabditis elegans germ line. *Advances in experimental medicine and biology* **757**, 205-247, doi:10.1007/978-1-4614-4015-4_8 (2013).

[6] Anderson, P. & Kedersha, N. RNA granules: post-transcriptional and epigenetic modulators of gene expression. *Nat Rev Mol Cell Biol* **10**, 430-436, doi:10.1038/nrm2694 (2009).

[7] Decker, C. J. & Parker, R. P-bodies and stress granules: possible roles in the control of translation and mRNA degradation. *Cold Spring Harbor perspectives in biology* **4**, a012286, doi:10.1101/cshperspect.a012286 (2012).

[8] Sheth, U. & Parker, R. Decapping and decay of messenger RNA occur in cytoplasmic processing bodies. *Science (New York, N.Y.)* **300**, 805-808, doi:10.1126/science.1082320 (2003).

[9] Parker, R. & Sheth, U. P bodies and the control of mRNA translation and degradation. *Molecular cell* **25**, 635-646, doi:10.1016/j.molcel.2007.02.011 (2007).

[10] Anderson, P. & Kedersha, N. RNA granules. *The Journal of Cell Biology* **172**, 803-808, doi:10.1083/jcb.200512082 (2006).

[11] Anderson, P. & Kedersha, N. Stress granules: the Tao of RNA triage. *Trends Biochem Sci* **33**, 141-150, doi:10.1016/j.tibs.2007.12.003 (2008).

[12] Grousl, T. *et al.* Robust heat shock induces eIF2alpha-phosphorylation-independent assembly of stress granules containing eIF3 and 40S ribosomal subunits in budding yeast, Saccharomyces cerevisiae. *J Cell Sci* **122**, 2078-2088, doi:10.1242/jcs.045104 (2009).

[13] Teixeira, D., Sheth, U., Valencia-Sanchez, M. A., Brengues, M. & Parker, R. Processing bodies require RNA for assembly and contain nontranslating mRNAs. *RNA* **11**, 371-382, doi:10.1261/rna.7258505 (2005).

[14] Marnef, A. & Standart, N. Pat1 proteins: a life in translation, translation repression and mRNA decay. *Biochem Soc Trans* **38**, 1602-1607, doi:10.1042/bst0381602 (2010).

[15] Presnyak, V. & Coller, J. The DHH1/RCKp54 family of helicases: an ancient family of proteins that promote translational silencing. *Biochimica et biophysica acta* **1829**, 817-823, doi:10.1016/j.bbagrm.2013.03.006 (2013).

[16] Carroll, J. S., Munchel, S. E. & Weis, K. The DExD/H box ATPase Dhh1 functions in translational repression, mRNA decay, and processing body dynamics. *J Cell Biol* **194**, 527-537, doi:10.1083/jcb.201007151 (2011).

[17] Coller, J. & Parker, R. General translational repression by activators of mRNA decapping. *Cell* **122**, 875-886, doi:10.1016/j.cell.2005.07.012 (2005).

[18] Teixeira, D. & Parker, R. Analysis of P-body assembly in Saccharomyces cerevisiae. *Molecular biology of the cell* **18**, 2274-2287, doi:10.1091/mbc.E07-03-0199 (2007).

[19] Kanai, Y., Dohmae, N. & Hirokawa, N. Kinesin transports RNA: isolation and characterization of an RNA-transporting granule. *Neuron* **43**, 513-525, doi:10.1016/j.neuron.2004.07.022 (2004).

[20] Fenger-Gron, M., Fillman, C., Norrild, B. & Lykke-Andersen, J. Multiple processing body factors and the ARE binding protein TTP activate mRNA decapping. *Molecular cell* **20**, 905-915, doi:10.1016/j.molcel.2005.10.031 (2005).

[21] Drummond, S. P. *et al.* Diauxic shift-dependent relocalization of decapping activators Dhh1 and Pat1 to polysomal complexes. *Nucleic acids research* **39**, 7764-7774, doi:10.1093/nar/gkr474 (2011).

[22] Bahassou-Benamri, R. *et al.* Subcellular localization and interaction network of the mRNA decay activator Pat1 upon UV stress. *Yeast (Chichester, England)* **30**, 353-363, doi:10.1002/yea.2968 (2013).

[23] Mitchell, S. F., Jain, S., She, M. & Parker, R. Global analysis of yeast mRNPs. *Nat Struct Mol Biol* **20**, 127-133, doi:10.1038/nsmb.2468 (2013).

[24] Kato, M. *et al.* Cell-free formation of RNA granules: low complexity sequence domains form dynamic fibers within hydrogels. *Cell* **149**, 753-767, doi:10.1016/j.cell.2012.04.017 (2012).

[25] Winston, F., Dollard, C. & Ricupero-Hovasse, S. L. Construction of a set of convenient Saccharomyces cerevisiae strains that are isogenic to S288C. *Yeast (Chichester, England)* **11**, 53-55, doi:10.1002/yea.320110107 (1995).

[26] Ho, C. H. *et al.* A molecular barcoded yeast ORF library enables mode-of-action analysis of bioactive compounds. *Nat Biotechnol* **27**, 369-377, doi:10.1038/nbt.1534 (2009).

[27] Rose MD, W. F., Hieter P. . (Cold Spring Harbor, NY, 1990).

[28] Huh, W. K. *et al.* Global analysis of protein localization in budding yeast. *Nature* **425**, 686-691, doi:10.1038/nature02026 (2003).

[29] Tian, Y., Zhou, Y., Elliott, S., Aebersold, R. & Zhang, H. Solid-phase extraction of N-linked glycopeptides. *Nat Protoc* **2**, 334-339, doi:10.1038/nprot.2007.42 (2007).

[30] Craig, R. & Beavis, R. C. TANDEM: matching proteins with tandem mass spectra. *Bioinformatics* **20**, 1466-1467, doi:10.1093/bioinformatics/bth092 (2004).

[31] Keller, A., Eng, J., Zhang, N., Li, X. J. & Aebersold, R. A uniform proteomics MS/MS analysis platform utilizing open XML file formats. *Mol Syst Biol* **1**, 2005 0017, doi:10.1038/msb4100024 (2005).

[32] Nesvizhskii, A. I., Keller, A., Kolker, E. & Aebersold, R. A statistical model for identifying proteins by tandem mass spectrometry. *Analytical chemistry* **75**, 4646-4658 (2003).

[33] Vogel, C. & Marcotte, E. M. Label-free protein quantitation using weighted spectral counting. *Methods in molecular biology (Clifton, N.J.)* **893**, 321-341, doi:10.1007/978-1-61779-885-6_20 (2012).

[34] Braisted, J. C. *et al.* The APEX Quantitative Proteomics Tool: generating protein quantitation estimates from LC-MS/MS proteomics results. *BMC bioinformatics* **9**, 529, doi:10.1186/1471-2105-9-529 (2008).

[35] Han, D. K., Eng, J., Zhou, H. & Aebersold, R. Quantitative profiling of differentiation-induced microsomal proteins using isotope-coded affinity tags and mass spectrometry. *Nat Biotechnol* **19**, 946-951, doi:10.1038/nbt1001-946 (2001).

[36] Dutrow, N. *et al.* Dynamic transcriptome of Schizosaccharomyces pombe shown by RNA-DNA hybrid mapping. *Nature genetics* **40**, 977-986, doi:10.1038/ng.196 (2008).

[37] Smyth, G. K. in *Bioinformatics and Computational Biology Solutions using R and Bioconductor* (ed R. Gentleman and V. Carey and S. Dudoit and R. Irizarry and W. Huber) 397-420 (Springer, 2005).

[38] Cristea, I. M., Williams, R., Chait, B. T. & Rout, M. P. Fluorescent proteins as proteomic probes. *Molecular & cellular proteomics : MCP* **4**, 1933-1941, doi:10.1074/mcp.M500227-MCP200 (2005).

[39] Oeffinger, M. *et al.* Comprehensive analysis of diverse ribonucleoprotein complexes. *Nature methods* **4**, 951-956, doi:10.1038/nmeth1101 (2007).

[40] Sweet, T., Kovalak, C. & Coller, J. The DEAD-box protein Dhh1 promotes decapping by slowing ribosome movement. *PLoS Biol* **10**, e1001342, doi:10.1371/journal.pbio.1001342 (2012).

[41] Cougot, N., Cavalier, A., Thomas, D. & Gillet, R. The dual organization of P-bodies revealed by immunoelectron microscopy and electron tomography. *Journal of molecular biology* **420**, 17-28, doi:10.1016/j.jmb.2012.03.027 (2012).

[42] Swisher, K. D. & Parker, R. Localization to, and effects of Pbp1, Pbp4, Lsm12, Dhh1, and Pab1 on stress granules in Saccharomyces cerevisiae. *PloS one* **5**, e10006, doi:10.1371/journal.pone.0010006 (2010).

[43] Aizer, A. *et al.* The dynamics of mammalian P body transport, assembly, and disassembly in vivo. *Molecular biology of the cell* **19**, 4154-4166, doi:10.1091/mbc.E08-05-0513 (2008).

[44] Tackett, A. *et al.* I-DIRT, a general method for distinguishing between specific and nonspecific protein interactions. *J. Proteome Res.* **4**, 1752-1756, doi:10.1021/pr050225e (2005).

[45] Tsvetanova, N. G., Klass, D. M., Salzman, J. & Brown, P. O. Proteome-wide search reveals unexpected RNA-binding proteins in Saccharomyces cerevisiae. *PloS one* **5**, doi:10.1371/journal.pone.0012671 (2010).

[46] Narayanaswamy, R. *et al.* Widespread reorganization of metabolic enzymes into reversible assemblies upon nutrient starvation. *Proceedings of the National Academy of Sciences of the United States of America* **106**, 10147-10152, doi:10.1073/pnas.0812771106 (2009).

[47] Han, T. W. *et al.* Cell-free formation of RNA granules: bound RNAs identify features and components of cellular assemblies. *Cell* **149**, 768-779, doi:10.1016/j.cell.2012.04.016 (2012).

[48] Alberti, S., Halfmann, R., King, O., Kapila, A. & Lindquist, S. A systematic survey identifies prions and illuminates sequence features of prionogenic proteins. *Cell* **137**, 146-158, doi:10.1016/j.cell.2009.02.044 (2009).

[49] Summers, D. W., Douglas, P. M. & Cyr, D. M. Prion propagation by Hsp40 molecular chaperones. *Prion* **3**, 59-64 (2009).

[50] Stribinskis, V. & Ramos, K. S. Rpm2p, a protein subunit of mitochondrial RNase P, physically and genetically interacts with cytoplasmic processing bodies. *Nucleic acids research* **35**, 1301-1311, doi:10.1093/nar/gkm023 (2007).

[51] Chen, C. Y. & Shyu, A. B. Deadenylation and P-bodies. *Advances in experimental medicine and biology* **768**, 183-195, doi:10.1007/978-1-4614-5107-5_11 (2013).

[52] Scarcelli, J. J. *et al.* Synthetic genetic array analysis in Saccharomyces cerevisiae provides evidence for an interaction between RAT8/DBP5 and genes encoding P-body components. *Genetics* **179**, 1945-1955, doi:10.1534/genetics.108.091256 (2008).

[53] Reijns, M. A., Alexander, R. D., Spiller, M. P. & Beggs, J. D. A role for Q/N-rich aggregation-prone regions in P-body localization. *J Cell Sci* **121**, 2463-2472, doi:10.1242/jcs.024976 (2008).

[54] Lu, Z. & Cyr, D. M. The conserved carboxyl terminus and zinc finger-like domain of the co-chaperone Ydj1 assist Hsp70 in protein folding. *The Journal of biological chemistry* **273**, 5970-5978 (1998).

[55] Tsai, J. & Douglas, M. G. A conserved HPD sequence of the J-domain is necessary for YDJ1 stimulation of Hsp70 ATPase activity at a site distinct from substrate binding. *The Journal of biological chemistry* **271**, 9347-9354 (1996).

[56] Nadler-Holly, M. *et al.* Interactions of subunit CCT3 in the yeast chaperonin CCT/TRiC with Q/N-rich proteins revealed by high-throughput microscopy analysis. *Proceedings of the National Academy of Sciences of the United States of America* **109**, 18833-18838, doi:10.1073/pnas.1209277109 (2012).

[57] Matsumoto, K. *et al.* Hsp90 is involved in the formation of P-bodies and stress granules. *Biochemical and biophysical research communications* **407**, 720-724, doi:10.1016/j.bbrc.2011.03.088 (2011).

[58] Petersen, C. P., Bordeleau, M. E., Pelletier, J. & Sharp, P. A. Short RNAs repress translation after initiation in mammalian cells. *Molecular cell* **21**, 533-542, doi:10.1016/j.molcel.2006.01.031 (2006).

[59] Drinnenberg, I. A. *et al.* RNAi in budding yeast. *Science (New York, N.Y.)* **326**, 544-550, doi:10.1126/science.1176945 (2009).

[60] Baker, C. R., Hanson-Smith, V. & Johnson, A. D. Following gene duplication, paralog interference constrains transcriptional circuit evolution. *Science (New York, N.Y.)* **342**, 104-108, doi:10.1126/science.1240810 (2013).

[61] Jourdain, A. A. *et al.* GRSF1 regulates RNA processing in mitochondrial RNA granules. *Cell metabolism* **17**, 399-410, doi:10.1016/j.cmet.2013.02.005 (2013).

[62] Daoud, R., Forget, L. & Lang, B. F. Yeast mitochondrial RNase P, RNase Z and the RNA degradosome are part of a stable supercomplex. *Nucleic acids research* **40**, 1728-1736, doi:10.1093/nar/gkr941 (2012).

[63] Morales, M. J., Wise, C. A., Hollingsworth, M. J. & Martin, N. C. Characterization of yeast mitochondrial RNase P: an intact RNA subunit is not essential for activity in vitro. *Nucleic acids research* **17**, 6865-6881 (1989).

[64] Stribinskis, V., Gao, G. J., Sulo, P., Ellis, S. R. & Martin, N. C. Rpm2p: separate domains promote tRNA and Rpm1r maturation in Saccharomyces cerevisiae mitochondria. *Nucleic acids research* **29**, 3631-3637 (2001).

[65] Borowski, L. S., Szczesny, R. J., Brzezniak, L. K. & Stepien, P. P. RNA turnover in human mitochondria: more questions than answers? *Biochimica et biophysica acta* **1797**, 1066-1070, doi:10.1016/j.bbabio.2010.01.028 (2010).

[66] Bruni, F., Gramegna, P., Lightowlers, R. N. & Chrzanowska-Lightowlers, Z. M. The mystery of mitochondrial RNases. *Biochem Soc Trans* **40**, 865-869, doi:10.1042/bst20120022 (2012).

[67] Luban, C., Beutel, M., Stahl, U. & Schmidt, U. Systematic screening of nuclear encoded proteins involved in the splicing metabolism of group II introns in yeast mitochondria. *Gene* **354**, 72-79, doi:10.1016/j.gene.2005.03.023 (2005).

[68] Saldanha, R., Mohr, G., Belfort, M. & Lambowitz, A. M. Group I and group II introns. *FASEB J* **7**, 15-24 (1993).

[69] Jackson, S. A., Koduvayur, S. & Woodson, S. A. Self-splicing of a group I intron reveals partitioning of native and misfolded RNA populations in yeast. *RNA* **12**, 2149-2159, doi:10.1261/rna.184206 (2006).

[70] Checkley, M. A., Nagashima, K., Lockett, S. J., Nyswaner, K. M. & Garfinkel, D. J. P-body components are required for Ty1 retrotransposition during assembly of retrotransposition-competent virus-like particles. *Molecular and cellular biology* **30**, 382-398, doi:10.1128/mcb.00251-09 (2010).

[71] Cooper, C. *et al.* Steroid Receptor RNA Activator bi-faceted genetic system: Heads or Tails? *Biochimie* **93**, 1973-1980, doi:10.1016/j.biochi.2011.07.002 (2011).

[72] Kung, J. T., Colognori, D. & Lee, J. T. Long noncoding RNAs: past, present, and future. *Genetics* **193**, 651-669, doi:10.1534/genetics.112.146704 (2013).

Chapter 3: Identification and characterization of a drug sensitive strain enables puromycin-based translational assays in *Saccharomyces cerevisiae*

Gregory A. Cary[1,2], Sung Hwan Yoon[3], David R. Goodlett[3], Aimée M. Dudley[1,2]

[1]Institute for Systems Biology, Seattle, Washington
[2]Molecular and Cellular Biology Program, University of Washington, Seattle, Washington
[3]Department of Pharmaceutical Sciences, University of Maryland, Baltimore, Maryland

Abstract

Puromycin is an aminonucleoside antibiotic with structural similarity to aminoacyl tRNA. This structure allows the drug to bind the ribosomal A-site and incorporate into nascent polypeptides causing chain termination, ribosomal subunit dissociation, and widespread translational arrest at high concentrations. In contrast, at sufficiently low concentrations, puromycin incorporates primarily at the C-terminus of proteins. While a number of techniques utilize puromycin incorporation as a tool for probing translational activity *in vivo*, these methods cannot be applied in yeasts that are insensitive to puromycin. Here, we describe a mutant strain of the yeast *Saccharomyces cerevisiae* that is sensitive to puromycin and characterize the cellular response to the drug. Puromycin inhibits the growth of yeast cells mutant for *erg6Δ, pdr1Δ,* and *pdr3Δ* (EPP) on both solid and liquid media. Puromycin also induces the aggregation of the cytoplasmic processing body component Edc3 in the mutant strain. We establish that puromycin is rapidly incorporated into yeast proteins and test the effects of puromycin on translation *in vivo*. This work establishes the EPP strain as a valuable tool for implementing puromycin-based assays in yeast, which will enable new avenues of inquiry into protein production and maturation.

Introduction

Recent work in a variety of organisms has underscored the importance of post-transcriptional regulation in many biological processes[1,2,3,4,5]. The ability to identify and characterize the subset of transcripts actively translated at a given time is central to

understanding post-transcriptional regulation. Techniques such as ribosome footprinting[6], polyribosome profiling[7], and ribosome affinity purification[8] have been used to differentiate translating from non-translating RNAs and gain unprecedented insight into translational control. While robust and powerful, a common limitation to these approaches is their focus on ribosome-associated mRNA without direct measurement of the protein products of translation. In contrast, approaches that label translational products directly by feeding cells isotopically labeled or chemically derivatized amino acids[9,10] require special media conditions, expensive or radioactive amino acids, and labeling times that preclude their application to the study of global translational dynamics. For example, while posttranscriptional events such as P-body induction or tRNA sequestration to the nucleus can occur within minutes[11,12], intrinsic metabolic labeling of proteins *in vivo* (e.g. stable isotopic labeling by amino acids in cell culture, SILAC) can take several hours to be detected following a pulse[13], presumably due to the time necessary for the isotopic amino acid to be taken up by the cell and incorporated into aminoacylated tRNA pools.

The aminonucleoside puromycin has been used as a tool for studying translation *in vitro* for many years[14]. Puromycin has characteristics of both amino acids and nucleic acids and is structurally similar to aminoacylated tRNA. This structure allows puromycin to bind the A-site of actively translating ribosomes[15], where it becomes a substrate for ribosomal peptidyl transferase activity and is incorporated into nascent polypeptide chains. Puromycin incorporation is a chain terminating event, leading to ribosomal subunit dissociation and, at high levels, general translational arrest[16]. Global

translational arrest is the mechanism by which puromycin inhibits cell growth, however at sublethal concentrations the drug is preferentially incorporated at the C-terminus of nascent proteins[17]. This property makes puromycin useful for the study of translation and protein dynamics, both *in vitro* and *in vivo*. Recently several techniques have exploited this property of puromycin including mRNA display[18,19], the generation of fluorescently labeled proteins for protein interaction arrays[20], proteomic measurements of translation state by purification and mass spectrometric identification of *ex vivo* puromycinylated proteins (PUNCH-P)[21], and the global detection of translation *in vivo* through the visualization of puromycin labeled proteins by immunocytochemistry (SUnSET)[22]. In a recent paper, Liu *et al.* demonstrated the ability to both visualize protein translation *in vivo* and enrich puromycin-incorporated proteins using an alkyne analog of puromycin and subsequent copper-catalyzed azide-alkyne cycloaddition (CuAAC) “click” chemistry[23]. Puromycin-based assays take advantage of the fact that the drug is non-radioactive, relatively inexpensive, and rapidly incorporated. Protein labeling with puromycin can also be accomplished without the use of amino acid auxotrophies or limiting media conditions, permitting a wider range of experimental designs. However, because yeasts and Gram negative bacteria exhibit little or no uptake of the drug and are generally insensitive to its effects on growth[24,25,26], these recent technologies are inaccessible to researchers studying these organisms.

Here we report a strain of *Saccharomyces cerevisiae* that is sensitive to puromycin at the level of growth on both liquid and solid media. We also characterize a common cellular response to puromycin treatment, the induction of cytoplasmic processing

bodies (P-bodies). Finally, we demonstrate the utility of puromycin as a probe for translation by showing that yeast proteins rapidly incorporate puromycin *in vivo*.

Materials and methods

Yeast strains and media

All *S. cerevisiae* strains used in this study [Table 3.1] are in the isogenic FY strain background[27]. Unless noted, standard media and methods were used for growth and genetic manipulation of yeast[28].

Puromycin (FW 544.43, A.G. Scientific, Inc., Product Number: P-1033) was prepared by dissolving the puromycin dihydrochloride powder in sterile water to a concentration of 50 mM and added to growth media to achieve the final concentrations listed. Puromycin was added to YPD agar plates prior to pouring.

O-propargyl-puromycin (OP-puromycin) was custom synthesized (Medchem Source LLP, Federal Way, WA) following the synthesis scheme established by Liu *et al.*[23]. OP-puromycin was dissolved in dimethyl sulfoxide (DMSO) to a working concentration of 150 mM and subsequently diluted to achieve the final concentrations listed.

Antibodies

The 12D10 monoclonal antibody against puromycin-incorporated proteins and peptides (gift from Philippe Pierre, now commercially available, Millipore, MABE343) was used at a 1:5000 dilution for western blot analyses. Mouse anti-HA antibody clone 12CA5 (Santa Cruz Biotechnology, sc-57592) was used at a 1:100 dilution and the

Table 3.1 *S. cerevisiae* strains used in this study.

Strain	Genotype	Reference
YAD1	MATa *his3Δ1 leu2Δ0 met15Δ0 ura3Δ0*	
YAD241	MATα *his3Δ1 leu2Δ0 lys2Δ0 ura3Δ0 erg6Δ::LEU2 pdr1Δ::*natMX *pdr3Δ::*hphMX	[29]
YAD337	MATa *his3Δ1 met15Δ0 ura3Δ0 erg6Δ::LEU2 pdr3Δ*::Hyg *pdr1Δ*::KanMX4	*This study*
YAD336	MATa *his3Δ1 leu2Δ0 met15Δ0 ura3Δ0 pdr1Δ::*KanMX4	[30]
YAD521	MATa *his3Δ1 leu2Δ0 met15Δ0 ura3Δ0 pdr3Δ::*KanMX4	[30]
YAD522	MATa *his3Δ1 leu2Δ0 met15Δ0 ura3Δ0 erg6Δ::*KanMX4	[30]
YAD267	MATa *met15Δ0 ura3Δ0 erg6Δ*::Leu *pdr1Δ*::Nat EDC3-GFP::HIS3MX6	*This study*
YAD269	MATa *met15Δ0 ura3Δ0 erg6*Δ::Leu *pdr3*Δ::Hyg EDC3-GFP::HIS3MX6	*This study*
YAD271	MATa *met15Δ0 ura3Δ0 pdr1Δ*::Nat *pdr3Δ*::Hyg EDC3-GFP::HIS3MX6	*This study*
YAD50	MATa *his3Δ1 leu2Δ0 met15Δ0 ura3Δ0* EDC3-GFP::HIS3MX6	[31]
YAD273	MATα *met15Δ0 ura3Δ0 erg6Δ*::Leu *pdr3Δ*::Hyg *pdr1Δ*::Nat EDC3-GFP::His3MX6	*This study*
YAD517	MATa *his3Δ1 met15Δ0 ura3Δ0 erg6Δ*::Leu *pdr3Δ*::Hyg *pdr1Δ*::KanMX4 pGal1:3xHA-ADE17::NatNT2	*This study*
YAD518	MATa *his3Δ1 met15Δ0 ura3Δ0 erg6Δ*::Leu *pdr3Δ*::Hyg *pdr1Δ*::KanMX4 pGal1:3xHA-HSP104::NatNT2	*This study*
YAD519	MATa *his3Δ1 met15Δ0 ura3Δ0 erg6Δ*::Leu *pdr3Δ*::Hyg *pdr1Δ*::KanMX4 pGal1:3xHA-NEW1::NatNT2	*This study*

pan-actin antibody mAbGEa (Novus Biologicals, NB100-74340) at a 1:1000 dilution was used for loading control. All antibodies were detected using the goat anti-mouse IRDye 800CW (LiCor, 926-32210) at a 1:10000 dilution and detected using a LiCor Odyssey Infrared Imaging System.

Growth assays

Strains were grown overnight in liquid YPD and normalized by cell count to the lowest cell concentration. Eight 5-fold serial dilutions were prepared and 5 µl of each dilution was plated onto YPD agar plates with or without puromycin. Plates were incubated at 30º C and imaged on an Epson Perfection 2480 Photo scanner at 300 dpi resolution every 24 hours for 2 days. Two replicate assays were performed.

For liquid growth assays, strains were grown overnight and counted the following day. Cells were diluted in YPD and $5x10^3$ cells (in 135 µl total volume) were added to each well of a tissue culture treated, flat bottomed, 96-well plate. Then, 15 µl of a 10x working drug stock was added to each well to achieve the final drug concentration. Each strain and drug concentration pair was assayed in triplicate for every experiment. Plates were sealed with sterile, gas-permeable, optical adhesive sealing film for microplates and incubated in a Sunrise 96-well optical plate reader (Tecan Austria GmbH, Austria) controlled by the Tecan Magellan v6.55 software. Cells were grown at 30º C with continuous shaking. Prior to reading, the plate was subjected to 15 seconds of high intensity shaking, and the OD_{600} was read using the Tecan accuracy method. Growth was measured for 2-3 days or until the OD of the wells exhibiting growth had plateaued. For puromycin spike-in assays, cells and 96-well plates were prepared as

above and grown to log phase (OD_{600} ~ 0.4) at which point the Tecan was stopped, the plate was removed, and 15 µl of a 10x working drug stock was added to each well. The plates were then re-sealed and returned to the Tecan for continued growth monitoring.

Growth rates were calculated from liquid growth assays by applying a linear fit in 90-minute sliding windows to the log-transformed OD_{600} values. Once the growth rates in the sliding windows had been estimated, the maximum growth rate achieved was reported for each dose and strain combination. For comparisons across strain backgrounds, the maximum growth rate for each strain at each drug concentration was normalized to its maximum growth rate in YPD. For analysis of the puromycin spike-in experiments, growth rates following the puromycin spike-in were normalized to growth rates in YPD and the maximum decrease in the relative rate for each dose is reported. The number of minutes required to achieve a 25% reduction in growth rate at various doses was also calculated using the normalized growth rate parameter.

Microscopy and image analysis

For microscopic evaluation of Edc3-GFP aggregation following puromycin treatment, cells were grown to log phase (OD_{600} ~ 0.8) and incubated with puromycin or vehicle for 30 minutes or 120 minutes. Following puromycin treatment, cells were fixed in 3.7% formaldehyde in PBS for 2 minutes at room temperature, followed by a 10-minute incubation in PBS on ice. Fixed cells were imaged using a DeltaVision deconvolution imaging system (Applied Precision, Issaquah, WA) outfitted with an Olympus IX-71 wide field microscope. Cells were imaged with a PlanApo 60x oil objective (N.A. 1.42) using differential interference contrast (DIC) bright field illumination

and a 250W xenon LED transillumination light source. For GFP fluorescence imaging a polychroic beam splitter was used along with excitation 490/20 and emission 528/38 bandpass filters. A set of up to 30, 0.2 micron z-sections were captured for each image, deconvolved, and exported as tiff files. Tiff files were imported into ImageJ to generate image stacks and image levels were adjusted to be identical across all images. Tiff stacks were then batch analyzed by the Cell3 MATLAB program for segmentation of the bright field and GFP images[32]. We implemented the local comparison and selection (LOC-CS) algorithm within Cell3 for fluorescent segmenation[33]. The LOC-CS parameters were r=5 and alpha=0.6. For bright field segmentation, the minimum was set to 120 pixels, the maximum to 2040 pixels, and any item smaller than 40 pixels or larger than 3000 pixels was excluded[34]. Statistical significance was determined using the Mann Whitney Rank-Sum U test implemented in the R statistical computing language.

Puromycin Incorporation, HA-protein induction, and Western Blot Analysis

To test the in vivo incorporation of puromycin into yeast proteins, overnight cultures were diluted to an OD_{600} of 0.2 and allowed to grow to log phase (OD_{600} ~ 0.8). Puromycin was added directly to the culture at the concentrations indicated and allowed to grow for the amount of time indicated, at which time cells were rapidly pelleted (5min at 3000g), and cell pellets were frozen in liquid nitrogen and stored at -80°C for further analysis. Lysates were prepared by alkaline lysis[35] and volumes corresponding to equivalent cell numbers were used for western blot analysis with the

anti-puromycin antibody and Coomassie stain (Imperial Stain, Thermo Pierce) loading control.

For galactose induction of the HA-tagged constructs, overnight cultures in SC medium with 2% raffinose were diluted to an OD_{600} of ~0.2 into a fresh aliquot of the same medium. The culture was grown to log phase (OD_{600} ~ 0.7) and galactose was added to a final concentration of 2%. After 15 minutes of galactose induction, 0 mM-2 mM puromycin was added to the cultures. The cultures were allowed to grow in galactose and puromycin for an additional 15 to 30 minutes before collection and analysis as above. The induced proteins were visualized by anti-HA western blot.

CuAAC Click Reaction & Mass Spectrometry

To test OP-puromycin-peptide fragmentation by tandem mass spectrometry (MS), a synthetic peptide was ordered with the sequence NH_2-ISHVSTGGGASLELLEG[K(N_3)]-COOH containing an azide-modified lysine terminal residue (Thermo Fisher Scientific). This peptide was resuspended in PBS (pH 7.4) and mixed with OP-puromycin at a molar ratio of 1:2 peptide:OP-puromycin, 250 μM $CuSO_4$, 1.25 mM Tris(3-hydroxyropyltiazolmethyl)amine (THPTA) ligand (gift from M.G. Finn, Scripps), 5 mM aminioguanidine, and 5 mM ascorbic acid. The mixture was incubated at 30 ºC for 1 hour. The reaction was then desalted on C18 resin, evaporated on a speedvac and resuspended in 5% acetonitrile and 0.1% formic acid to prepare for mass spectrometry.

The experiments were carried out on the LTQ ion trap MS of an LTQ-FT MS instrument (Thermo Scientific, San Jose, CA) the front end of which, including the ion

source, was replaced by a homebuilt electrodynamic ion funnel[36,37]. Samples were dissolved into a solution mixture of H_2O/MeOH (1:1 v:v). A direct infusion with 2kV of spray voltage was used for ionization. A sample flow rate of 3 μl/min flow rate was applied and an atmospheric pressure ionization (API) inlet capillary temperature of 300 °C was used. Collision induced dissociation was used for the structural identification. Normalized collision energies of 20% for OP-puromycin at 495 m/z, 24% for Pgk1 azido peptide at 1781 m/z, 35% for the CuAAC product at 1135 m/z, and 20% or 27% for the CuAAC product at 755 m/z were used. To mitigate the effect of instantaneous signal fluctuations, the analyzed data were produced from mass spectra averaged over one minute.

Results and discussion

Identification and characterization of a puromycin-sensitive *S. cerevisiae* strain

Despite the fact that puromycin is able to disassemble yeast ribosomes *in vitro*[38,39], the commonly used laboratory strain of *S. cerevisiae* is insensitive to the antibiotic effects of puromycin[24,25]. To identify a strain with the potential to incorporate puromycin into proteins *in vivo*, we first set out to identify strains that were sensitive to the antibiotic properties of the drug. Yeast strains harboring mutations in the genes encoding the Pdr1p and Pdr3p pleiotropic drug resistance transcription factors and the Erg6p methyltransferase involved in the biosynthesis of the sterol component of yeast membranes (ergosterol) have previously been shown to sensitize strains to a variety of drugs[29]. To test whether an *erg6Δ*, *pdr1Δ*, *pdr3Δ* triple mutant (EPP) could sensitize

yeast to puromycin, we compared the growth of the EPP strain to wild type cells on YPD agar plates supplemented with puromycin at a range of concentrations (Figure 3.1A). While puromycin concentrations as high as 1 mM had no effect on the growth of wild-type cells, puromycin at concentrations of 40 μM slowed the growth of the EPP strain, with complete growth inhibition at 200 μM. Puromycin showed a similar effect on EPP growth in liquid culture, although the drug concentrations required were higher than those required on solid media (Figure 3.1B). Thus, the triple mutant EPP strain is sensitive to puromycin, although less sensitive by an order of magnitude than metazoan cell culture systems that typically use between 2 μM and 20 μM puromycin[40,41,42].

To characterize the contribution of the individual mutations on the sensitivity of the EPP triple mutant, we examined the puromycin sensitivity of strains harboring each single and all combinations of double *erg6Δ*, *pdr1Δ*, and *pdr3Δ* mutations. With the exception of a modest effect on an *erg6Δ* mutant on solid medium, there were no measurable effects of puromycin on the growth of any of the single mutants on solid or liquid media. All double mutant strains showed some level of sensitivity to puromycin in liquid culture (Figure 3.1C), with the *pdr1Δ pdr3Δ* mutant being the most sensitive of the panel. However, none of the strains were as sensitive to puromycin as the triple mutant. Thus, the strong sensitivity of the EPP strain requires the deletion of all three genes.

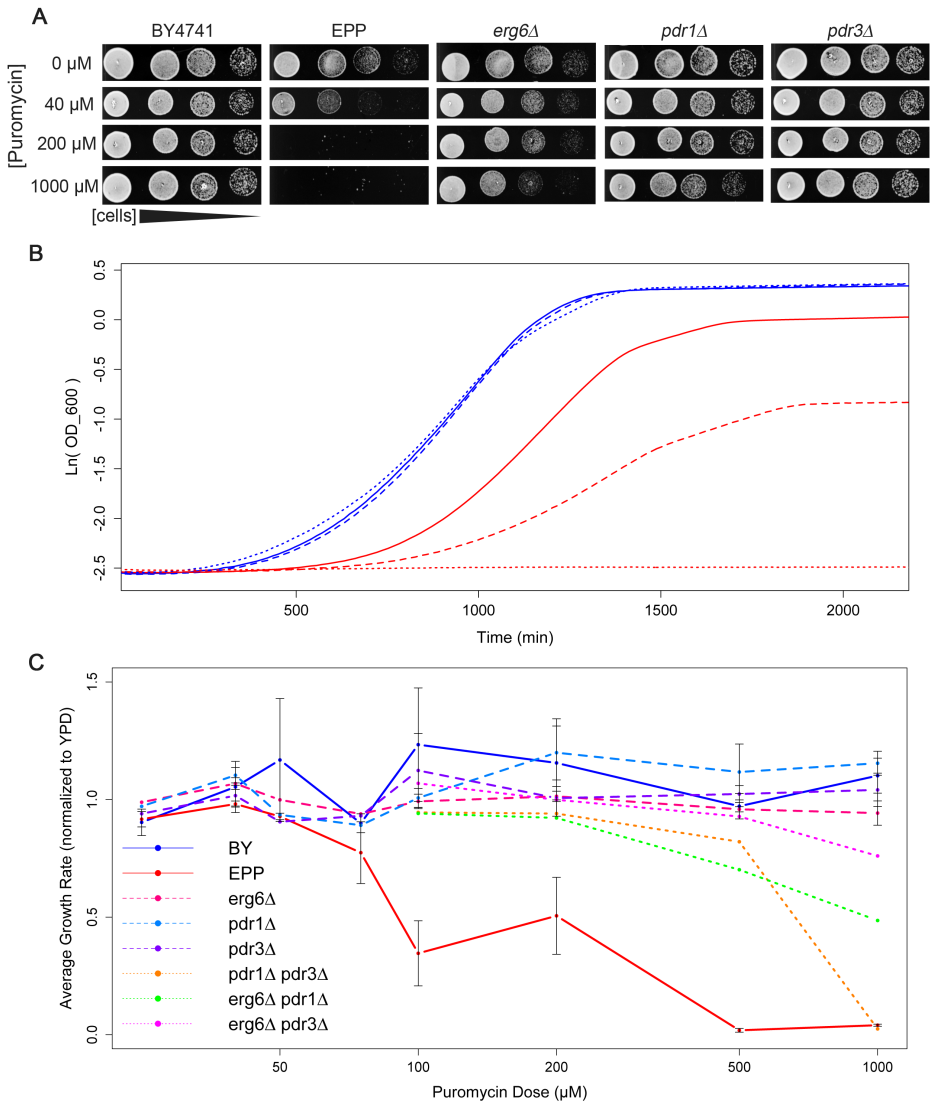

Figure 3.1 Characterization of a puromycin-sensitive yeast strain.

(A) Growth of 5-fold serial dilutions of wild-type (BY4741), EPP (*erg6Δ pdr1Δ pdr3Δ*) triple deletion mutant, and single deletion mutants cells spotted on YPD agar containing 0 μM, 40 μM, 200 μM and 1000μM puromycin. (B) Growth curves for BY4741 (blue) and the EPP triple mutant (red) in liquid media containing 0 μM (solid), 200 μM (dash), and 1000 μM (dot) puromycin. Curves are the average of 6 biological replicates. Growth curves were measure using a Tecan Sunrise plate reader sampling OD_{600} at 15 min intervals at a constant temperature of 30°C. (C) Average maximum growth rate (maximum change in log(OD)/minute) calculated for each strain grown at each concentration of puromycin, normalized to average maximum growth rate for each strain in YPD without puromycin. Error bars +/- SEM. Wild type (blue, solid line), EPP (red, solid line), *erg6Δ* (magenta, dash line), *pdr1Δ* (light blue, dash line), *pdr3Δ* (purple, dash line), *pdr1Δ pdr3Δ* (orange, dotted line), *erg6Δ pdr1Δ* (green, dotted line), and *erg6Δ pdr3Δ* (pink, dotted line).

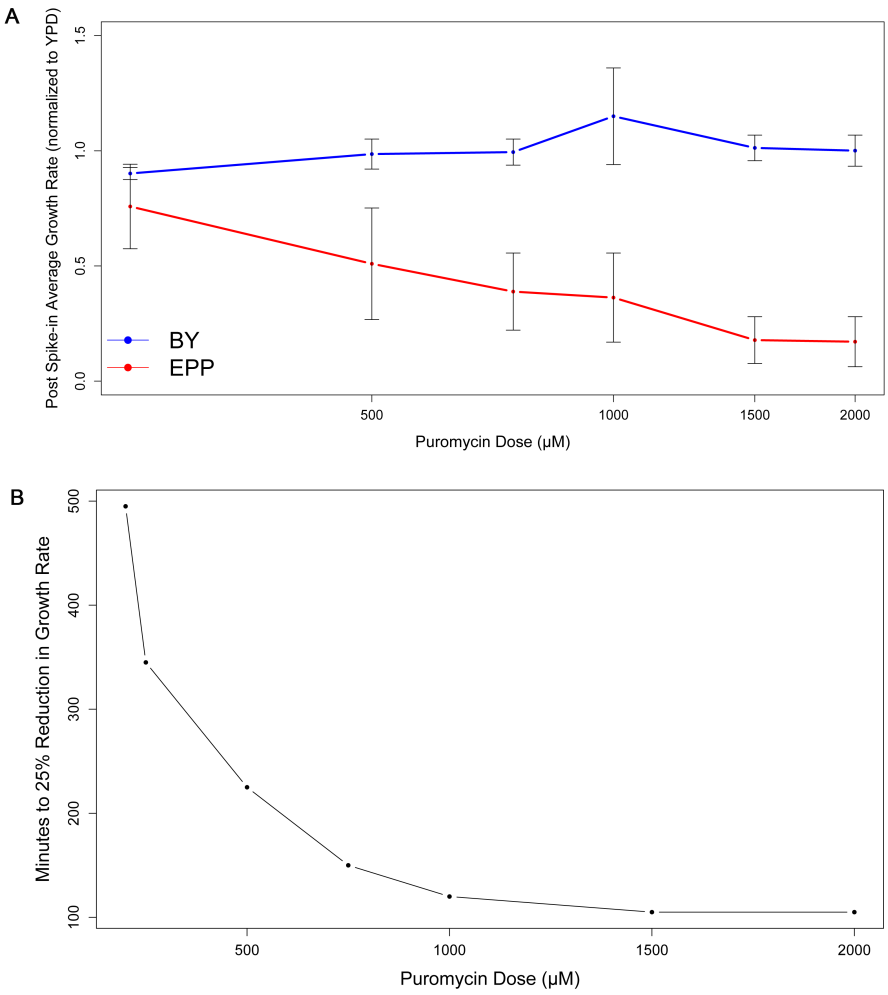

Figure 3.2 Characterization of puromycin spike-in kinetics.
(A) Minimum pre-saturation average growth rate following puromycin spike-in at several doses normalized to growth rate prior to puromycin addition. (B) Length of time to reduce growth rate to 25% of rate in YPD by spike-in of puromycin.

Studies using puromycin as a probe for of translational dynamics would be likely to pulse the drug into the growth medium at a specific stage of growth or following an environmental perturbation. To assess the response of the EPP strain to a puromycin pulse, we added puromycin to cultures of logarithmically growing EPP cells and measured the subsequent effects on growth. While the addition of puromycin to EPP cells in mid-log phase growth strongly inhibited their growth, higher doses of the drug were required to achieve similar levels of growth inhibition compared to continuous culture with the drug (Figure 3.2A). The concentration of puromycin applied also affected the rate of growth inhibition; 2 mM puromycin slowed cells to 75% of their maximal growth rate after 105 minutes, while 1 mM puromycin took 120 minutes and 0.5 mM took 225 minutes to slow to the same degree (Figure 3.2B). These data provide an initial framework for dose selection with the EPP strain.

Puromycin exposure induces aggregation of the P-body protein Edc3-GFP

Processing bodies (P-bodies) are cytoplasmic RNP complexes that are conserved across eukaryotes and are composed of RNA decay enzymes, translational repressors and non-translating mRNPs[43]. P-bodies are sensitive to environmental perturbations and typically increase in size and number when cells are exposed to conditions that inhibit translation[11]. Puromycin treatment is known to induce the aggregation of P-body proteins into cytoplasmic foci in metazoan systems[16,44,45], a response that likely coincides with ribosomal subunit dissociation and translational arrest. To test whether puromycin exposure could also induce P-bodies in yeast, we introduced a florescent P-body reporter (the P-body component Edc3p fused to GFP)

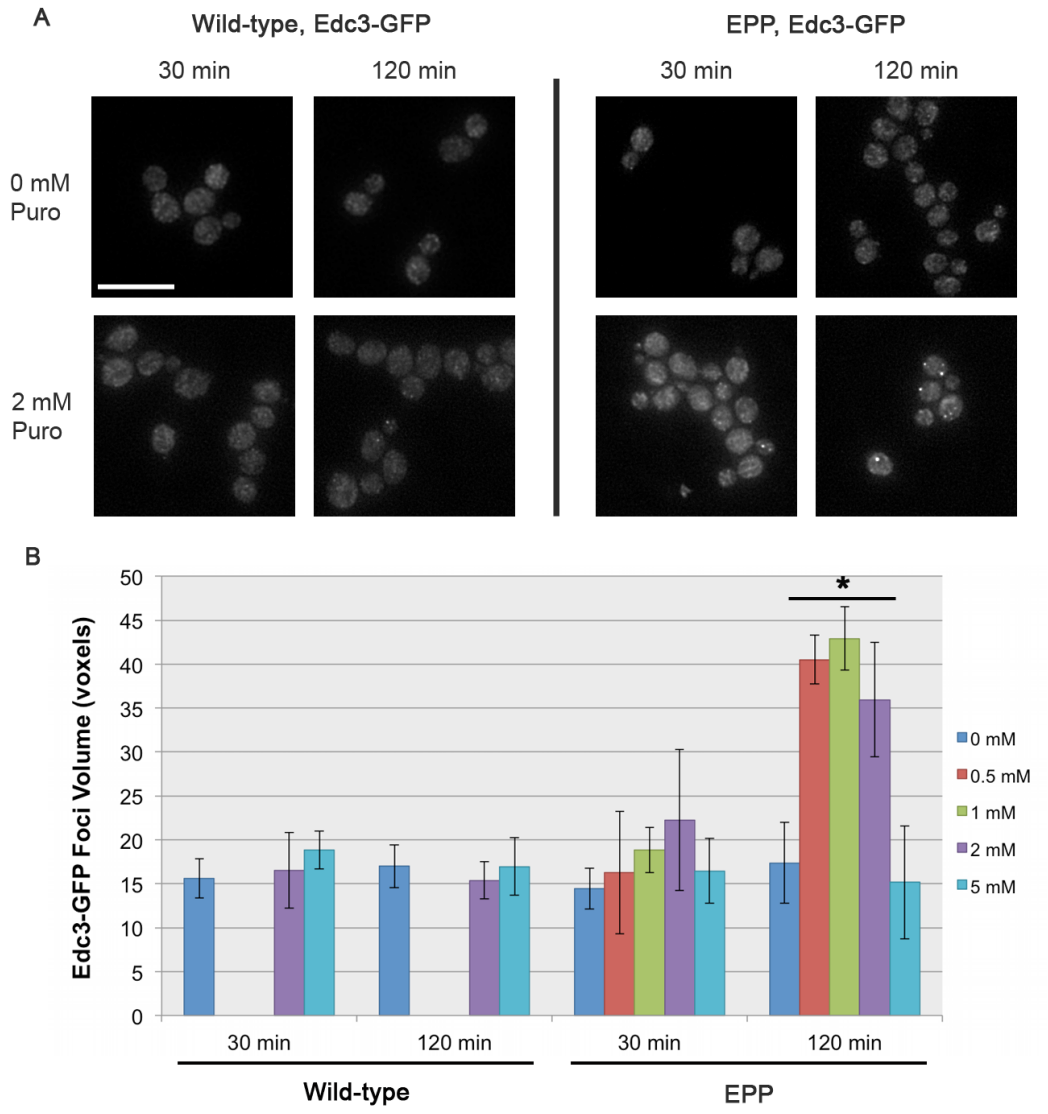

Figure 3.3 Exposure to puromycin induces Edc3-GFP accumulation into cytoplasmic foci. (A) Images of Edc3-GFP in wild-type and EPP cells grown in 0 mM or 2 mM puromycin for 30 min and 120 min. Scale bar = 10 μm. (B) Edc3-GFP foci volume (in voxels) in wild type and EPP cells after 30 min and 120 min of exposure to a range of concentrations from 0 mM to 5 mM puromycin. The conditions in which a statistically significant difference in Edc3-GFP foci volume relative to 0 mM puromycin treatment are marked (*; $p < 2.2x10^{-16}$).

into the EPP strain background. Puromycin was added to cells growing in log phase, and cells were fixed and imaged following 30 minutes and 120 minutes of drug exposure. While no change was observed in the localization of Edc3-GFP in the wild-type strain background, in the EPP strain Edc3-GFP accumulated in distinct cytoplasmic foci (P-bodies) after 120 minutes of exposure to 2 mM puromycin (Figure 3.3A). To provide a more objective assessment of Edc3 aggregation, we used automated image analysis to measure P-body volume (Materials and Methods). In the wild-type strain background we observed no significant ($p < 0.01$) increases in P-body volume at any of the doses tested. However, after 2 hours of incubation with puromycin, all EPP mutants treated with concentrations of drug below 5 mM showed significant increases in the volume of Edc3-GFP foci ($p < 2.2x10^{-16}$) (Figure 3.3B). Interestingly, at 5 mM puromycin there is no increase in Edc3-GFP accumulation, perhaps representing extreme toxicity of a high dose. These results demonstrate that upon sensitization to the drug via the introduction of the EPP deletion mutations, the effects of puromycin on yeast cellular physiology are similar to those that have been observed in other eukaryotes.

Puromycin is rapidly incorporated into proteins in the sensitized strain

To test whether puromycin could be incorporated into yeast proteins *in vivo*, thereby enabling a number of puromycin based techniques, we used the anti-puromycin monoclonal antibody 12D10[22], which has been used to detect puromycin incorporation into human proteins by western blot and flow cytometry. We observed a dose- and time-dependent increase in 12D10 immunoreactivity in yeast lysates

prepared from EPP strains exposed to puromycin for 30 and 120 minutes (Figure 3A), with the highest levels detected in lysates from cells treated for 120 minutes with 2 mM puromycin. We also observed low levels of 12D10 immunoreactivity in wild-type cells treated with puromycin (Figure 3.4A), suggesting that wild- type cells are at least minimally permeable to the drug. To assess how rapidly puromycin is detectable in yeast proteins, we prepared yeast lysates of the EPP strain harvested at different times following the addition of puromycin. Here we observed puromycin immunoreactivity by western blot with the 12D10 antibody as early as 5-10 minutes after the drug was administered (Figure 3.4B). Taken together, these results demonstrate that that puromycin is rapidly taken up by the mutant strain, available to ribosomes *in vivo*, and able to be incorporated into nascent proteins in yeast.

To examine the incorporation of puromycin into individual proteins *in vivo*, we constructed an EPP strain in which ADE17 is N-terminally 3xHA tagged and expressed under the transcriptional control of the *GAL1* promoter. The *GAL1* promoter is tightly repressed in the presence of glucose, highly expressed in the presence of galactose, and in the presence of neutral carbon sources, such as raffinose, poised to rapidly initiate transcription upon addition of galactose[46]. To facilitate the detection of puromycin incorporation into newly synthesized proteins, the EPP strain containing the galactose-inducible 3xHA-ADE17 was grown in raffinose, its transcription was induced by the addition of galactose for 15 minutes, and different concentrations of puromycin were added to label proteins synthesized after this timepoint. The results show that while steady state levels of protein do not change (Figure 3.5, Actin, lanes 1-6), there is

a galactose-dependent induction of the 3xHA-ADE17 protein (Figure 3.5, 3xHA-ADE17, lanes 1 and 2). As described above (Figure 3.4), we observed drug-dependent puromycin immunoreactivity in total proteins (Figure 3.5, anti-puromycin, lanes 1-2 versus lanes 3-5) that appeared to decrease at the highest concentration of puromycin (Figure 3.5, anti-puromycin, lane 6). These results support the hypothesis that puromycin inhibits translation *in vivo* in a dose-dependent manner and provide further evidence that 5 mM puromycin represents an extreme dose with distinct physiological and translational responses. Finally, in the presence of various concentrations of puromycin, we were able to detect a nascent molecules of a specific protein, 3xHA-ADE17 (Figure 3.5, 3xHA-ADE17, lanes 3-6), although at a significantly reduced level relative to the no-drug control (Figure 3.5, 3xHA-ADE17, lane 2).

In addition to dose dependent effects of puromycin treatment, we also examined time-dependent translational kinetics using three galactose inducible N-terminally 3xHA-tagged proteins of increasing length: Ade17p (592 amino acids), Hsp104p (908 amino acids) and New1p (1196 amino acids). Cells were collected in a time course following puromycin or vehicle addition. In cultures not treated with puromycin, anti-HA immunoreactivity increases starting at 15 minutes of growth in galactose (Figure 3.6). The larger proteins exhibited reduced signal compared with HA-Ade17p, which presumably reflects the extra time involved in translating the additional 300-600 residues per protein and also the decreased efficiency for western blot transfer of large proteins[47]. When the same strains were treated with puromycin, the production of HA signal was reduced for all three proteins relative to the untreated cells (Figure 3.6). This

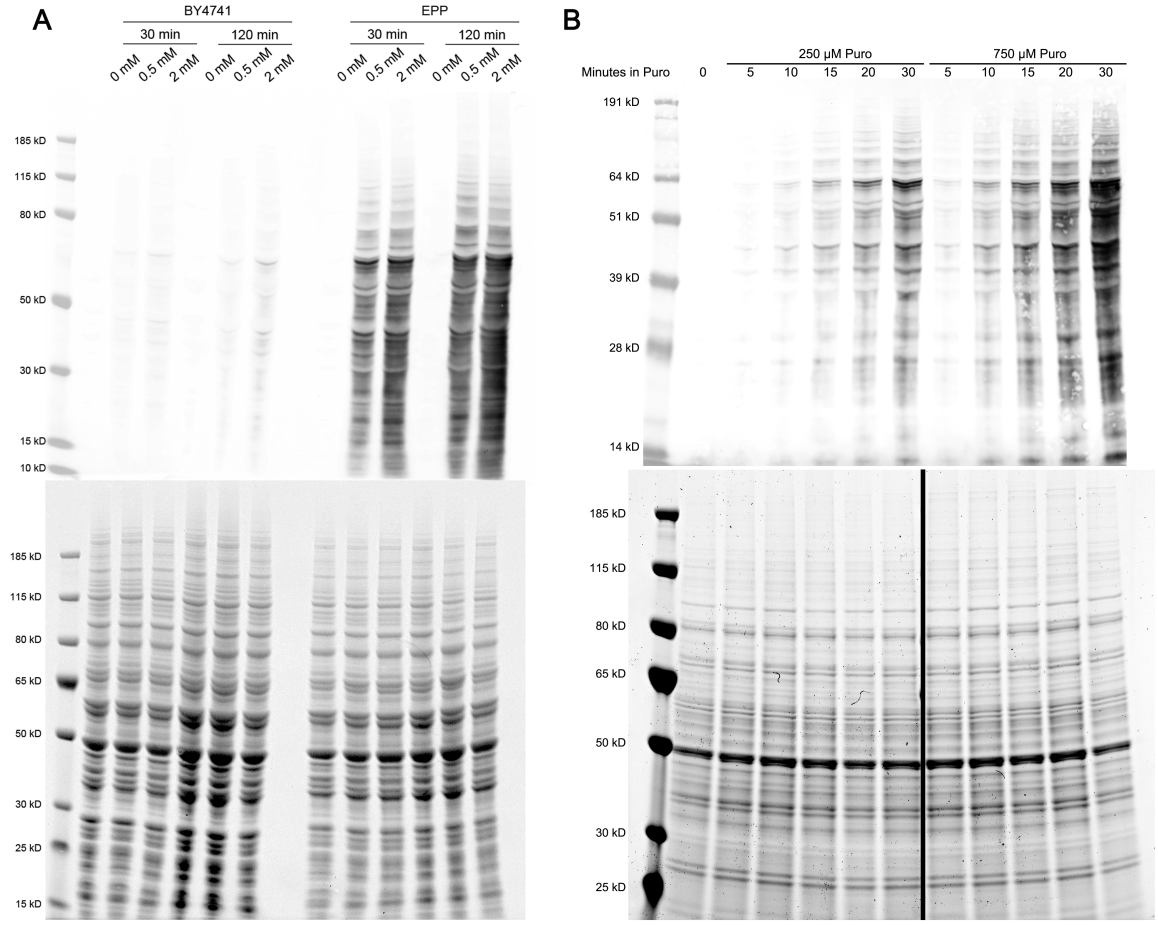

Figure 3.4 Puromycin is rapidly incorporated into proteins in the EPP strain.
(A) Anti-puromycin (12D10) western blot of lysates from wild type and EPP strains following 30 min and 120 min of exposure to puromycin and a Coomassie stain demonstrating loading equivalency. (B) Time-course of the EPP strain grown in 250 µM and 750 µM puromycin and a Coomassie stain demonstrating loading equivalency.

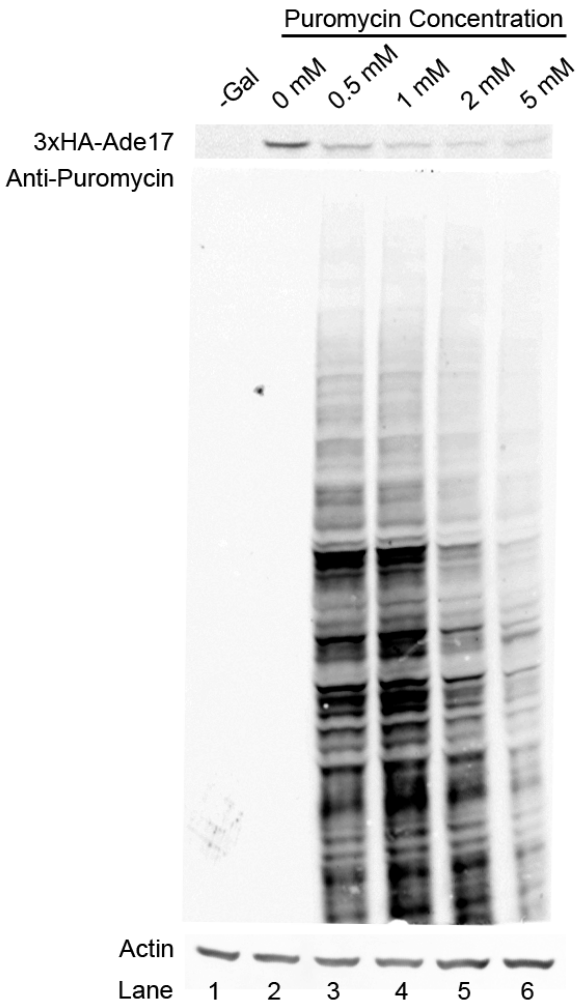

Figure 3.5 Dose-response effect of puromycin treatment on protein translation *in vivo*. Anti-HA (12CA5) and anti-puromycin (12D10) western blots of a galactose-induced 3xHA-Ade17p strain grown in 0mM-2mM puromycin for 15 minutes. No galactose induction was present for the sample marked –Gal, while the other samples were grown in 2% galacotse for 15 minutes prior to puromycin addition. Anti-actin is shown to demonstrate loading equivalency.

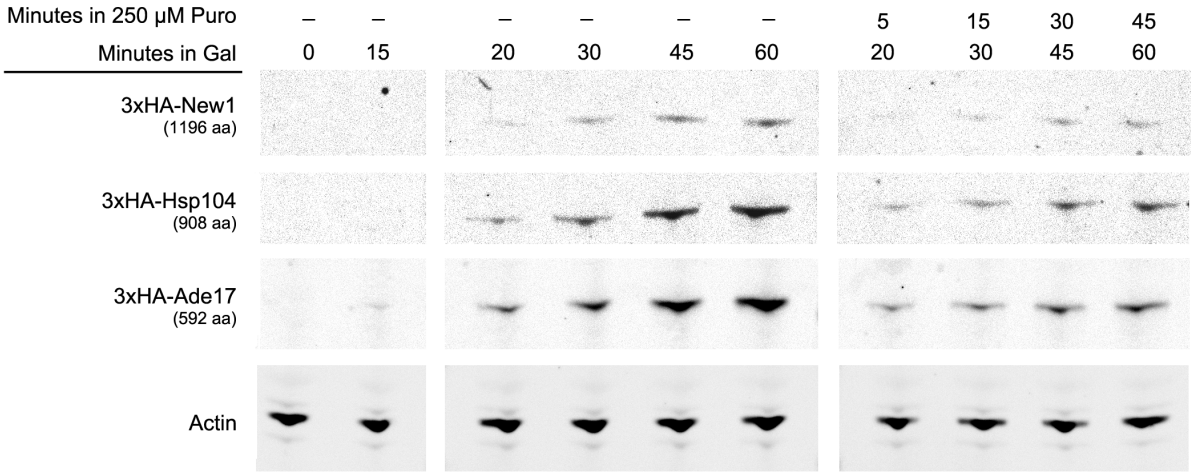

Figure 3.6 Time course of translation in the presence and absence of puromycin
Time course of strains expressing galactose-induced N-terminally 3xHA-tagged ORFs grown in 0 μM or 250 μM puromycin. The ORFs tested are 3xHA-Ade17p (592 amino acids); 3xHA-Hsp104p (908 amino acids); 3xHA-New1p (1196 amino acids). Anti-actin is shown to demonstrate loading equivalency.

signifies that proteins of a range of sizes are affected by puromycin incorporation and there does not appear to be a drastic bias toward longer or shorter proteins for puromycin incorporation.

Puromycin analogs, such as O-propargyl-puromycin (OP-puromycin), enable more sophisticated inquiries into translational activity including visualization of translational activity and capture of nascent proteins. We tested whether the EPP mutant strain is also able to incorporate OP-puromycin. Growing the EPP strain in 500μM OP-puromycin was sufficient to inhibit the expression of HA-Ade17p and incorporate into proteins, generating 12D10 immunoreactivity (Figure 3.7). While the anti-puromycin immunoreactivity of the OP-puromycin treated lysates was reduced compared to the cells treated with an equal dose of puromycin, inhibition of the production of the HA-tagged ORF is equivalent. This suggests there may be different sensitivities of the 12D10 antibody to puromycin and OP-puromycin labeled proteins.

We also tested the effects of OP-puromycin on peptide fragmentation by collision-induced dissociation (CID) in an ion trap mass spectrometer (MS). To do so OP-puromycin was conjugated to a synthetic peptide with an azido-lysine terminal residue using CuAAC chemistry. However, the puromycin orientation with respect to the peptide is not as would be expected for *in vivo* incorporated puromycin peptides, through a peptide linkage, but rather conjugated to the terminal lysine side chain (Figure 3.8A and 3.8B). Subjecting OP-puromycin to CID, the base peak of the tandem mass spectrum corresponds to loss of the dimethyl-aminopurine ring (Figure 3.8C). This reflects what is known concerning the mass spectrometric fragmentation of

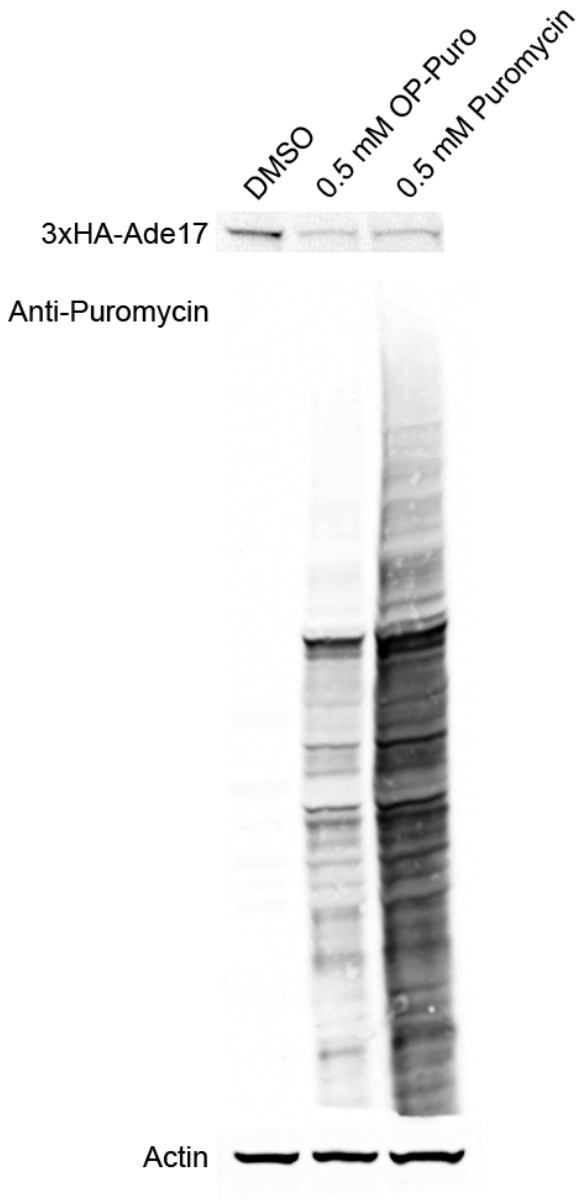

Figure 3.7 OP-puromycin incorporation and effects on translation
Anti-puromycin (12D10) western blot of cells grown in either 0.5mM OP-puromycin, puromycin or DMSO and anti-HA (12CA5) western blot of 3xHA-Ade17p expression in each condition.

Figure 3-S3

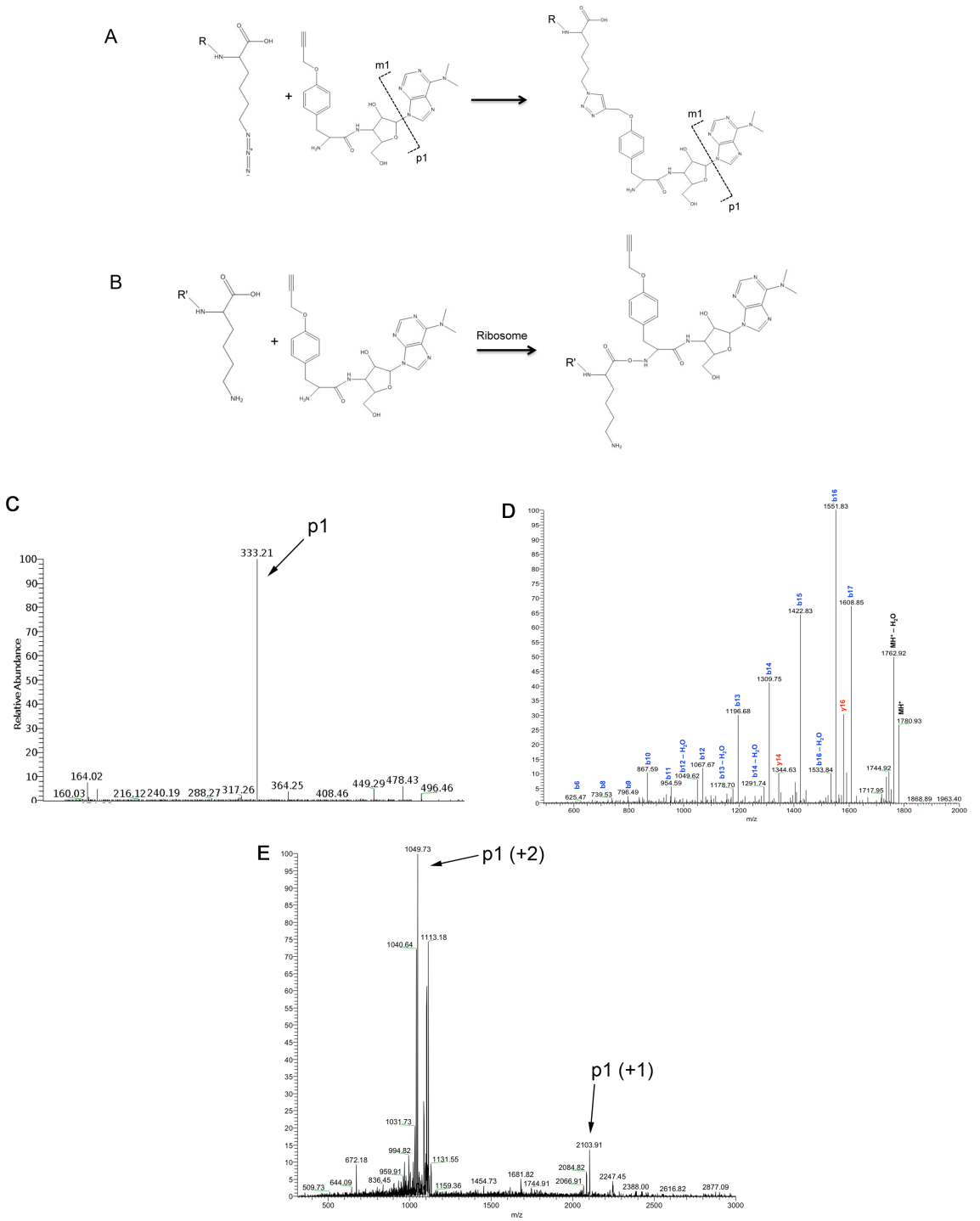

Figure 3.8 Mass spectrometric analysis of OP-puromycin and OP-puromycin-peptide adducts.

(A) Structures of the peptide CuAAC scheme. In our experiments R corresponds to the synthetic peptide ISHVVSTGGGASLELLEG with the terminal azido-lysine shown. The expected masses of m1 and p1 from OP-puromycin are 162m/z and 333m/z respectively whereas the expected masses of m1 and p1 from the CuAAC product are 162m/z and 2108m/z respectively. (B) Hypothetical *in vivo* ribosome mediated puromycinylation. Tandem mass spectra of (C) OP-Puromycin, (D) ISHVVSTGGGASLELLEG-K_{azide}, (E) and the CuAAC product, OP-puromycin conjugated peptide in +2 charge states, p1 (+1) corresponds to the singly charged fragment ion and p1 (+2) corresponds to the doubly charged fragment ion.

puromycin and related compounds, where a common fragment ion forms due to loss of the purine ring from the sugar[48]. Tandem MS of the pre-conjugated synthetic peptide resulted in observation of the b- and y-series fragment ions common to peptides subjected to CID, and which correspond well to the consensus fragmentation pattern reported in the PeptideAtlas for the native peptide (Figure 3.8D). When we subjected the product of the peptide-OP-puromycin conjugation to CID, the base peak in the tandem mass spectra corresponded to loss of dimethylaminopurine (Figure 3.8E) with no detectable b- and y- fragment ions. These data indicate that the loss of the purine ring from a puromycin-peptide represents cleavage of the most labile bond producing a tandem mass spectrum devoid of peptide backbone fragment ions. This suggests that efficient identification of puromycin labeled proteins and peptides of unknown sequence by mass spectrometry will require either enrichment by puromycin capture or the development of MS3 based tandem MS approaches popular in the phosphoproteomic field for similar reasons; i.e. facile loss of phosphate during CID resulting in few detectable b- or y-ions. In such an MS3 based strategy after MS2 detection of the loss of dimethylaminopurine would trigger MS2 on the subsequent base peak.

This work demonstrates *in vivo* puromycin sensitivity in *S. cerevisiae*. The increase in sensitivity is attributable to an increase in cell permeability by disruption of the multi-drug efflux system and sterol synthesis. Both the physiological effect of P-body induction and the increase in puromycin immunoreactivity indicate that puromycin is acting *in vivo* in a similar manner to its actions in other systems. Because puromycin

incorporation acts as a label of translational activity, the characterization of the EPP strain enables yeast researchers to utilize the tools of puromycin-based assays including visualizing the location of protein translation across conditions or cell states, the ability to capture puromycin labeled proteins and peptides for proteomic analysis, and the assessment of co-translational versus post-translational protein modifications. Furthermore, development of these and other puromycin-based assays will be facilitated by the many advantages of the yeast model. Yeast researchers have been on the forefront of developing and implementing assays to explore translation, and the ability to incorporate puromycin *in vivo* enables the development of new and complementary techniques to enrich the understanding post-transcriptional regulatory mechanisms.

References

[1] McCarthy, J. E. Posttranscriptional control of gene expression in yeast. *Microbiology and molecular biology reviews : MMBR* **62**, 1492-1553 (1998).

[2] Kim, W. & Kyung Lee, E. Post-transcriptional regulation in metabolic diseases. *RNA biology* **9**, 772-780, doi:10.4161/rna.20091 (2012).

[3] Anderson, P. Post-transcriptional regulons coordinate the initiation and resolution of inflammation. *Nature reviews. Immunology* **10**, 24-35, doi:10.1038/nri2685 (2010).

[4] Freeman, J. A. & Espinosa, J. M. The impact of post-transcriptional regulation in the p53 network. *Briefings in functional genomics* **12**, 46-57, doi:10.1093/bfgp/els058 (2013).

[5] Nousch, M. & Eckmann, C. R. Translational control in the Caenorhabditis elegans germ line. *Advances in experimental medicine and biology* **757**, 205-247, doi:10.1007/978-1-4614-4015-4_8 (2013).

[6] Ingolia, N. T., Ghaemmaghami, S., Newman, J. R. & Weissman, J. S. Genome-wide analysis in vivo of translation with nucleotide resolution using ribosome profiling. *Science (New York, N.Y.)* **324**, 218-223, doi:10.1126/science.1168978 (2009).

[7] Pospisek, M. & Valasek, L. Polysome profile analysis--yeast. *Methods in enzymology* **530**, 173-181, doi:10.1016/b978-0-12-420037-1.00009-9 (2013).

[8] Halbeisen, R. E., Scherrer, T. & Gerber, A. P. Affinity purification of ribosomes to access the translatome. *Methods (San Diego, Calif.)* **48**, 306-310, doi:10.1016/j.ymeth.2009.04.003 (2009).

[9] Ong, S. E. *et al.* Stable isotope labeling by amino acids in cell culture, SILAC, as a simple and accurate approach to expression proteomics. *Molecular & cellular proteomics : MCP* **1**, 376-386 (2002).

[10] Hinz, F. I., Dieterich, D. C., Tirrell, D. A. & Schuman, E. M. Non-canonical amino acid labeling in vivo to visualize and affinity purify newly synthesized proteins in larval zebrafish. *ACS chemical neuroscience* **3**, 40-49, doi:10.1021/cn2000876 (2012).

[11] Brengues, M., Teixeira, D. & Parker, R. Movement of eukaryotic mRNAs between polysomes and cytoplasmic processing bodies. *Science (New York, N.Y.)* **310**, 486-489, doi:10.1126/science.1115791 (2005).

[12] Whitney, M. L., Hurto, R. L., Shaheen, H. H. & Hopper, A. K. Rapid and reversible nuclear accumulation of cytoplasmic tRNA in response to nutrient availability. *Molecular biology of the cell* **18**, 2678-2686, doi:10.1091/mbc.E07-01-0006 (2007).

[13] Schwanhausser, B., Gossen, M., Dittmar, G. & Selbach, M. Global analysis of cellular protein translation by pulsed SILAC. *Proteomics* **9**, 205-209, doi:10.1002/pmic.200800275 (2009).

[14] Hansen, W. J., Lingappa, V. R. & Welch, W. J. Complex environment of nascent polypeptide chains. *The Journal of biological chemistry* **269**, 26610-26613 (1994).

[15] Schmeing, T. M. *et al.* A pre-translocational intermediate in protein synthesis observed in crystals of enzymatically active 50S subunits. *Nature structural biology* **9**, 225-230, doi:10.1038/nsb758 (2002).

[16] Eulalio, A., Behm-Ansmant, I., Schweizer, D. & Izaurralde, E. P-body formation is a consequence, not the cause, of RNA-mediated gene silencing. *Molecular and cellular biology* **27**, 3970-3981, doi:10.1128/mcb.00128-07 (2007).

[17] Miyamoto-Sato, E., Nemoto, N., Kobayashi, K. & Yanagawa, H. Specific bonding of puromycin to full-length protein at the C-terminus. *Nucleic acids research* **28**, 1176-1182 (2000).

[18] Tabuchi, I. Next-generation protein-handling method: puromycin analogue technology. *Biochemical and biophysical research communications* **305**, 1-5 (2003).

[19] Roberts, R. W. & Szostak, J. W. RNA-peptide fusions for the in vitro selection of peptides and proteins. *Proceedings of the National Academy of Sciences of the United States of America* **94**, 12297-12302 (1997).

[20] Starck, S. R., Green, H. M., Alberola-Ila, J. & Roberts, R. W. A general approach to detect protein expression in vivo using fluorescent puromycin conjugates. *Chemistry & biology* **11**, 999-1008, doi:10.1016/j.chembiol.2004.05.011 (2004).

[21] Aviner, R., Geiger, T. & Elroy-Stein, O. Novel proteomic approach (PUNCH-P) reveals cell cycle-specific fluctuations in mRNA translation. *Genes & development* **27**, 1834-1844, doi:10.1101/gad.219105.113 (2013).

[22] Schmidt, E. K., Clavarino, G., Ceppi, M. & Pierre, P. SUnSET, a nonradioactive method to monitor protein synthesis. *Nature methods* **6**, 275-277, doi:10.1038/nmeth.1314 (2009).

[23] Liu, J., Xu, Y., Stoleru, D. & Salic, A. Imaging protein synthesis in cells and tissues with an alkyne analog of puromycin. *Proceedings of the National Academy of Sciences of the United States of America* **109**, 413-418, doi:10.1073/pnas.1111561108 (2012).

[24] Schindler, D. & Davies, J. Inhibitors of macromolecular synthesis in yeast. *Methods in cell biology* **12**, 17-38 (1975).

[25] Melcher, U. Metabolism of puromycin by yeast cells. *Biochimica et biophysica acta* **246**, 216-224 (1971).

[26] Halegoua, S., Hirashima, A. & Inouye, M. Puromycin-resistant biosynthesis of a specific outer-membrane lipoprotein of Escherichia coli. *Journal of bacteriology* **126**, 183-191 (1976).

[27] Winston, F., Dollard, C. & Ricupero-Hovasse, S. L. Construction of a set of convenient Saccharomyces cerevisiae strains that are isogenic to S288C. *Yeast (Chichester, England)* **11**, 53-55, doi:10.1002/yea.320110107 (1995).

[28] Rose MD, W. F., Hieter P. . (Cold Spring Harbor, NY, 1990).

[29] Dunstan, H. M. *et al.* Cell-based assays for identification of novel double-strand break-inducing agents. *Journal of the National Cancer Institute* **94**, 88-94 (2002).

[30] Giaever, G. *et al.* Functional profiling of the Saccharomyces cerevisiae genome. *Nature* **418**, 387-391, doi:10.1038/nature00935 (2002).

[31] Huh, W. K. *et al.* Global analysis of protein localization in budding yeast. *Nature* **425**, 686-691, doi:10.1038/nature02026 (2003).

[32] Selinummi, J. *Supplement Site for Cell3 Software*, <https://sites.google.com/site/cell3supplement/> (

[33] Ruusuvuori, P. *et al.* Evaluation of methods for detection of fluorescence labeled subcellular objects in microscope images. *BMC bioinformatics* **11**, 248, doi:10.1186/1471-2105-11-248 (2010).

[34] Niemisto, A. *et al.* A K-means segmentation method for finding 2-D object areas based on 3-D image stacks obtained by confocal microscopy. *Conference proceedings : ... Annual International Conference of the IEEE Engineering in Medicine and Biology Society. IEEE Engineering in Medicine and Biology Society. Conference* **2007**, 5559-5562, doi:10.1109/iembs.2007.4353606 (2007).

[35] Kushnirov, V. V. Rapid and reliable protein extraction from yeast. *Yeast (Chichester, England)* **16**, 857-860, doi:10.1002/1097-0061(20000630)16:9<857::aid-yea561>3.0.co;2-b (2000).

[36] Shaffer, S. A. *et al.* A novel ion funnel for focusing ions at elevated pressure using electrospray ionization mass spectrometry. *Rapid Communications in Mass Spectrometry* **11**, 1813-1817, doi:10.1002/(SICI)1097-0231(19971030)11:16<1813::AID-RCM87>3.0.CO;2-D (1997).

[37] Page, J. S., Tang, K. & Smith, R. D. An electrodynamic ion funnel interface for greater sensitivity and higher throughput with linear ion trap mass spectrometers. *International Journal of Mass Spectrometry* **265**, 244-250, doi:http://dx.doi.org/10.1016/j.ijms.2007.02.032 (2007).

[38] Barbacid, M., Fresno, M. & Vazquez, D. Inhibitors of polypeptide elongation on yeast polysomes. *The Journal of antibiotics* **28**, 453-462 (1975).

[39] Pfund, C. *et al.* The molecular chaperone Ssb from Saccharomyces cerevisiae is a component of the ribosome-nascent chain complex. *The EMBO journal* **17**, 3981-3989, doi:10.1093/emboj/17.14.3981 (1998).

[40] Medina, D., Moskowitz, N., Khan, S., Christopher, S. & Germino, J. Rapid purification of protein complexes from mammalian cells. *Nucleic acids research* **28**, E61 (2000).

[41] Iwaki, T. & Castellino, F. J. A single plasmid transfection that offers a significant advantage associated with puromycin selection in Drosophila Schneider S2 cells expressing heterologous proteins. *Cytotechnology* **57**, 45-49, doi:10.1007/s10616-008-9129-0 (2008).

[42] Iwaki, T. & Umemura, K. A single plasmid transfection that offers a significant advantage associated with puromycin selection, fluorescence-assisted cell sorting, and doxycycline-inducible protein expression in mammalian cells. *Cytotechnology* **63**, 337-343, doi:10.1007/s10616-011-9357-6 (2011).

[43] Parker, R. & Sheth, U. P bodies and the control of mRNA translation and degradation. *Molecular cell* **25**, 635-646, doi:10.1016/j.molcel.2007.02.011 (2007).

[44] Aizer, A. *et al.* The dynamics of mammalian P body transport, assembly, and disassembly in vivo. *Molecular biology of the cell* **19**, 4154-4166, doi:10.1091/mbc.E08-05-0513 (2008).

[45] Swetloff, A. *et al.* Dcp1-bodies in mouse oocytes. *Molecular biology of the cell* **20**, 4951-4961, doi:10.1091/mbc.E09-02-0123 (2009).

[46] Longtine, M. S. *et al.* Additional modules for versatile and economical PCR-based gene deletion and modification in Saccharomyces cerevisiae. *Yeast (Chichester, England)* **14**, 953-961, doi:10.1002/(sici)1097-0061(199807)14:10<953::aid-yea293>3.0.co;2-u (1998).

[47] Bolt, M. W. & Mahoney, P. A. High-efficiency blotting of proteins of diverse sizes following sodium dodecyl sulfate-polyacrylamide gel electrophoresis. *Analytical biochemistry* **247**, 185-192, doi:10.1006/abio.1997.2061 (1997).

[48] Eggers, S. H., Biedron, S. I. & Hawtrey, A. O. Mass spectra of puromycin and some derivatives. *Tetrahedron letters* **28**, 3271-3280 (1966).

Chapter 4: Perspectives & Future Directions

The work presented in this dissertation provides new techniques and novel perspectives to the field of post-transcriptional research. Within this work, I have characterized yeast strains sensitive to puromycin and demonstrated the utility of this approach for the examination of protein biosynthesis *in vivo*. This enables the implementation of the array of puromycin-based assays of translational activity in yeast. For example, O-propargyl-puromycin has been used to visualize intracellular sites of translational activity[1] and a similar assay could be used to investigate the hypothesis that P-body localization to the bud site prior to bud emergence is involved in the localized translation of bud-specific proteins [Garmendia Torres and Dudley, personal communication]. Recent work has demonstrated the utility of ribosome mediated protein puromycinylation for the purposes of measuring the translatome by tandem mass spectrometry in human cells[2]. Implementation of an analogous approach in yeast would facilitate the further development of these technologies. For example, the authors needed to label proteins *ex vivo*, but utilization of OP-puromycin in yeast could enable the labeling and capture of *in vivo* puromycinylated proteins. In addition, the authors made no report of puromycin incorporation sites within the proteins identified, likely due to the inability to measure peptide backbone fragmentation in puromycin-incorporated peptides. The development of methods to measure puromycin incorporation on the peptide level could be accomplished more easily by utilizing the

relatively simple yeast proteome. Ribosome mediated puromycin labeling of proteins *in vivo* could also enable more precise investigation of protein modifications that occur co-translationally versus those that occur post-translationally. N-terminal acylation of proteins affects a variety of important expression characteristics including intracellular localization, protein interactions, and stability[3] and the modification is known to occur both co- and post-translationally[4]. Using puromycin incorporation to label nascent proteins could be a useful tool for dissecting the relative contributions, timing, and significance of these and other protein modifications. Finally, puromycin labeling could be useful for exploring protein quality control as other groups have shown that puromycin labeled proteins are targeted to ubiquitinylated aggregate structures within human cells[5]. The development of these and other technologies will be facilitated by the ability to work in the yeast model system because of its relative simplicity and because of the many complementary techniques and data sources already available.

This work also demonstrates the first specific enrichment of an RNA granule complex measuring both protein and RNA constituents. Because RNA granules are highly dynamic non-membrane bound organelles *in vivo*, it was important to consider approaches to stabilize the complex *in vitro* for enrichment by immunoprecipitation. However, by implementing a number of experimental strategies specifically designed to minimize dynamic exchange during the purification process, we were able to demonstrate reproducible and specific enrichment of RNA granules from the yeast lysate. The ability to enrich these structures allows for the interrogation of protein and RNA constituents as well as the exploration of *in vivo* compositional dynamics.

A striking difference between the stress induced and the uninduced complexes we measured was the increase in abundance of many metabolic enzymes in the stress induced condition. This result suggests that yeast RNA granules associate with metabolic enzymes primarily in response to cell stress. Intriguingly, many metabolic enzymes have been observed to form reversible cytoplasmic foci upon nutrient deprivation[6]. These foci were observed to persist for up to a week in continuous culture of cells in stationary phase and also rapidly disassembled in response to nutrient re-addition[7]. Therefore, these foci are most likely not due to a buildup of protein degradation substrates, but rather represent a potential mechanism for cellular protein storage in conditions where these metabolic pathways are of limited utility. These assemblies can maintain the constituent proteins - presumably in inactive states - until they are needed again by the cell. A similar logic may underlie the accumulation of RNA granule proteins and translationally quiescent mRNAs during stress. Because translation is one of the most energetically expensive processes within the cell[8], it is deleterious for cells to unnecessarily produce proteins when they are not necessary to the survival of the cell. For example the overexpression of ectopic mRNA in cells unable to form P-body aggregates leads to an increase in ectopic RNA translation, increased sensitivity to various stress conditions, and a decrease in cellular viability relative to wild type cells[9]. Also, in response to various stresses yeast are known to rapidly and reversibly accumulate tRNA in the nucleus, potentially as a mechanism to sequester a critical substrate in protein biosynthesis and impede translation for the duration of the stress[10,11]. In addition, the formation of RNA granule foci is important for the long-term survival of cells in stationary phase[12]. The accumulation of metabolic

enzymes along with RNA granule complexes suggests a common cellular mechanism to sequester energetically expensive biological processes not essential to survival during exposure to specific stressors. Further experiments should explore interactions between these structures and aim to identify common regulatory mechanisms and organizational principles.

Finally, it is becoming increasingly clear the central role these RNA granule aggregates have in neurodegenerative processes. Many genes for RNA granule components have been genetically associated with neurodegenerative pathologies - including the genes TDP-43, FUS, SMN1, FMR1, and ATXN2. The clustering of mutations in genes whose protein product localizes to RNA granules suggests that RNA granule processes may be associated with these pathologies. Recent reviews have explored these potential associations to great lengths[13-15]. It appears that motorneurons may be especially susceptible to RNA granule associated pathologies as many of these gene products are associated with motorneuronopathies including amyotrophic lateral sclerosis (TDP-43, ATXN2) and spinal muscular atrophy (SMN1). In addition to the localization of many of these disease-associated proteins with RNA granule structures, there are other RNA granule associated functions that are perturbed in these disease processes. We observe an association between yeast RNA granules and proteins containing domains of low complexity as well as chaperones, and demonstrate that the Hsp40 chaperone Ydj1p is involved in the aggregation of P-body proteins. These results highlight the role of protein folding and aggregation in RNA granule accumulation; protein mis-folding and aggregation are phenotypes common to many neurological pathologies[16-18]. We, and others, have shown that RNA granules are

associated with intracellular transport mechanisms including cytoskeleton-dependent transport; defects in protein and organelle intracellular trafficking have been reported in several neurodegenerative disease models[19-21]. Finally, we demonstrate a close association with metabolic pathways by demonstrating the condition-specific association between metabolic enzymes and RNA granules as well as association between critical mitochondrial RNA processing factors and P-bodies; defects in energy homeostasis have also been associated with neurodegenerative phenotypes[22]. These common functions suggest that mi-regulation of post-transcriptional processes in or associated with RNA granules may be broadly associated with neurological pathologies. For this reason, it is critical to continue to study the specific mis-regulation of post-transcriptional processes that occur within degenerating neurons and associated tissues. A more complete understanding of the basic mechanics underlying post-transcriptional regulatory processes including how and why RNA granule proteins aggregate, how transcripts are targeted to or excluded from RNA granule aggregates, and how cells regulate which transcripts are translated at a given time and place will add to our understanding of how mis-regulation of these processes can lead to disease. Finally, as demonstrated in this work, yeast represents a powerful model for interrogating post-transcriptional regulatory processes and the approaches presented here should allow for further investigations into the role of post-transcriptional regulatory dynamics associated with RNA granules in the future.

References

[1] Liu, J., Xu, Y., Stoleru, D. & Salic, A. Imaging protein synthesis in cells and tissues with an alkyne analog of puromycin. *Proceedings of the National Academy of Sciences of the United States of America* **109**, 413-418, doi:10.1073/pnas.1111561108 (2012).

[2] Aviner, R., Geiger, T. & Elroy-Stein, O. Novel proteomic approach (PUNCH-P) reveals cell cycle-specific fluctuations in mRNA translation. *Genes & development* **27**, 1834-1844, doi:10.1101/gad.219105.113 (2013).

[3] Hollebeke, J., Van Damme, P. & Gevaert, K. N-terminal acetylation and other functions of Nalpha-acetyltransferases. *Biological chemistry* **393**, 291-298, doi:10.1515/hsz-2011-0228 (2012).

[4] Iqbal, Z. *et al.* Influence of the sequence environment and properties of neighboring amino acids on amino-acetylation: relevance for structure-function analysis. *Journal of cellular biochemistry* **114**, 874-887, doi:10.1002/jcb.24426 (2013).

[5] Lelouard, H. *et al.* Dendritic cell aggresome-like induced structures are dedicated areas for ubiquitination and storage of newly synthesized defective proteins. *J Cell Biol* **164**, 667-675, doi:10.1083/jcb.200312073 (2004).

[6] O'Connell, J. D., Zhao, A., Ellington, A. D. & Marcotte, E. M. Dynamic reorganization of metabolic enzymes into intracellular bodies. *Annual review of cell and developmental biology* **28**, 89-111, doi:10.1146/annurev-cellbio-101011-155841 (2012).

[7] Narayanaswamy, R. *et al.* Widespread reorganization of metabolic enzymes into reversible assemblies upon nutrient starvation. *Proceedings of the National Academy of Sciences of the United States of America* **106**, 10147-10152, doi:10.1073/pnas.0812771106 (2009).

[8] Topisirovic, I. & Sonenberg, N. mRNA translation and energy metabolism in cancer: the role of the MAPK and mTORC1 pathways. *Cold Spring Harbor symposia on quantitative biology* **76**, 355-367, doi:10.1101/sqb.2011.76.010785 (2011).

[9] Lavut, A. & Raveh, D. Sequestration of highly expressed mRNAs in cytoplasmic granules, P-bodies, and stress granules enhances cell viability. *PLoS Genet* **8**, e1002527, doi:10.1371/journal.pgen.1002527 (2012).

[10] Whitney, M. L., Hurto, R. L., Shaheen, H. H. & Hopper, A. K. Rapid and reversible nuclear accumulation of cytoplasmic tRNA in response to nutrient availability. *Molecular biology of the cell* **18**, 2678-2686, doi:10.1091/mbc.E07-01-0006 (2007).

[11] Miyagawa, R., Mizuno, R., Watanabe, K. & Ijiri, K. Formation of tRNA granules in the nucleus of heat-induced human cells. *Biochemical and biophysical research communications* **418**, 149-155, doi:10.1016/j.bbrc.2011.12.150 (2012).

[12] Ramachandran, V., Shah, K. H. & Herman, P. K. The cAMP-dependent protein kinase signaling pathway is a key regulator of P body foci formation. *Molecular cell* **43**, 973-981, doi:10.1016/j.molcel.2011.06.032 (2011).

[13] Ramaswami, M., Taylor, J. P. & Parker, R. Altered ribostasis: RNA-protein granules in degenerative disorders. *Cell* **154**, 727-736, doi:10.1016/j.cell.2013.07.038 (2013).

[14] Vanderweyde, T., Youmans, K., Liu-Yesucevitz, L. & Wolozin, B. Role of Stress Granules and RNA-Binding Proteins in Neurodegeneration: A Mini-Review. *Gerontology* **59**, 524-533, doi:10.1159/000354170 (2013).

[15] Wolozin, B. Regulated protein aggregation: stress granules and neurodegeneration. *Molecular neurodegeneration* **7**, 56, doi:10.1186/1750-1326-7-56 (2012).

[16] Jellinger, K. A. Interaction between pathogenic proteins in neurodegenerative disorders. *Journal of cellular and molecular medicine* **16**, 1166-1183, doi:10.1111/j.1582-4934.2011.01507.x (2012).

[17] Olanow, C. W. & Brundin, P. Parkinson's disease and alpha synuclein: is Parkinson's disease a prion-like disorder? *Movement disorders : official journal of the Movement Disorder Society* **28**, 31-40, doi:10.1002/mds.25373 (2013).

[18] Forloni, G., Sclip, A., Borsello, T. & Balducci, C. The neurodegeneration in Alzheimer disease and the prion protein. *Prion* **7**, 60-65, doi:10.4161/pri.23286 (2013).

[19] Atkin, J. D. *et al.* Mutant SOD1 inhibits ER-Golgi transport in amyotrophic lateral sclerosis. *Journal of neurochemistry*, doi:10.1111/jnc.12493 (2013).

[20] Lucin, K. M. *et al.* Microglial beclin 1 regulates retromer trafficking and phagocytosis and is impaired in Alzheimer's disease. *Neuron* **79**, 873-886, doi:10.1016/j.neuron.2013.06.046 (2013).

[21] Eisbach, S. E. & Outeiro, T. F. Alpha-synuclein and intracellular trafficking: impact on the spreading of Parkinson's disease pathology. *Journal of molecular medicine (Berlin, Germany)* **91**, 693-703, doi:10.1007/s00109-013-1038-9 (2013).

[22] Weydt, P. *et al.* Thermoregulatory and metabolic defects in Huntington's disease transgenic mice implicate PGC-1alpha in Huntington's disease neurodegeneration. *Cell metabolism* **4**, 349-362, doi:10.1016/j.cmet.2006.10.004 (2006).

Appendix: Androgen receptor function in motor neuron survival and degeneration

Gregory A. Cary, BA[a,b], Albert R. La Spada, MD, PhD[a,c,d,e,f,*]

[a]Department of Laboratory Medicine, University of Washington Medical Center, Box 357110, Room NW 120, Seattle, WA 98195-7110, USA

[b]Molecular & Cellular Biology Program, University of Washington, Seattle, WA, USA

[c]Department of Neurology, University of Washington, Seattle, WA, USA

[d]Department of Medicine, University of Washington, Seattle, WA, USA

[e]Department of Pathology, University of Washington, Seattle, WA, USA

[f]Center for Neurogenetics & Neurotherapeutics, University of Washington, Seattle, WA, USA

Phys Med Rehabil Clin N Am 19 (2008) 479–494
doi:10.1016/j.pmr.2008.03.002

Abstract

Polyglutamine repeat expansion in the androgen receptor is responsible for the motor neuron degeneration in X-linked spinal and bulbar muscular atrophy (SBMA; Kennedy's disease). This mutation, like the other polyglutamine repeat expansions, has proven to be toxic itself by a gain-of-function effect; however, a growing body of evidence indicates that loss of androgen receptor normal function simultaneously contributes to SBMA disease pathology, and, conversely, that normal androgen receptor signaling mediates important trophic effects upon motor neurons. This review considers the trophic requirements of motor neurons, focusing upon the role of known neurotrophic factors in motor neuron disease natural history, and the interactions of androgen receptor signaling pathways with motor neuron disease pathogenesis and progression. A thorough understanding of androgen receptor signaling in motor neurons should provide important inroads toward the development of effective treatments for a variety of devastating motor neuron diseases.

Introduction

The androgen receptor (AR) is a nuclear hormone receptor of approximately 110 kd that is responsible for the biological actions of androgens, including testosterone and its metabolite dihydrotestosterone (DHT). Androgens regulate a wide range of developmental and physiologic processes including the growth of muscle and bone, spermatogenesis, and the development of secondary sexual characteristics [1]. The AR mediates these effects primarily by influencing the expression of androgen responsive

genes. The AR affects transcription in a ligand-dependent manner by nuclear translocation, dimerization, DNA binding, and association with various co-activators/co-repressors and other components of the transcriptional machinery [2]. The functional domains of the AR – an N-terminal transcriptional activation domain, a DNA-binding domain (DBD) and a C-terminal ligand-binding domain (Fig. 1) – reflect these processes involved in androgen signaling. Both gain-of-function and loss-of-function mutations have been identified in the AR, and these alterations respectively give rise to distinct pathologies. These conditions include the various forms of androgen insensitivity syndromes (AIS): ranging from testicular feminization (Tfm) and partial androgen insensitivity syndrome (PAIS) to male infertility, prostate cancer (CaP), breast cancer susceptibility, and X-linked spinal and bulbar muscular atrophy (SBMA), which is also known as Kennedy's disease [3]. SBMA is of particular interest because it exhibits characteristics of both loss-of-function and gain-of-function mutations in the AR.

SBMA is a heritable, adult onset disease that causes preferential degeneration of lower motor neurons leading to weakness and atrophy of bulbar, facial, and limb muscles [4,5]. It is clinically similar to amyotrophic lateral sclerosis (ALS), another form of motor neuron disease (MND). The main clinical distinction between the two diseases is that ALS involves degeneration of both upper and lower motor neurons, whereas the affected cell type in SBMA is lower motor neurons. Another interesting difference is that Onuf's nucleus, an androgen-sensitive spinal cord motor neuron nucleus, is spared in ALS, although it degenerates in SBMA [6,7]. Degeneration of sensory neurons of the dorsal root ganglia is also a typical sign associated with SBMA, often preceding the onset of motor dysfunction [8,9]. In addition to the neurological

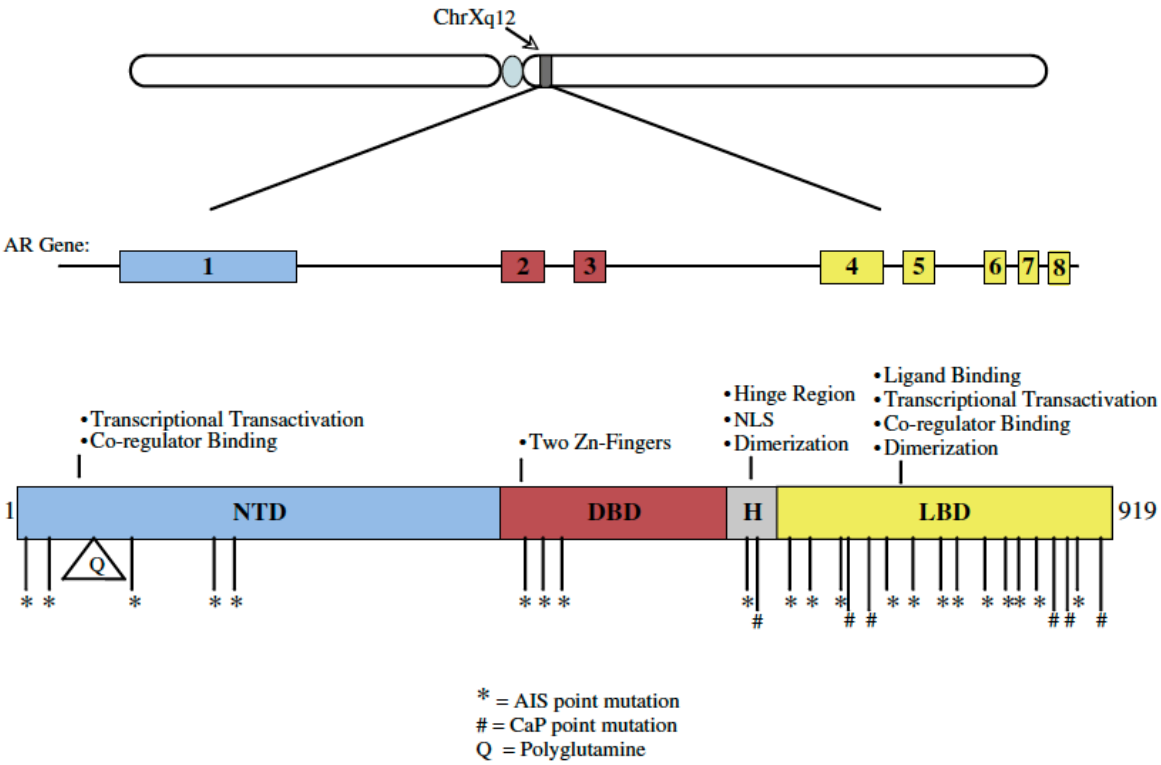

Appendix Figure 1 Schematic illustration of the androgen receptor.

The location of the androgen receptor locus on the long arm of the X chromosome at q12 (gray bar) and an expanded map of the androgen receptor gene, depicting the relative sizes and distribution of its eight exons, are shown. The colors of the exons reflect the different functional domains of the translated protein that are encoded by the various exons, including the amino-terminal domain (NTD; blue), the DNA-binding domain (DBD; red) and the ligand-binding domain (LBD; yellow). An illustration of the final protein product is shown below, highlighting these functional domains, along with the short hinge region (H). Representative disease-causing mutations have been identified and mapped onto the protein, including mutations that cause androgen insensitivity syndrome (AIS; *), mutations that are associated with prostate cancer (CaP; #), and the polyglutamine tract that is expanded in SBMA (Q).

phenotype, SBMA patients display some of the characteristic signs of androgen insensitivity syndromes including testicular atrophy, decreased fertility, gynecomastia, and elevated androgen levels [10,11]. This mild androgen insensitivity, along with the X-linked pattern of inheritance, caused the AR to be considered as a candidate gene for SBMA. This association was further supported by linkage mapping of the SBMA gene to a locus on the X chromosome that includes the AR gene [12]. Ultimately, the work to identify the gene responsible for SBMA led to the discovery of a novel mutation, the expansion of a trinucleotide CAG repeat, in the first exon of the AR gene [13]. This CAG repeat encodes a stretch of glutamine residues within the N-terminal transcriptional activation domain of the AR. Unaffected individuals have a polyglutamine repeat size that ranges between 5 and 35 glutamines, while symptomatic individuals always have a polyglutamine stretch of at least 37 glutamines [13]. This absolute association indicates that the polyglutamine expansion in the AR is the source of the pathology in SBMA. SBMA is a member of a family of nine dominantly inherited neurodegenerative diseases caused by polyglutamine (polyQ) repeat expansions in specific proteins. Other polyQ diseases include Hungtington's disease (HD), dentatorubral-pallidoluysian atrophy, and six forms of spinocerebellar ataxia. Interestingly, though each of the polyQ diseases has a CAG repeat expansion in a different gene, and each disease seems to specifically affect different subsets of neuronal populations, SBMA is the only polyQ repeat expansion disease known to cause selective degeneration of motor neurons [14]. This observation implies that there is something unique about AR biology that is important for motor neuron function.

Studies of other polyQ expansion diseases, as well as research specifically

investigating SBMA, indicate that the pathology associated with polyQ-expanded proteins is due to a toxic gain of function of the mutant protein [14–16]. The polyQ expansion of the AR in SBMA, like all polyQ repeat expansion diseases, is a dominantly inherited mutation; numerous lines of investigation, including ascertainment of homozygous females with CAG repeat expansions [17] and androgen ablation experiments in SBMA transgenic mouse models [18], have shown that SBMA disease pathogenesis requires AR activation by ligand binding. Heterozygous female carriers are thus spared the neurodegenerative SBMA phenotype due to a significantly reduced concentration of available ligands for the AR. Although considerable work in the polyQ research field has emphasized the polyQ protein misfolding gain-of-function toxicity as the principal mechanism for molecular pathology, gain-of-function and loss-of-function are not mutually exclusive explanations for the etiology of the disease. Indeed, numerous studies have implicated loss of polyQ protein normal function in the pathogenesis of each disease [19–25]. In the case of SBMA, one of the primary indicators of a loss of normal AR function is the mild androgen insensitivity phenotype that is seen in affected patients. This insensitivity reflects the fact that polyQ-expanded AR is not competent to fully stimulate androgen-dependent physiologic pathways or to fully maintain male secondary sexual characteristics. Consequently, in a motor neuron-like cell culture model of SBMA, cells transfected with polyQ-expanded AR differentially express genes in response to androgens when compared with cells expressing a non-pathologic form of AR [26], confirming that polyQ-expanded AR is not functionally interchangeable with unexpanded AR. In a highly representative SBMA transgenic mouse model, the authors' lab has further demonstrated that endogenous

mouse AR partially compensates for, and thus retards, motor neuron loss, as SBMA mice develop a more severe motor neuron phenotype when the endogenous AR is absent [18]. These observations indicate that normal AR might be playing a role in supporting motor neurons and protecting them from degeneration. Hence, polyQ-expanded AR is dysfunctional in this protective capacity, an effect that agonizes the process of motor neuron degeneration in SBMA. This article examines the evidence supporting the idea that normal AR has a protective, trophic role in motor neuron biology, first by examining the trophic requirements of motor neurons in general, and then by delineating the trophic properties of the AR in the central nervous system.

Trophic requirements of motor neurons

The neuronal requirements for trophic factor support are well established and have been investigated for over 50 years. Nerve growth factor (NGF) was the first target-derived neuronal growth factor identified. Since its discovery in 1951, a whole family of similar trophic factors, called neurotrophins, have been recognized [27–29]. Neurotrophins are small peptide growth hormones that promote neuronal differentiation, synaptic plasticity, regeneration, and survival [27–29]. The family includes molecules such as neurotrophin-3 (NT-3), brain-derived neurotrophic factor (BDNF), ciliary neurotrophic factor (CNTF), and glial cell line-derived neurotrophic factor (GDNF) [27–29]. Neurotrophin signals are transduced in a variety of ways, but most involve the activation of receptor tyrosine kinases. NGF, BDNF, and NT-3 involve signaling through the Trk receptors (ie, TrkA, TrkB, and TrkC) and also through the $p75^{NTR}$ (neurotrophin receptor). GDNF signals through the RET family of receptor

tyrosine kinases and CNTF signals through a receptor that is structurally very similar to the IL-6 receptor.

Of all of these neurotrophic factors, GDNF, BDNF, and CNTF display the greatest growth promotion and neuroprotective effects on motor neuron populations. GDNF is produced by glial cells of the CNS; is a very potent neuroprotective agent; and exerts its effects on both astrocytes and motor neurons. Mutations in murine GDNF are associated with a loss of 20%–30% of motor neurons [30], whereas GDNF over-expression prevents the developmental programmed cell death of motor neurons [31] and axotomy-induced motor neuron cell death [32]. Muscle from patients who have SBMA and ALS demonstrates decreased expression of GDNF [33]. BDNF is target-derived and retrogradely transported by motor neurons from muscle [34,35]. BDNF can also protect motor neurons from axotomy-induced cell death [36–38], as well as prevent toxic neuronal nitric oxide synthase production [39] and glutamate excitotoxicity [40,41]. Despite these protective effects, BDNF has shown little promise in the treatment of several MNDs, including ALS [42], though it did ameliorate the disease phenotype in the Wobbler mouse [43]. CNTF is a peptide growth factor that is produced predominantly by glial cells postnatally, but, unlike the other neurotrophins, does not contain a signal sequence, indicating that it is not normally secreted [44]. This has led some to hypothesize that CNTF release occurs in response to nerve injury [28]. Despite some conflicting reports [45,46], CNTF appears to rescue axotomized neurons from cell death [47]. In addition, both homozygous null CNTF mice [48] and mice deficient in the CNTFa receptor [49] develop motor neuron loss.

Beyond these classical neurotrophic factors, there are several other growth factors

that display motor neuron specific trophism, including vascular endothelial growth factor (VEGF) and insulin-like growth factor 1 (IGF-1). VEGF is a cytokine that is typically associated with angiogenesis and can support motor neurons by increasing local blood supply, but also exhibits many direct neuroprotective effects on motor neurons [50–52]. VEGF is able to promote the survival of motor neurons in vitro [53], and increase neurogenesis after axotomy [54]. Decreased VEGF levels have been correlated with various forms of MND including ALS, both in patients [55] and in mouse models, including the authors' transgenic mouse model of SBMA [56]. Intriguingly, deletion of a hypoxia-responsive element within the promoter of VEGF leads to the degeneration of motor neurons [57] and a correlation between VEGF promoter haplotypes and ALS has been observed [58]. In addition, VEGF treatment has been beneficial in a variety of models of MND [50–52,59].

IGF-1 is a peptide hormone produced by oligodendrocytes, Schwann cells, and muscle [60–62]. IGF-1 is a very potent trophic factor for motor neurons; it increases motor neuron survival both in vitro [63] and in an in vivo axotomy model [64]. IGF-1 also promotes motor neuron axonal sprouting, regeneration, and muscle innervation in vitro [65]. Targeting of IGF-1 to motor neurons slows the typical force decline seen in aging muscle [66]. Because IGF-1 is trophic for both motor neurons and muscle, there has been considerable interest in its potential protective capacity in various forms of MND. Most notably, viral delivery of IGF-1 dramatically slowed the progression of ALS in the SOD1 transgenic mouse model [67]. Additionally, the beneficial effects of IGF-1 in the Wobbler mouse model of MND are potentiated by glycosaminoglycans [68], and the neuroprotective effects of IGF-1 and GDNF act additively in the SOD1 mouse

model of ALS [69]. IGF-1 can decrease the toxicity associated with polyQ-expanded AR in vitro by stimulating the Akt phosphoylation of the AR, thereby preventing ligand binding and receptor activation [70]. These trophic factors play an important role in protecting motor neurons from many of the cytotoxic insults that lead to motor neuron cell death.

Trophic effects of the AR

The trophic effects of androgens on reproductive organs are well established. AR signaling is essential for the normal development of male sexual features, including sexual organ development as well as the formation and maintenance of secondary sexual characteristics, including increased body hair and muscle mass [1]. Beyond sexual development, androgen signaling has been associated with neoplastic prostate growth [71,72] and male breast carcinoma [73], which demonstrates the strong trophism of androgens. Hormonal castration, the prevention of androgen signaling, and silencing prostate AR expression have all been demonstrated to retard cancerous growth of the prostate [74,75]. In this context, the trophic effects of androgens have been causally linked with the ability of the AR to stimulate VEGF expression, thereby increasing angiogenesis. However, androgens, as well as other sex hormones, have also demonstrated trophic actions in non-reproductive tissues. Immunohistochemical investigation has confirmed the presence of the AR in a wide variety of human fetal extra-genital tissues including the thymus, bronchial epithelium, cardiac valves and surrounding muscle, and in the spinal cord [76]. The presence of the AR in these early tissues suggests that androgen signaling might not simply affect sexual differentiation,

but may be a broader signal for early growth and development of these tissues.

It is clear that AR expression in the spinal cord occurs as early as the first trimester and that high expression of AR within the spinal cord continues into adulthood. In a classic paper in 1977, Sar and Stumpf [77] demonstrated that androgen receptor expression is especially high in the ventral spinal cord. Therefore, it is reasonable to predict that AR signaling is important to the development and maintenance of this tissue, including especially spinal cord motor neurons. Studies of cell culture and animal models of spinal cord development have provided clues to the functions of androgens in such cell types. AR-expressing motor neuron-like cells in vitro exhibit changes in morphology in response to androgen treatment, including developing larger cell bodies and broader fields of neurite processes [78]. Further exploration of these effects indicates that this increased neurite outgrowth might be due to androgen-dependent up-regulation of neuritin, a protein previously demonstrated to be important for neurite elongation [79]. Another indication of the function of androgens in developing spinal cord motor neurons comes from careful investigation of the spinal nucleus of the bulbocavernosus (SNB), a sexually dimorphic nucleus of androgen-sensitive motor neurons in rodents that is analogous to Onuf's nucleus in humans. Androgen signaling has been demonstrated to influence soma size and dendrite length in SNB motor neurons [80]. These effects are linked to the expression of both BDNF and its receptor TrkB [81]. Furthermore, androgens and CNTF interact early in postnatal development to increase SNB motor neuron number [82]. These in vivo data confirm the in vitro observation that androgen signaling plays a crucial role in motor neuron development, especially with regard to the establishment of neurites (in vitro)

and dendrites (in vivo). However, remaining questions are: to what degree does the AR maintain this trophic influence in adult motor neurons, and how might androgen signaling protect adult motor neurons from degeneration?

Trophism of adult neurons is frequently inferred from the ability of a trophic factor to protect neurons from a variety of insults. The AR has demonstrated a wide variety of neuroprotective effects. AR signaling protects many cells (including neuroblastoma cells [83], primary cerebellar granule cells [84] and striatal cells in vivo [85]) against oxidative stress-induced cell death. This protection may result from an AR-specific increase in catalase activity [83,84]. Another example of AR neuroprotection comes from an experiment in which the excitotoxin kainate was noted to kill more hippocampal neurons in gonadectomized male rats versus sham-operated controls; this cell death was then reversed by supplementation of the gonadectomized rats with DHT [86]. Androgens have even been shown to protect neurons from the toxic effects of the beta-amyloid peptide (Ab1-42), believed to be a causative agent in Alzheimer's disease pathogenesis [87]. Both androgens and estrogen can protect neurons from Ab toxicity by increasing the levels of the chaperone protein Hsp70, which is thought to prevent Ab aggregate formation [88]. Additionally, androgens may protect against Ab toxicity through a receptor-dependent activation of the MAPK/ERK signaling pathway in neurons, leading to downstream activation of Rsk and inactivation of Bad, a pro-apoptotic Bcl-2 family member [89].

Importantly, in the spinal cord, signaling through the AR can elicit specific motor neuron protection, both in vitro and in vivo. AR expressing motor neuron-like MN-1 cells not only exhibit larger somas and broader neurite arbors in response to

androgens, but they are also protected from serum deprivation-induced cell death [26,78]. This seems to be a common function of AR signaling in neurons, as androgens promote the survival of human primary neurons in low serum conditions in a receptor-dependent fashion [90]. Evidence from in vivo motor neuron injury models indicates that AR signaling protects motor neurons from axotomy-induced death. Androgens interact with BDNF in the SNB to promote motor neuron survival and maintenance of the SNB dendritic arbor post-axotomy [80]. Furthermore, androgens are particularly trophic in a hamster facial motor neuron axotomy model, promoting survival of axotomized neurons and increasing the rate of functional recovery [91–93]. AR signaling is clearly involved in protecting adult neurons, including motor neurons, from toxicity, injury and death.

How might androgen signaling be promoting neuronal survival? Since the AR functions primarily as a transcription factor, it is logical to predict that this protective effect might be tied to the ability of the AR to induce the expression of genes that are involved in promoting motor neuron survival (Fig. 2). Indeed, AR mediated up-regulation of neuritin expression is directly responsible for neurite elongation in motor neuron-like cultures, as neuritin silencing by siRNA abolishes the trophic response to androgens [79]. Similarly, inhibition of neurotrophin and CNTF signaling prevents the sparing of SNB motor neurons normally observed after administration of androgens to neonatal rats [94]. Trophic factor signaling is thus an important aspect of AR trophism and might function downstream of androgen signaling.

Several trophic factors that are important for motor neuron biology have been associated with AR signaling. AR activation stimulates the production of VEGF mRNA

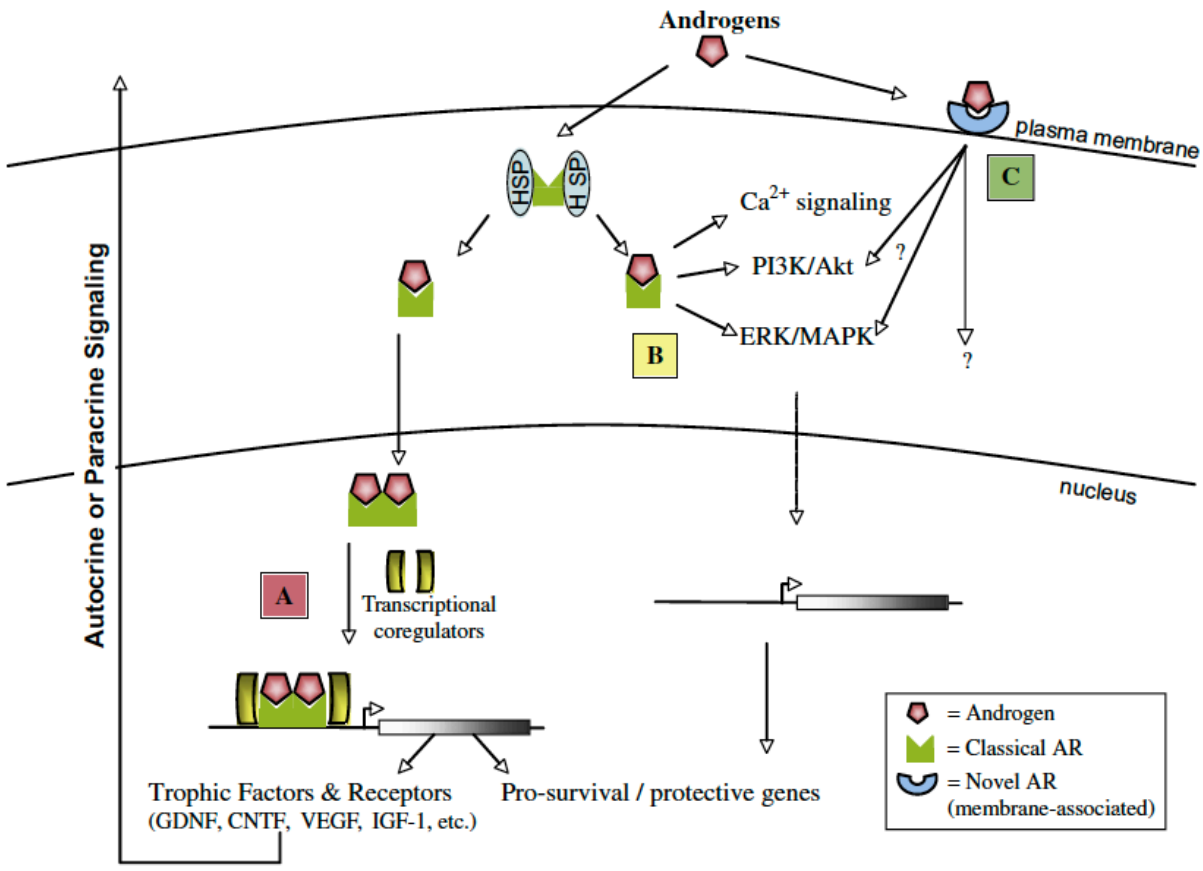

Appendix Figure 2 Proposed mechanisms for androgen receptor (AR) protection of motor neurons.

This figure summarizes three mechanisms by which AR may exert its trophic effects on motor neurons. (A) In the classical model of androgen receptor signaling, AR binds ligand, releasing it from its molecular chaperone and allowing it to undergo nuclear translocation to form homodimers. AR then associates with transcriptional co-regulators at androgen-responsive genes to promote their transcription. (B) In this non-genomic pathway of androgen receptor action, AR signaling does not involve direct interaction with genomic elements. Rather, ligand-bound AR interacts with second messenger signaling cascades, such as ERK/MAPK and PI3K/Akt, to influence the molecular status of the cell. This mechanism has not been validated yet in motor neurons. (C) Lastly, in the membrane-associated model for androgen receptor signaling, the authors postulate the interaction of androgens with putative novel membrane-associated ARs that would signal through second messenger signaling cascades.

in prostate cancer cells [74]; and in vivo siRNA silencing of AR has been demonstrated to slow neoplastic prostate growth and repress VEGF expression [75]. AR stimulation of VEGF signaling increases BDNF levels and ultimately neurogenesis in the brains of adult songbirds [95], which demonstrates the possible multi-potency of AR-stimulated VEGF expression. Transgenic mice carrying a polyQ-expanded AR express less VEGF, and this reduction has been implicated in the pathology of SBMA [56]. In another mouse model of SBMA, polyQ-expanded AR is associated with decreased GDNF and IGF-1 expression [96]. Researchers have identified androgen response elements in the upstream promoter of the IGF-1 gene [97], and testosterone has been observed to stimulate IGF-1 transcription in prostate [98]. Interestingly, IGF-1 can facilitate AR signaling by de-repressing Foxo1 [99] or by stabilization of beta-catenin, an AR co-activator [100]. The authors' group, in collaboration with workers at the National Institutes of Health, has recently identified a mechanism through which IGF-1 prevents the deleterious effects of polyQ-expanded AR by stimulating Akt-mediated AR phosphorylation which blocks ligand binding and receptor activation [70]. These results indicate that while IGF-1 and AR signaling in motor neurons are intertwined, it is possible that AR stimulation of IGF-1 expression is a protective mechanism for motor neurons. CNTF is another important trophic factor that has been demonstrated to be androgen-responsive. Expression of the CNTF receptor alpha subunit is regulated by the AR in both spinal cord and muscle [101,102]. Furthermore, CNTF receptor knock-out mice do not exhibit the sexual dimorphism normally present in the SNB [103]; and SNB motor neuron death in androgen-insensitive rats can be prevented by CNTF administration [104]. These results, together with the previously noted observation that

blocking CNTF signaling prevents the AR-mediated rescue of early SNB motor neurons, indicate that AR-mediated expression of the CNTF receptor is necessary for the sexually dimorphic sparing of SNB motor neurons in rodents. These data support a model in which AR-mediated expression of trophic factor signaling genes is a mechanism by which androgens convey their neuroprotection.

A complication of this interpretation comes from recent observations that AR signaling might not be restricted to direct genomic interaction and the subsequent regulation of transcription through binding of androgen response elements in the promoters of target genes (See Fig. 2). Indeed, it has been reported that the androgen antagonists flutamide and cyproterone acetate both exhibit agonist effects, including hippocampal neuroprotection, in an AR-dependent manner [105]. These antagonists have been shown to block AR DNA binding and disrupt AR co-regulator associations, respectively, ultimately preventing the transcriptional effects of the AR [106]. This suggests that either these compounds are not true anti-androgens or, more likely, that signaling through the AR is not limited to influencing transcription. Indeed, the AR, like many hormone receptors [107], can rapidly signal through ERK/MAPK and the PI3K/Akt pathways without direct genomic interaction [89,108–110]. These interactions could promote cell survival, however, rapid signaling of the AR through these second messenger pathways has not been directly observed in motor neurons. In addition, Gatson and colleagues [111] recently described the discovery of a novel membrane-associated androgen receptor action in a glial cell model. This membrane-associated receptor, triggered by a cell-impermeable BSA-conjugated DHT, was shown to have the opposite effect upon MAPK and Akt signaling pathways that had been elicited by

non-BSA-conjugated DHT treatment. This group then further characterized their system in primary astrocyte cultures, and demonstrated that signaling through this potentially novel androgen pathway actually promotes astrocyte cell death [112]. These data indicate that despite years of research, there may be numerous aspects of AR signaling that are not fully understood.

Summary

Motor neurons are acutely dependent upon trophic factor support, as a variety of MND have responded very positively to trophic factor intervention. However, as most of these molecules are peptide hormones, there is the intrinsic problem of delivery across the blood-brain-barrier to the CNS. Many delivery paradigms have been employed with varying success – from systemic administration and use of motor neuron retrograde transport mechanisms, to viral and cellular delivery of specific trophic factors [113,114]. The cumulative data presented here suggest that these trophic signaling pathways might be prone to manipulation in other ways, including via signaling through the AR. Further supporting the involvement of AR in MND is evidence that AR signaling is perturbed not only in SBMA, but also in ALS. The incidence of ALS is strongly sexually dimorphic, with male predominance [115], and recently, Militello and colleagues [116] documented decreased serum levels of free testosterone in ALS patients. Completing the picture of how normal AR signaling promotes motor neuron health may be informative not only for SBMA, but also for other MND, including especially ALS.

The trophic effects of androgen signaling have been enumerated, but many

questions still remain. One question is whether the beneficial effects of AR signaling in motor neurons occur by androgen acting directly upon the AR in the motor neurons themselves, or whether AR signaling in supporting cells, such as glia or muscle, might be promoting motor neuron health. As IGF-1 is produced by glial cells and muscle fibers, and IGF-1 expression is responsive to AR signaling, it is tempting to speculate that muscle production of IGF-1 drives AR-dependent trophic actions in a paracrine fashion to support motor neurons. There may also be a set of trophic autocrine signaling loops that are stimulated by AR activation. Future studies should test the ability of other steroid hormones to promote the protection of motor neurons. Finally, the relative contributions of the genomic and novel non-genomic signaling mechanisms of the AR on the neuroprotective functions of androgens on motor neurons needs to be resolved. Ultimately, there is a very compelling case that androgen signaling is protective in motor neurons. An understanding of AR biology in motor neurons will likely be required to fully appreciate the etiology of SBMA and other MND, and thereby devise effective treatments for these devastating disorders.

References

[1] Mooradian AD, Morley JE, Korenman SG. Biological actions of androgens. Endocr Rev 1987;8:1–28.

[2] Gelmann EP. Molecular biology of the androgen receptor. J Clin Oncol 2002;20:3001–15.

[3] Gottlieb B, Beitel LK, Wu JH, et al. The androgen receptor gene mutations database (ARDB): 2004 update. Hum Mutat 2004;23:527–33.

[4] Kennedy WR, Alter M, Sung JH. Progressive proximal spinal and bulbar muscular atrophy of late onset. A sex-linked recessive trait. Neurology 1968;18(7):671–80.

[5] Li M, Miwa S, Kobayashi Y, et al. Nuclear inclusions of the androgen receptor protein in spinal and bulbar muscular atrophy. Ann Neurol 1998;44:249–54.

[6] Kihira T, Yoshida S, Yoshimasu F, et al. Involvement of Onuf's nucleus in amyotrophic lateral sclerosis. J Neurol Sci 1997;147(1):81–8.

[7] Schroder HD, Reske-Nielsen E. Preservation of the nucleus X-pelvic floor motosystem in amyotrophic lateral sclerosis. Clin Neuropathol 1984;3(5):210–6.

[8] Olney RK, Aminoff MJ, So YT. Clinical and electrodiagnostic features of X-linked recessive bulbospinal neuronopathy. Neurology 1991;41:823–8.

[9] Barkhaus PE, Kennedy WR, Stern LZ, et al. Hereditary proximal spinal and bulbar motor neuron disease of late onset. A report of six cases. Arch Neurol 1982;39:112–6.

[10] Dejager S, Bry-Gauillard H, Bruckert E, et al. A comprehensive endocrine description of Kennedy's disease revealing androgen insensitivity linked to CAG repeat length. J Clin Endocrinol Metab 2002;87:3893–901.

[11] Arbizu T, Santamarıa J, Gomez JM, et al. A family with adult spinal and bulbar muscular atrophy, X-linked inheritance and associated testicular failure. J Neurol Sci 1983;59: 371–82.

[12] Fischbeck KH, Ionasescu V, Ritter AW, et al. Localization of the gene for X-linked spinal muscular atrophy. Neurology 1986;36:1595–8.

[13] La Spada AR, Wilson EM, Lubahn DB, et al. Androgen receptor gene mutations in X-linked spinal and bulbar muscular atrophy. Nature 1991;352:77–9.

[14] Zoghbi HY, Orr HT. Glutamine repeats and neurodegeneration. Annu Rev Neurosci 2000; 23:217–47.

[15] Ordway JM, Tallaksen-Greene S, Gutekunst CA, et al. Ectopically expressed CAG repeats cause intranuclear inclusions and a progressive late onset neurological phenotype in the mouse. Cell 1997;91:753–63.

[16] Paulson HL, Bonini NM, Roth KA. Polyglutamine disease and neuronal cell death. Proc Natl Acad Sci USA 2000;97:12957–8.

[17] Schmidt BJ, Greenberg CR, Allingham-Hawkins DJ, et al. Expression of X-linked bulbospinal muscular atrophy (Kennedy disease) in two homozygous women. Neurology 2002; 59:770–2.

[18] Thomas PS, Fraley GS, Damian V, et al. Loss of endogenous androgen receptor protein accelerates motor neuron degeneration and accentuates androgen insensitivity in a mouse model of X-linked spinal and bulbar muscular atrophy. Hum Mol Genet 2006;15:2225–38.

[19] Dragatsis I, Levine MS, Zeitlin S. Inactivation of Hdh in the brain and testis results in progressive neurodegeneration and sterility in mice. Nat Genet 2000;26:300–6.

[20] Leavitt BR, Guttman JA, Hodgson JG, et al. Wild-type huntingtin reduces the cellular toxicity of mutant huntingtin in vivo. Am J Hum Genet 2001;68:313–24.

[21] Rigamonti D, Bauer JH, De-Fraja C, et al. Wild-type huntingtin protects from apoptosis upstream of caspase-3. J Neurosci 2000;20:3705–13.

[22] Leavitt BR, van Raamsdonk JM, Shehadeh J, et al. Wild-type huntingtin protects neurons from excitotoxicity. J Neurochem 2006;96:1121–9.

[23] Gauthier LR, Charrin BC, Borrell-Page` s M, et al. Huntingtin controls neurotrophic support and survival of neurons by enhancing BDNF vesicular transport along microtubules. Cell 2004;118:127–38.

[24] Palhan VB, Chen S, Peng GH, et al. Polyglutamine-expanded ataxin-7 inhibits STAGA histone acetyltransferase activity to produce retinal degeneration. Proc Natl Acad Sci U S A 2005;102:8472–7.

[25] Donaldson KM, Li W, Ching KA, et al. Ubiquitin-mediated sequestration of normal cellular proteins into polyglutamine aggregates. Proc Natl Acad Sci USA 2003;100:8892–7.

[26] Lieberman AP, Harmison G, Strand AD, et al. Altered transcriptional regulation in cells expressing the expanded polyglutamine androgen receptor. Hum Mol Genet 2002;11: 1967–76.

[27] Sendtner M, Holtmann B, Hughes RA. The response of motoneurons to neurotrophins. Neurochem Res 1996;21:831–41.

[28] Thoenen H, Hughes RA, Sendtner M. Trophic support of motoneurons: physiological, pathophysiological, and therapeutic implications. Exp Neurol 1993;124:47–55.

[29] Kilpatrick TJ, Soilu-Hai nninen M. Molecular mechanisms regulating motor neuron development and degeneration. Mol Neurobiol 1999;19:205–28.

[30] Henderson CE, Phillips HS, Pollock RA, et al. GDNF: a potent survival factor for motoneurons present in peripheral nerve and muscle. Science 1994;266:1062–4.

[31] Zhao Z, Alam S, Oppenheim RW, et al. Overexpression of glial cell line-derived neurotrophic factor in the CNS rescues motoneurons from programmed cell death and promotes their long-term survival following axotomy. Exp Neurol 2004;190:356–72.

[32] Yan Q, Matheson C, Lopez OT. In vivo neurotrophic effects of GDNF on neonatal and adult facial motor neurons. Nature 1995;373:341–4.

[33] Yamamoto M, Mitsuma N, Inukai A, et al. Expression of GDNF and GDNFR-alpha mRNAs in muscles of patients with motor neuron diseases. Neurochem Res 1999;24(6): 785–90.

[34] Henderson CE, Camu W, Mettling C, et al. Neurotrophins promote motor neuron survival and are present in embryonic limb bud. Nature 1993;363:266–70.

[35] DiStefano PS, Friedman B, Radziejewski C, et al. The neurotrophins BDNF, NT-3, and NGF display distinct patterns of retrograde axonal transport in peripheral and central neurons. Neuron 1992;8:983–93.

[36] Gimei nez y Ribotta M, Revah F, Pradier L, et al. Prevention of motoneuron death by adenovirus-mediated neurotrophic factors. J Neurosci Res 1997;48:281–5.

[37] Yan Q, Elliott J, Snider WD. Brain-derived neurotrophic factor rescues spinal motor neurons from axotomy-induced cell death. Nature 1992;360:753–5.

[38] Koliatsos VE, Clatterbuck RE, Winslow JW, et al. Evidence that brain-derived neurotrophic factor is a trophic factor for motor neurons in vivo. Neuron 1993;10:359–67.

[39] Estei vez AG, Spear N, Manuel SM, et al. Nitric oxide and superoxide contribute to motor neuron apoptosis induced by trophic factor deprivation. J Neurosci 1998;18:923–31.

[40] Lindholm D, Dechant G, Heisenberg CP, et al. Brain-derived neurotrophic factor is a survival factor for cultured rat cerebellar granule neurons and protects them against glutamate-induced neurotoxicity. Eur J Neurosci 1993;5:1455–64.

[41] Shimohama S, Tamura Y, Akaike A, et al. Brain-derived neurotrophic factor pretreatment exerts a partially protective effect against glutamate-induced neurotoxicity in cultured rat cortical neurons. Neurosci Lett 1993;164:55–8.

[42] Ochs G, Penn RD, York M, et al. A phase I/II trial of recombinant methionyl human brain derived neurotrophic factor administered by intrathecal infusion to patients with amyotrophic lateral sclerosis. Amyotroph Lateral Scler Other Motor Neuron Disord 2000;1:201–6.

[43] Ikeda K, Klinkosz B, Greene T, et al. Effects of brain-derived neurotrophic factor on motor dysfunction in wobbler mouse motor neuron disease. Ann Neurol 1995;37:505–11.

[44] Negro A, Tolosano E, Skaper SD, et al. Cloning and expression of human ciliary neurotrophic factor. Eur J Biochem 1991;201:289–94.

[45] Sendtner M, Arakawa Y, Stoi ckli KA, et al. Effect of ciliary neurotrophic factor (CNTF) on motoneuron survival. J Cell Sci Suppl 1991;15:103–9.

[46] Clatterbuck RE, Price DL, Koliatsos VE. Further characterization of the effects of brain-derived neurotrophic factor and ciliary neurotrophic factor on axotomized neonatal and adult mammalian motor neurons. J Comp Neurol 1994;342:45–56.

[47] Tan SA, Dei glon N, Zurn AD, et al. Rescue of motoneurons from axotomy-induced cell death by polymer encapsulated cells genetically engineered to release CNTF. Cell Transplant 1996;5:577–87.

[48] Gatzinsky KP, Holtmann B, Daraie B, et al. Early onset of degenerative changes at nodes of Ranvier in alpha-motor axons of Cntf null (-/-) mutant mice. Glia 2003;42:340–9.

[49] DeChiara TM, Vejsada R, Poueymirou WT, et al. Mice lacking the CNTF receptor, unlike mice lacking CNTF, exhibit profound motor neuron deficits at birth. Cell 1995;83:313–22.

[50] Azzouz M, Ralph GS, Storkebaum E, et al. VEGF delivery with retrogradely transported lentivector prolongs survival in a mouse ALS model. Nature 2004;429:413–7.

[51] Storkebaum E, Lambrechts D, Carmeliet P. VEGF: once regarded as a specific angiogenic factor, now implicated in neuroprotection. Bioessays 2004;26:943–54.

[52] Storkebaum E, Lambrechts D, Dewerchin M, et al. Treatment of motoneuron degeneration by intracerebroventricular delivery of VEGF in a rat model of ALS. Nat Neurosci 2005;8: 85–92.

[53] Van Den Bosch L, Storkebaum E, Vleminckx V, et al. Effects of vascular endothelial growth factor (VEGF) on motor neuron degeneration. Neurobiol Dis 2004;17:21–8.

[54] Hobson MI, Green CJ, Terenghi G. VEGF enhances intraneural angiogenesis and improves nerve regeneration after axotomy. J Anat 2000;197(Pt 4):591–605.

[55] Devos D, Moreau C, Lassalle P, et al. Low levels of the vascular endothelial growth factor in CSF from early ALS patients. Neurology 2004;62:2127–9.

[56] Sopher BL, Thomas PS, LaFevre-Bernt MA, et al. Androgen receptor YAC transgenic mice recapitulate SBMA motor neuronopathy and implicate VEGF164 in the motor neuron degeneration. Neuron 2004;41:687–99.

[57] Oosthuyse B, Moons L, Storkebaum E, et al. Deletion of the hypoxia-response element in the vascular endothelial growth factor promoter causes motor neuron degeneration. Nat Genet 2001;28:131–8.

[58] Terry PD, Kamel F, Umbach DM, et al. VEGF promoter haplotype and amyotrophic lateral sclerosis (ALS). J Neurogenet 2004;18(2):429–34.

[59] Zheng C, Nennesmo I, Fadeel B, et al. Vascular endothelial growth factor prolongs survival in a transgenic mouse model of ALS. Ann Neurol 2004;56(4):564–7.

[60] Wilkins A, Chandran S, Compston A. A role for oligodendrocyte-derived IGF-1 in trophic support of cortical neurons. Glia 2001;36:48–57.

[61] Hansson HA, Dahlin LB, Danielsen N, et al. Evidence indicating trophic importance of IGF-I in regenerating peripheral nerves. Acta Physiol Scand 1986;126:609–14.

[62] Dobrowolny G, Giacinti C, Pelosi L, et al. Muscle expression of a local Igf-1 isoform protects motor neurons in an ALS mouse model. J Cell Biol 2005;168:193–9.

[63] Ang LC, Bhaumick B, Munoz DG, et al. Effects of astrocytes, insulin and insulin-like growth factor I on the survival of motoneurons in vitro. J Neurol Sci 1992;109:168–72.

[64] Hughes RA, Sendtner M, Thoenen H. Members of several gene families influence survival of rat motoneurons in vitro and in vivo. J Neurosci Res 1993;36:663–71.

[65] Caroni P, Grandes P. Nerve sprouting in innervated adult skeletal muscle induced by exposure to elevated levels of insulin-like growth factors. J Cell Biol 1990;110:1307–17.

[66] Payne AM, Zheng Z, Messi ML, et al. Motor neurone targeting of IGF-1 prevents specific force decline in ageing mouse muscle. J Physiol 2006;570:283–94.

[67] Kaspar BK, Lladoi J, Sherkat N, et al. Retrograde viral delivery of IGF-1 prolongs survival in a mouse ALS model. Science 2003;301:839–42.

[68] Gorio A, Lesma E, Madaschi L, et al. Co-administration of IGF-I and glycosaminoglycans greatly delays motor neurone disease and affects IGF-I expression in the wobbler mouse: a long-term study. J Neurochem 2002;81:194–202.

[69] Bilak MM, Corse AM, Kuncl RW. Additivity and potentiation of IGF-I and GDNF in the complete rescue of postnatal motor neurons. Amyotroph Lateral Scler Other Motor Neuron Disord 2001;2:83–91.

[70] Palazzolo I, Burnett BG, Young JE, et al. Akt blocks ligand binding and protects against expanded polyglutamine androgen receptor toxicity. Hum Mol Genet 2007;16:1593–603.

[71] Leav I, Lau KM, Adams JY, et al. Comparative studies of the estrogen receptors beta and alpha and the androgen receptor in normal human prostate glands, dysplasia, and in primary and metastatic carcinoma. Am J Pathol 2001;159(1):79–92.

[72] Waltregny D, Leav I, Signoretti S, et al. Androgen-driven prostate epithelial cell proliferation and differentiation in vivo involve the regulation of p27. Mol Endocrinol 2001; 15(5):765–82.

[73] Kidwai N, Gong Y, Sun X, et al. Expression of androgen receptor and prostate-specific antigen in male breast carcinoma. Breast Cancer Res 2004;6(1):R18–23.

[74] Sordello S, Bertrand N, Plouei t J. Vascular endothelial growth factor is up-regulated in vitro and in vivo by androgens. Biochem Biophys Res Commun 1998;251:287–90.

[75] Compagno D, Merle C, Morin A, et al. SIRNA-directed in vivo silencing of androgen receptor inhibits the growth of castration-resistant prostate carcinomas. PLoS ONE 2007;2:e1006.

[76] Sajjad Y, Quenby S, Nickson P, et al. Androgen receptors are expressed in a variety of human fetal extragenital tissues: an immunohistochemical study. Asian J Androl 2007;9:751–9.

[77] Sar M, Stumpf WE. Androgen concentration in motor neurons of cranial nerves and spinal cord. Science 1977;197:77–9.

[78] Brooks BP, Merry DE, Paulson HL, et al. A cell culture model for androgen effects in motor neurons. J Neurochem 1998;70:1054–60.

[79] Marron TU, Guerini V, Rusmini P, et al. Androgen-induced neurite outgrowth is mediated by neuritin in motor neurones. J Neurochem 2005;92:10–20.

[80] Yang LY, Verhovshek T, Sengelaub DR. Brain-derived neurotrophic factor and androgen interact in the maintenance of dendritic morphology in a sexually dimorphic rat spinal nucleus. Endocrinology 2004;145:161–8.

[81] Ottem EN, Beck LA, Jordan CL, et al. Androgen-dependent regulation of brain-derived neurotrophic factor and tyrosine kinase B in the sexually dimorphic spinal nucleus of the bulbocavernosus. Endocrinology 2007;148(8):3655–65.

[82] Varela CR, Bengston L, Xu J, et al. Additive effects of ciliary neurotrophic factor and testosterone on motoneuron survival; differential effects on motoneuron size and muscle morphology. Exp Neurol 2000;165:384–93.

[83] Chisu V, Manca P, Lepore G, et al. Testosterone induces neuroprotection from oxidative stress. Effects on catalase activity and 3-nitro-L-tyrosine incorporation into alpha-tubulin in a mouse neuroblastoma cell line. Arch Ital Biol 2006;144:63–73.

[84] Ahlbom E, Prins GS, Ceccatelli S. Testosterone protects cerebellar granule cells from oxidative stress-induced cell death through a receptor mediated mechanism. Brain Res 2001;892:255–62.

[85] Tunez I, Feijoo M, Collado JA, et al. Effect of testosterone on oxidative stress and cell damage induced by 3-nitropropionic acid in striatum of ovariectomized rats. Life Sci 2007;80(13):1221–7.

[86] Ramsden M, Shin TM, Pike CJ. Androgens modulate neuronal vulnerability to kainate lesion.

Neuroscience 2003;122:573–8.

[87] Magranei J, Smith RC, Walsh K, et al. Heat shock protein 70 participates in the neuroprotective response to intracellularly expressed beta-amyloid in neurons. J Neurosci 2004;24: 1700–6.

[88] Zhang Y, Champagne N, Beitel LK, et al. Estrogen and androgen protection of human neurons against intracellular amyloid beta1-42 toxicity through heat shock protein 70. J Neurosci 2004;24:5315–21.

[89] Nguyen TV, Yao M, Pike CJ. Androgens activate mitogen-activated protein kinase signaling: role in neuroprotection. J Neurochem 2005;94:1639–51.

[90] Hammond J, Le Q, Goodyer C, et al. Testosterone-mediated neuroprotection through the androgen receptor in human primary neurons. J Neurochem 2001;77:1319–26.

[91] Drengler SM, Handa RJ, Jones KJ. Effects of axotomy and testosterone on androgen receptor mRNA expression in hamster facial motoneurons. Exp Neurol 1997;146(2):374–9.

[92] Huppenbauer CB, Tanzer L, DonCarlos LL, et al. Gonadal steroid attenuation of developing hamster facial motoneuron loss by axotomy: equal efficacy of testosterone, dihydrotestosterone, and 17-beta estradiol. J Neurosci 2005;25(16):4004–13.

[93] Kujawa KA, Emeric E, Jones KJ. Testosterone differentially regulates the regenerative properties of injured hamster facial motoneurons. J Neurosci 1991;11(12):3898–906.

[94] Xu J, Gingras KM, Bengston L, et al. Blockade of endogenous neurotrophic factors prevents the androgenic rescue of rat spinal motoneurons. J Neurosci 2001;21:4366–72.

[95] Louissaint A, Rao S, Leventhal C, et al. Coordinated interaction of neurogenesis and angiogenesis in the adult songbird brain. Neuron 2002;34:945–60.

[96] Yu Z, Dadgar N, Albertelli M, et al. Androgen-dependent pathology demonstrates myopathic contribution to the Kennedy disease phenotype in a mouse knock-in model. J Clin Invest 2006;116:2663–72.

[97] Wu Y, Zhao W, Zhao J, et al. Identification of androgen response elements in the insulin-like growth factor I upstream promoter. Endocrinology 2007;148:2984–93.

[98] Pandini G, Mineo R, Frasca F, et al. Androgens up-regulate the insulin-like growth factor-I receptor in prostate cancer cells. Cancer Res 2005;65:1849–57.

[99] Fan W, Yanase T, Morinaga H, et al. Insulin-like growth factor 1/insulin signaling activates androgen signaling through direct interactions of Foxo1 with androgen receptor. J Biol Chem 2007;282:7329–38.

[100] Verras M, Sun Z. Beta-catenin is involved in insulin-like growth factor 1-mediated transactivation of the androgen receptor. Mol Endocrinol 2005;19:391–8.

[101] Xu J, Forger NG. Expression and androgen regulation of the ciliary neurotrophic factor receptor (CNTFRalpha) in muscles and spinal cord. J Neurobiol 1998;35:217–25.

[102] Forger NG, Wagner CK, Contois M, et al. Ciliary neurotrophic factor receptor alpha in spinal

motoneurons is regulated by gonadal hormones. J Neurosci 1998;18:8720–9.

[103] Forger NG, Howell ML, Bengston L, et al. Sexual dimorphism in the spinal cord is absent in mice lacking the ciliary neurotrophic factor receptor. J Neurosci 1997;17:9605–12.

[104] Forger NG, Wong V, Breedlove SM. Ciliary neurotrophic factor arrests muscle and motoneuron degeneration in androgen-insensitive rats. J Neurobiol 1995;28:354–62.

[105] Nguyen TV, Yao M, Pike CJ. Flutamide and cyproterone acetate exert agonist effects: induction of androgen receptor-dependent neuroprotection. Endocrinology 2007;148: 2936–43.

[106] Berrevoets CA, Umar A, Brinkmann AO. Antiandrogens: selective androgen receptor modulators. Mol Cell Endocrinol 2002;198(1–2):97–103.

[107] Loi sel R, Wehling M. Nongenomic actions of steroid hormones. Nat Rev Mol Cell Biol 2003;4:46–56.

[108] Kousteni S, Bellido T, Plotkin LI, et al. Nongenotropic, sex-nonspecific signaling through the estrogen or androgen receptors: dissociation from transcriptional activity. Cell 2001; 104:719–30.

[109] Michels G, Hoppe UC. Rapid actions of androgens. Front Neuroendocrinol 2007:10.1016/ j.yfrne.2007.1008.1004. In press.

[110] Rahman F, Christian HC. Non-classical actions of testosterone: an update. Trends Endocrinol Metab 2007;18:371–8.

[111] Gatson JW, Kaur P, Singh M. Dihydrotestosterone differentially modulates the mitogen-activated protein kinase and the phosphoinositide 3-kinase/Akt pathways through the nuclear and novel membrane androgen receptor in C6 cells. Endocrinology 2006;147:2028–34.

[112] Gatson JW, Singh M. Activation of a membrane-associated androgen receptor promotes cell death in primary cortical astrocytes. Endocrinology 2007;148:2458–64.

[113] Federici T, Boulis NM. Gene-based treatment of motor neuron diseases. Muscle Nerve 2006;33(3):302–23.

[114] Nayak MS, Kim YS, Goldman M, et al. Cellular therapies in motor neuron diseases. Biochim Biophys Acta 2006;1762(11–12):1128–38.

[115] Beghi E, Logroscino G, Chio` A, et al. The epidemiology of ALS and the role of population-based registries. Biochim Biophys Acta 2006;1762:1150–7.

[116] Militello A, Vitello G, Lunetta C, et al. The serum level of free testosterone is reduced in amyotrophic lateral sclerosis. J Neurol Sci 2002;195:67–70.